BEAM DEPTH SIZE EFFECT IN SIMPLY SUPPORTED REINFORCED CONCRETE DEEP BEAM

EUGENE KOK ZHEN YIN

UNIVERSITI TUNKU ABDUL RAHMAN

BEAM DEPTH SIZE EFFECT IN SIMPLY SUPPORTED REINFORCED CONCRETE DEEP BEAM
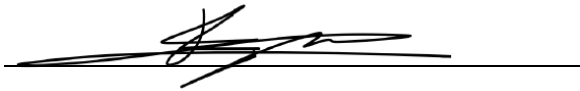
EUGENE KOK ZHEN YIN

A project report submitted in partial fulfilment of the requirements for the award of Bachelor of Engineering (Honours) Civil Engineering

Lee Kong Chian Faculty of Engineering and Science

Universiti Tunku Abdul Rahman

May 2022

DECLARATION

I hereby declare that this project report is based on my original work except for citations and quotations which have been duly acknowledged. I also declare that it has not been previously and concurrently submitted for any other degree or award at UTAR or other institutions.

Signature : _____

Name : Eugene Kok Zhen Yin

ID No. : 1704210

Date : 17-5-2022

APPROVAL FOR SUBMISSION

I certify that this project report entitled **"BEAM DEPTH SIZE EFFECT IN SIMPLY SUPPORTED REINFORCED CONCRETE DEEP BEAM"** was prepared by **EUGENE KOK ZHEN YIN** has met the required standard for submission in partial fulfilment of the requirements for the award of Bachelor of Engineering (Honours) Civil Engineering at Universiti Tunku Abdul Rahman.

Approved by,

Signature   :

Supervisor   :   Dr. Woon Kai Siong

Date   :   17/5/2022

ACKNOWLEDGEMENTS

I would like to thank everyone who had contributed to the successful completion of this project. I would like to express my gratitude to my research supervisor, Dr. Woon Kai Siong for his invaluable advice, guidance and his enormous patience throughout the development of the research.

In addition, I would also like to express my gratitude to my loving parents and friends who had helped and given me encouragement as well as support throughout the research study. Before I finish, I would like to thank my FYP coordinator, Dr Lee Yee Ling for her great efforts.

ABSTRACT

Reinforced concrete (RC) deep beam is different from slender beam in term of its load transferring mechanism. It is widely used in construction industry to transfer massive amount of load over a large span length mainly to free up more column spaces. Depth of deep beam would often be increased to withstand higher loading. However, the increase in depth of the beam may not resultes in a corresponding increment in beam shear strength where this phenomenon is referred as depth size effect. Therefore, this research study aims to focus on the depth size effect in simply supported RC deep beam. This research study utilized the ABAQUS Finite Element Analysis (FEA) software to simulate the numerical test specimen. Six numerical deep beam specimens were created which includes one reference beam, R-01, one control beam, C-01, and 4 numerical test specimens with different cross-sectional height denoted as D-400, D-500, D-600 and D-700 which were analysed by ABAQUS software. The numerical reference beam results were verified with the experimental results from Zhang and Tan (2007) to prove the reliability of numerical modelling technique. Then, similar numerical modelling technique was applied for all the numerical specimens. The difference in ultimate failure loads between numerical model and analytical model (Cracking Strut and Tie model) are found to range between 5.13% and 7.24%. Besides, size effect was observed in the study. On the first 100 mm beam height increment, the normalized shear stress decreased by 4.29 % and for the following 100 mm beam height incremental, the cumulative decrements are found to be 11.07 %, 13.97 % and 16.95 % respectively. The decrement in relative depth of compression zone is the contributing factor that resulted in size effect. Other than that, the von Mises stress contour and concrete tension damage contour was generated to study the behaviour of deep beam with different height in term of stress distribution and cracking propagation. The findings shows that the stress distribution and crack propagation of numerical deep beam specimens are about similar between each of the specimen. Therefore, it is inferred that the stress distribution and cracking propagation of deep beam does not greatly influence by the specimen's height.

TABLE OF CONTENTS

LIST OF TABLES

LIST OF FIGURES

LIST OF SYMBOLS / ABBREVIATIONS

a	shear span length, mm
b_w	specimen width, m
c	compression zone height, mm
d	effective depth, m
f'_c	concrete compressive cylinder strength, kPa
f_u	ultimate stress, kPa
f_y	steel yield stress, kPa
p	ratio of longitudinal reinforcement
w	strut width, mm
E	Young's modulus, GPa
K_c	ratio of the second stress invariant on the tensile meridian to compressive meridian
V	ultimate fail load, kN
V_n	shear capacity of strut, N
α	critical shear crack angle
β	strut efficiency
ε	strain, mm/mm
θ	strut angle
μ	viscosity
σ	concrete tensile stress, kPa
Ψ	dilation angle
ω	concrete density, kg/m^3
CDP	concrete damaged plasticity
CSC	critical shear crack
CSTM	cacking strut-and-tie model
FEM	finite element method
RC	reinforced concrete
STM	strut and tie method

LIST OF APPENDICES

CHAPTER 1

INTRODUCTION

1.1   General Introduction

Reinforced concrete (RC) deep beams have numerous applications in building construction due to its capability on supporting huge load over a large span length. RC deep beams can usually be found in design of pile caps in foundation, load bearing walls, wall footings, floor diaphragms, outriggers and it is widely used as transfer girders at the lower level of tall building due to their convenience and economical competency (Mohamed, Shoukry and Saeed, 2014). Different depth of beam is used for different application to support the applied load and the depth can be as large as 6m (Yu et al., 2016).

The RC deep beams are defined differently by different codes of practice. According on the ACI Committee 318, deep beams are defined as member with clear span equal to or less than four times the overall member height ($\ell/h \leq 4$) while BS EN 1992-1-1:2004 defined deep beams as member with clear span less than three times its overall height ($\ell/h < 3$). The definition is important to classify deep beam and slender beam as both beams require different theory of stress analysis. The usual assumption used for slender beam design are based on the Euler-Bernoulli hypothesis which assuming the structural cross-section remain plane before and after straining where this kind of assumption is not appropriate for deep beams design. The assumption only accounted for flexural strain and assuming there is no transverse strain which it is not valid for the case of deep beams where the effects due to shear deformation are significant for deep beam design (Ghugal and Dahake, 2012). The shear strength of a deep beam predicted using Euler-Bernoulli hypothesis may be two to three times lower than the actual shear strength possess by the deep beam specimen (Niranjan and Patil, 2012). Therefore, it is important to apply suitable method for deep beam design.

The two popular methods to estimate deep beams capacity are the strut and tie method (STM) and finite element method (FEM). STM could be computed manually using empirical formula suggested by ACI Committee 318 and past researchers. However, FEM is too complicated and could be very

tedious to solve manually. Therefore, software such as ABAQUS or ATENA will often be introduced to perform the numerical analysis of the RC deep beam.

1.2   Importance of the Study

Reinforced concrete deep beam is widely used in construction industry due to its capability of transferring massive amount of load and this subject of researches has attracted the attention of professionals and academician (Lafta and Ye, 2016). Deep beam members are essential especially for skyscraper buildings mainly to save up column usage in order to provide more free spaces. The size effect of deep beam is one of the major factors that needed to be considerate when comes to practical and economical design. Because of the complexities of evaluating the behaviour of deep beam member, determining the ultimate strength of the deep beams has been a significant challenge (Lafta and Ye, 2016). Several hypotheses such as Weibull's statistical theory by Weibull (1939), interface shear transfer by Taylor (1972), fracture mechanics by Reinhardt (1981), and out-of-plane action by Kotsovos and Pavlovic (1994) have previously been proposed to explain the size effect of deep beams. However, none of the proposed hypotheses has been truly reach an accepted consensus agreement by all researchers (Tan and Cheng, 2006).

The behaviour of deep beam is primarily controlled by shear rather than flexure members where their member strength behaves as arch action mechanism. The increasing depth of deep beams would not necessarily bring about a corresponding increase in the shear capacity of the deep beam itself and this is known to be the depth size effect. The experimental data on deep beams varied with beam sizes are relatively scarce (Zhang and Tan, 2007). Therefore, the research on this subject becomes significant in order to contribute and improve the design of deep beam in the industry.

1.3   Problem Statement

A great architect often designs aesthetic looking building and at the same time always trying to provide maximum building spaces to please client needs. However, when comes to high-rise building the challenging arise to structural design engineer as architects may wanted to have minimum amount of column in the building to free up more spaces. Engineers in the situation would need

to try their best to design internal structural elements according to the architect requirement. Deep beams design is usually required at the lower story of the high-rise building, especially at the car parking basement to support massive load over long span length when the column support is limited. Deep beams have different strength behaviour compared to slender beams; it is more critical on shear failure rather than flexural failure. Therefore, when the load capacity of the deep beams needed to be increased, one of the options is to provide more shear reinforcement in the deep beams to tackle shear failure. However, the shear reinforcement could not be increased overly as the excessive amount of reinforcement would cause reinforcement congestion which later would affect the casting process and decrease the durability of the beam. Hence, increasing the cross-sectional height of deep beam would be the better option to tackle further apply loading. However, increasing of depth of deep beams would induce depth size effect which is known as a phenomenon when the ultimate shear strength does not increased proportionally with the increased in sectional depth (Birrcher et al., 2014). Thus, it is important to investigate the percentage of change in normalized shear strength when the cross-sectional height of beam is increased in order to produce an optimum design.

1.4   Aim and Objectives

This report is aimed to study the depth size effect in simply supported reinforced concrete deep beams by finite element method. The study objectives are listed as follows:

i.   to create a numerical reference beam using ABAQUS software and verify the numerical reference beam results with the experimental results.

ii.   to evaluate the change in percentage of normalised shear strength of deep beam corresponding to the increment of beam's cross-sectional height.

iii. to study the stress behaviour and cracking pattern of deep beam when the cross-sectional height of the beam increases.

1.5   Scope and Limitation of the Study

The study is to model simply supported RC deep beam using ABAQUS software to predict the depth size effect of the beam. The scope of study is:

    i.   The deep beams are tested with two-point loading.

    ii.   The deep beams are support with roller and pinned support.

    iii.   The deep beams are designed with normal strength concrete of 25.9 Mpa.

    iv.   The deep beams are only tested for shear failure instead of flexural failure.

    v.   The deep beams are designed to have constant shear span-to-effective depth ratio (a/d) of 1.2.

    vi.   The longitudinal reinforcements ratio and vertical reinforcement ratio is fixed at 1.2 % and 0.4 % respectively.

    vii.   The sensitivity analysis will be focused on the viscosity parameter in Concrete Damaged Plasticity model.

1.6   Contribution of the Study

This study provides percentage of change in normalized shear strength of beam with different cross-sectional height. The outcome of this study can be served as reference for structural engineer when designing reinforced concrete deep beam. With the outcome of this study, structural engineer could have a better concept on size effect where instinctively increasing beam height in design would not necessarily provide the expected shear strength. Therefore, to lower the construction cost, structural engineer may look for other alternative to increase the beam strength to produce a cost-effective design.

Besides that, finite element analysis by ABAQUS software was performed in this study to simulate numerical deep beams. The results proved that numerical generated beam can well resemble the actual behaviour of experimental beam. This study promotes another alternative way for engineers to evaluate the stress and behaviour of deep beam other than by conventional beam casting which could take up a lot of time and costly.

1.7   Outline of the Report

This study consists of five chapter. Chapter 1 started with a general introduction about reinforced concrete deep beam follow with importance of this study and the problem arises to initiate this study. The aim, objectives, scope and limitation are highlighted in this chapter to list out the focal points of the study. Lastly, the contribution of the study was described in the following sub-chapter.

Chapter 2 contains literature reviews related to the study topic. This chapter mainly focuses on the theory review on size effect, past experimental study related to size effect, and the introduction of finite element modelling and analytical model in studying size effect.

Chapter 3 outlines the methodology work plan for the numerical study. The overall research's workflow for this study was presented in this chapter. There are three main parts for the numerical study which include the numerical modelling, numerical analysis and finally result verification.

Chapter 4 discusses the numerical results obtained from simulation process. The results such as load-displacement curve, normalised shear strength versus effective depth's curve, von Mises stress contour, concrete tension damage contour and plastic strain magnitude diagram was provided to study depth size effect.

Lastly, Chapter 5 concludes the whole analysis findings and discussion made in Chapter 4. The conclusion was made based on the aim and objectives outlined in Chapter 1. Also, several recommendation and suggestions have been made for future study purposes.

CHAPTER 2

LITERATURE REVIEW

2.1   Introduction

Reinforced concrete deep beam is different from the conventional slender beam in term of its effectiveness of load carrying mechanism as well as failure mode. The deep beam is then often chosen to be used to transmit huge load over its long span length typically in high-rise building (Mohamed, Shoukry and Saeed, 2014). Since deep beam is usually more critical on shear failure rather than flexural failure, the design of such beam is focuses on the shear capacity. In order to improve the deep beam shear capacity, several options can be considered. However, if the cross-sectional height of beam is selected as the manipulating parameter to increase the deep beam shear capacity; the depth size effect of the beam has to be considered in the design.

Depth size effect of deep beam is the focus of this study. In this Chapter 2, the parameters which can be used to improve the shear capacity of deep beam were briefly reviewed. Next, followed with theory explanations on the size effect in deep beam by different researchers. After that, several journal studies regarding the depth size effect were discussed. Followed with the comparison of depth size effect and bearing plate size effect aided with Finite Element Modelling (FEM) and Cracking Strut-and-Tie Model (CSTM).

2.2   Improvement on Deep Beam Load Carrying Capacity

A higher load carrying capacity is often needed by the deep beam in order to withstand huge load over the span length. The deep beam load carrying capacity is usually influence by the factor such as the shear span-to-effective depth ratio a/d, concrete's compressive strength, the reinforcement ratio and the cross-sectional area.

The shear capacity of a deep beam is largely influenced by its shear span-to-effective depth ratio a/d. Tan et al. (1995) found that the shear strength of deep beam concrete is higher when the a/d ratio is lower as shown in Figure 2.1. This is due to at lower a/d ratio, the mechanism called strut-and-tie action

taken place which enable the beam to transmit higher stresses in a way different from the conventional beam.

Shear strength vs. a/d ratio
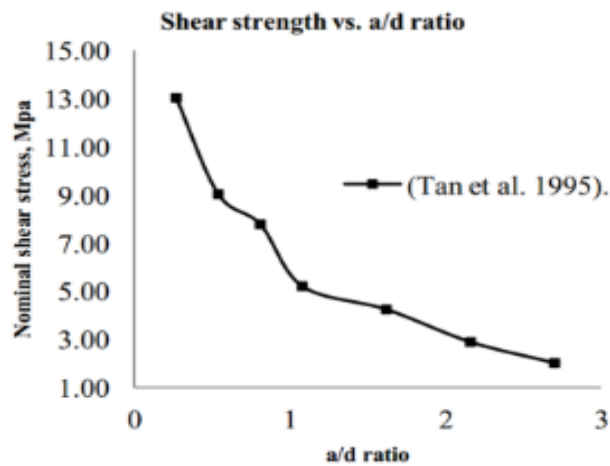
Figure 2.1: Shear Strength versus a/d Ratio (Tan et al. 1995).

Besides that, the shear strength of beam is a function of its concrete compressive strength. The shear strength of beam is higher when the concrete compressive strength is high as validated by the results done by Mphonde and Frantz (1984) up to a strength of 90MPa as shown in Figure 2.2.
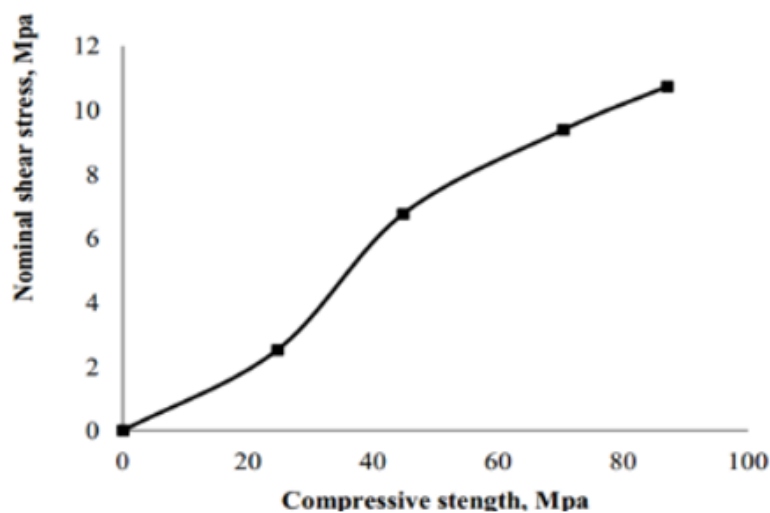
Figure 2.2: Shear Strength versus Compressive Strength (Mphonde and
Frantz, 1984).

Next, the other factor that contribute to the beam shear strength is the reinforcements provision. There are two types of common reinforcement used

in beam design which are the tension reinforcement and the shear reinforcement. Study shows that the uses of those reinforcement able to increase the shear strength of beams. However, the reinforcement can only be provided up to a certain limit as too much reinforcements would lead to reinforcement congestions. Therefore, optimum reinforcement is often needed to attain maximum beam capacity.

The next way to improve the beam capacity is by increasing the beam cross-sectional area. The increase in deep beam cross-sectional area able to increase the shear capacity of the beam. However, the normalised shear strength of the beam will decrease as has been examined by Birrcher et al. (2009). This phenomenon is due to the presence of depth size effect which will be the focus of this study.

2.3   Theory Explanations on Deep Beam Size Effect

The beam depth size effect is known to be the reduction of beam's ultimate shear strength when the cross-sectional depth of the beam increases. The shear strength is usually referred to normalised shear strength for which can be calculated using the formula as shown in Equation 2.1 (Hussein et al., 2018). As could be noted from the equation, an additional parameter of f_c' is introduced in the calculation of normalised shear strength as differs from the conventional formula in calculation of ultimate shear strength. The normalised shear strength is widely used by researchers to compare the depth size effect of specimens.

$$\text{Normalised Shear Strength} = \frac{V}{f_c' b_w d} \qquad (2.1)$$

where

V = vertical loading applied, kN

f_c' = concrete compressive cylinder strength, kPa

b_w = specimen width, m

d = specimen effective depth, m

There are quite a number of theories proposed by researchers to explain the depth size effect in deep beam, but there is not much consensus

among them. Out of the numerous theories, the three of the popular depth size effect hypotheses are based upon the material strength variation, interface shear transfer mechanism and the fracture mechanics.

One of the oldest depth size effect theories is based upon the work of Weibull (1939) that about the statistical strength variations. When the theory applied to reinforced beam, the theory suggests that the decrement of normalised shear strength in beams when the member size increase is due to the variability of material strength. This can be explained by comparing a reinforced concrete structure to a series of connection links where if any of the link break or fail, it would cause the entire chain to collapse. As the beam height increases, the number of links would also increase, when there is more links, the probability of link with lower strength will increase due to the randomness of material strength in concrete. Hence, the normalised shear strength reduces as beam height increases. However, the randomness of material strength is found to be insignificant in most beams as stated in the journal paper by Bazant and Xiang (1997).

Next, Taylor (1972) explains the depth size effect theory by interface shear transfer. When the aggregate size used for the specimen is kept constant while the size of the specimen is increased, it would cause the reduction of interface shear transfer action. Therefore, resulted lower nominal shear strength for higher beam. Besides that, as the specimens size becomes larger, the width of the diagonal cracks would also become wider. The increases of crack width would result in the reductions of concrete ability to transmit the shear by aggregate interlock across the diagonal crack. Hence, the efficiency of the interface shear transfer action is affected. This theory is accepted by Tan and Cheng (2006), where the authors uses this theory to incorporated with numerical analysis to explain depth size effect in deep beam.

Another theory explains the beam depth size effect is by fracture mechanics, proposed by Reinhardt (1981). Fracture mechanics concerned on the study of cracks propagation in materials. The author theorized that the rate of the stored energy in the beam is released during the period of crack propagation are different for each beam of different sizes. It is found that the beam with larger size will experience crack propagation faster than the beam

with smaller size. Tan and Lu (1999) found out that the larger beam cracks more extensively as compared to smaller beam at similar shear stress.

As mentioned at the beginning, those theories do not truly reach an accepted consensus agreement by all researchers. Therefore, another approach may be more proper to be used to study beam depth size effect. Strut-and-tie model analysis is suggested to be a better way to analyse and predict the deep beam depth size effect (Birrcher et al., 2014).

2.3.1 Strut-and-Tie Model

Load transmitted in deep beam is differ from slender beam as it is capable of transmitting additional loads after it crack diagonally due to the characteristic of tie arch mechanism. Besides that, the strain distribution in deep beam is nonlinear at the disturbed regions (Shah, Haq and Khan, 2011). Therefore, the conventional sectional analysis of slender beam could not be applied on deep beam. The Strut-and-Tie model (STM) which is an equilibrium model that based on the plasticity solution theory is introduced to be used to determine the capacity of a complicated disturbed regions in deep beam (Ismail, Guadagnini and Pilakoutas, 2017). The design of deep beam based on STM is allowed in many codes of design which included Eurocode 2 and ACI 318-14.

The typical STM composed of two components which are the concrete struts acting in compression and longitudinal reinforcement acting in tension. The struts form diagonally along the line linking the bearing point to the supports while the tie form along the tension reinforcement. Figure 2.3 illustrates the geometry of the STM. The STM only provide an approximation and simplified mechanism when compared to the actual mechanism that is in the deep beam. Birrcher et al. (2014) found out that the simplified coefficient of the strut efficiency that usually used in the codes result in high scatter between the comparison of predicted value by the STM and the actual test result observed by the authors. Besides that, Chen, Yi and Ma (2019) stated that the current code only calibrated by the experimental result of beam with height of less than 2m and it did not account for the effect of diagonal crack on the strut. Therefore, researchers are always trying to propose different type of modified STM to improve the estimating accuracy.
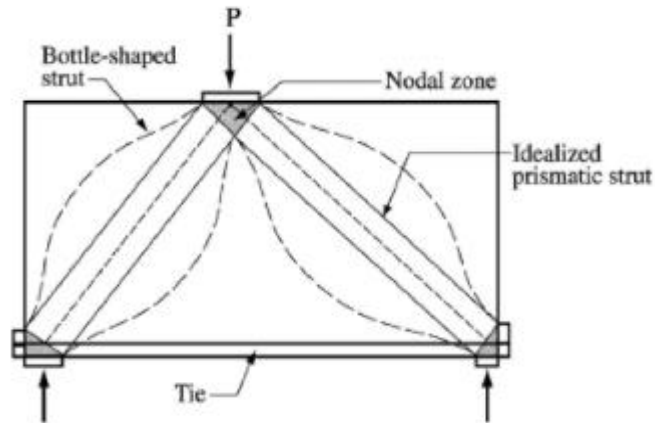
Figure 2.3: Geometry of STM (ACI 318-05).

Chen, Yi and Hwang (2018) proposed a modified STM known as Cracking Strut-and-Tie Model (CSTM). This model is designed to improve the shear strength estimation for RC deep beam by taking consideration of the diagonal shear crack and the strut efficiency. The configuration of cracks and strut of deep beams by CSTM are as shown in Figure 2.4. As illustrated, the critical shear crack (CSC) which is known as the diagonal crack located nearest to the support plate; is dividing the diagonal strut into two portions. The portion above the critical shear crack is considered to be unaffected by diagonal cracks but the portion below critical shear crack does crack diagonally.
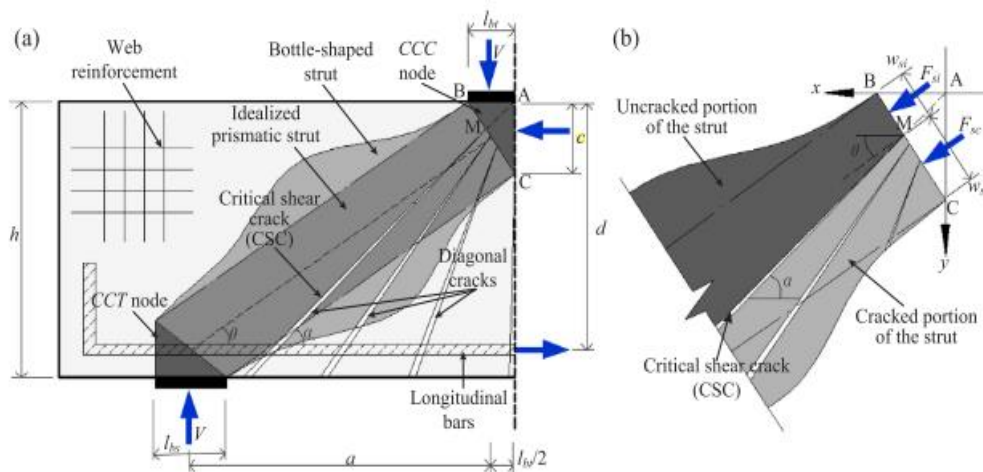
Figure 2.4: Configuration of Cracks and Strut in CSTM (Chen, Yi and Hwang, 2018).

The shear strength of the model is mainly depending on the compression failure of diagonal strut at interface BC which is the overall width of the strut. Therefore, the width of the strut is directly influencing the strength of the beam. The width of the strut can be split into two part which are the upper part (BM) and the lower part (MC) divided by the critical shear crack. The portion MC which is the cracked part will experience a resultant force F_{sc} where the stress is transfer through the cracked part region which results the degradation of compressive stress capacity. On the other hand, the portion BM which is the uncracked part will experience a resultant force F_{si} where the stress transmits through the uncracked portion which is theoretically having higher compressive stress capacity. Therefore, different value of strut efficiency is applied at the interfaces MC and BM to calibrate the strengths of both portions. The strut efficiency coefficient at interface MC is depends on the strength contributed by aggregate interlock, longitudinal reinforcement and web reinforcement. While, the strut efficiency at interface BM is based on the compression test and is assume to be 0.85 as suggested by the test results done by Laughery and Pujol (2015).

Chen, Yi and Hwang (2018) had provided a series of formula to predict the shear strength of deep beam. The deep beam shear strength predictions done by using CSTM has a good agreement with the experimental findings which had been compared by Chen, Yi and Ma (2019). The authors strongly recommended the CSTM to be use in the analysis for deep beam with depth larger than 2m.

2.4   Review on Past Experiment Investigations

The characteristic of deep beam with high load carrying capacity by forming an internal arch action mechanism for load transferring had attracted interest of researchers to carry out study on this subject. A number of experimental studies have been conducted in the past to study the reason behind the reduction of normalised shear strength of deep beams when the beam sizes increased, known as "size effect". Throughout this sub-topic, some of the published journals regarding deep beam size effect are reviewed. The discussion mainly focuses on the depth size effect in RC deep beam while bearing plate size effect in RC deep beam is also reviewed. The size effects

phenomenon supported by using STM and numerical model are presented in the following section.

2.4.1   Past Experimental Results on Depth Size Effect in Deep Beam

From the past two decades, Matsuo et al. (2001) had conducted an experiment with 9 specimens of reinforced concrete deep beams. All the test specimens were fixed at the (a/d) ratio of 1.0 and the width were made constant at 150 mm. The effective depth of the specimens ranged from 200mm to 600mm. In order to examine the effect of depth on deep beams, the bearing plates and support plates size for all of the specimens were increased proportionally to the respective height of beam at the ratio of 0.25. A total of 9 specimens were classified into 3 groups in the studied. The first group did not provide with any vertical reinforcement, the second group had 0.42% of vertical reinforcement and the third group had 0.84% of vertical reinforcement. Those specimens were loaded with single concentrated load at mid span.

The results from the study were shown in Figure 2.5. For the beams without vertical reinforcement, the normalised shear strength of the group shows a decreasing trend when the depth of the beam increases. Therefore, this phenomenon signifying the presence of depth size effect in deep beam. Moreover, the shear stress at failure for specimens with reinforcement did not show consistent decreasing trend. This finding inferred that the presence of vertical reinforcement in deep beams alleviate size effect to some degree. Matsuo et al. (2001) suggested that the size effect was due to the reduction on ratio of compression failure area to the total specimen region.
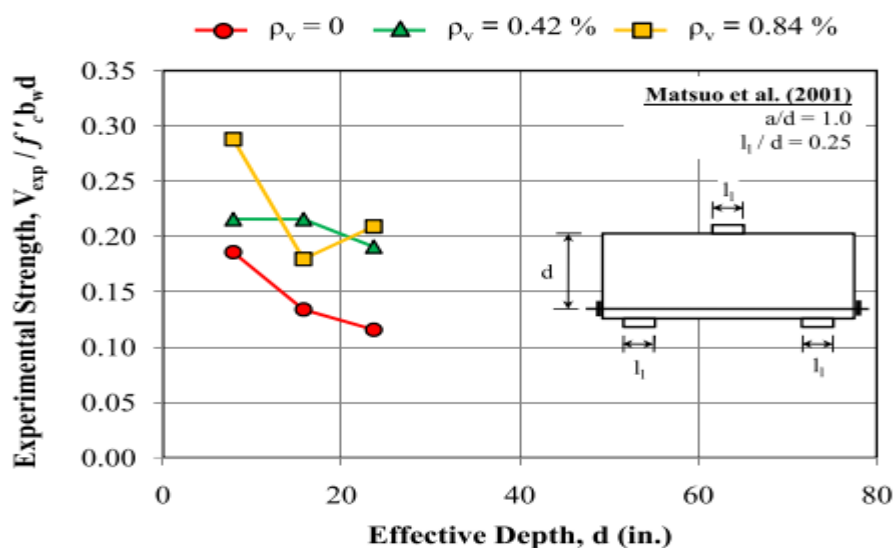
Figure 2.5: Size Effect Results by Matsuo et al. (2001).

The next findings were conducted by Zhang and Tan (2007). The authors had tested 12 reinforced concrete deep beams specimens with constant shear span-to-depth ratio (*a/d*) of 1.1. The concrete deep beams were separated into 3 groups of 4 and within each of the group, the specimens' effective depth varied from 313mm to 926mm. The first group beams were designed to have different width length which the width increased proportionally from 80mm to 230mm while keeping the height-to-width ratio (h/b) at 4.4. Besides that, web reinforcement was provided for Group 1 specimens with span to web steel ratio maintained around 0.4%. For the second group, the width of the beams was made constant at 80mm and there was no vertical reinforcement provided. While for the third group, the width of the beam was designed to varied in the same way as Group 1 but no vertical reinforcement was provided for the group of beams. Similar to the study done by Matsuo et al (2001), the width of the bearing plates and support plates were varied proportionally with the plate width-to-depth ratio kept at 0.15. The specimens in the study were loaded with two-point loads separated evenly from supports.

Based on the grouping characteristic, Group 3 specimens were designed to act as a control beam. By comparing Group 1 and Group 3 specimens, the beams size effect and the effect due to vertical reinforcement can be studied. While by comparing Group 2 and Group 3 beams, the beam width and depth effect can be analysed. The findings of the test are shown in

Figure 2.6. Based on the result, the line graph indicating normalised shear strength shows that Group 2 and Group 3 located at almost similar level which means that the width of deep beam do not result in size effect. Therefore, width size effect of deep beam is said to be negligible. Next, as could be observed; the Group 1 specimens achieved higher normalised shear strength as compared to both other groups of specimens. This denotes that the additional of 0.4% of web reinforcement does improve the beam's ultimate shear strength as the increment of reinforcement could contributes higher shear strength as been mentioned in sub-chapter 2.2.
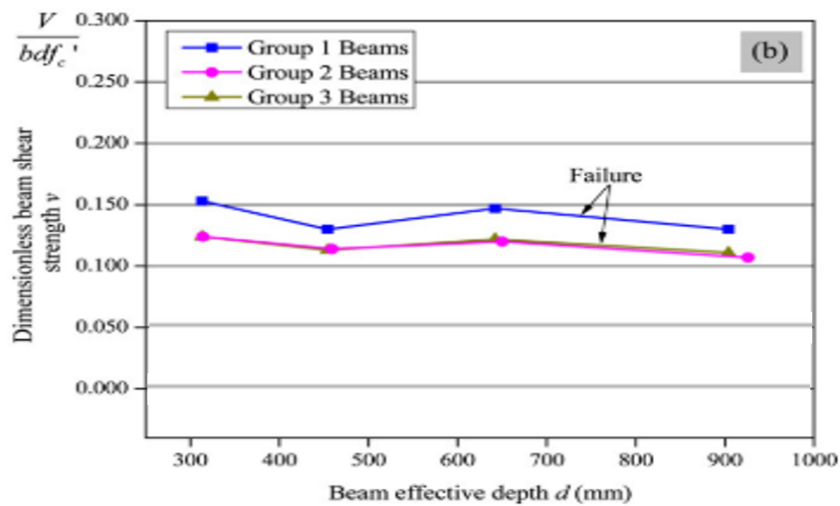
Figure 2.6: Size Effect Results by Zhang and Tan (2007).

Besides that, the results show all three groups of specimens exhibit a nearly flat trend line which infers that there was lack of size effect present in the study by Zhang and Tan (2007) as there were limited deduction in normalised shear strength when the depth of the specimens were increased. The authors stated that the size effect was mitigated by properly configured the support and bearing plate size proportionally to the height of the beam. This phenomenon can be explained from the strut-and-tie model perspective as the deep beam's strength is controlled by the nodes and strut width which could be affected by the support and bearing plate sizes. Therefore, when the support and bearing plate size is proportioned to the specimen's height, the size effect due to the steel bearing plates could be discounted. Hence, the change in normalised shear strength of specimens in each of the groups carried out by

Zhang and Tan (2007) was mainly due to the depth size effect without the interference of bearing plate size effect.

However, the findings from Zhang and Tan (2007) are contradicting to the test results by Matsuo et al. (2001). Zhang and Tan (2007) explained the size effect of deep beams was mitigated very obviously by increase proportionally the size of the support and bearing plates as proven by the result. But Matsuo et al. (2001) did also proportion their support and bearing plates in the same way, yet the size effect was not mitigated as obvious as presented by Zhang and Tan (2007). Therefore, there may be other factor that influence the contradictorily of both the results. The testing methods may be the reason behind the disagreement of the results. As could be noted, Matsuo et al. (2001) loaded the beams with a one-point load at middle of the span while Zhang and Tan (2007) loaded their beams with two-point loads separated evenly from supports. For the case of single point load, the load bearing stress are double as high as those on its support while for the case of double point load; the bearing stresses were equivalent to its support load. It could be noted that the height of specimens tested by both the researchers are relatively low which were less than 1m. This limitation may be due to some difficulties in casting larger specimens which required different set of skills and casting equipment. Although there is limitation on the experimental beam's height, this problem does not stop researchers from analysing depth size effect in deep beam with larger dimensions. Methods such as finite element model and strut and tie method had been introduced to numerically and mathematically predict size effect on larger beams.

2.4.2 Explanations on Depth Size Effect by Numerical and Mechanical Model

Chen et al. (2019) had done research on predicting the size effect on larger beams. They collected results from other researchers and used those results to serve as reference data and model higher beams size. The authors extrapolated the beam height to 4m using ATENA finite element model (FEM) and cracking strut-and-tie model (CSTM) to predict the size effect of deeper beam. The author used results obtained from Walraven and Lehwalter (1994) and Zhang and Tan (2007) to assess the depth beam effect as both of the authors tested

deep beams by increasing bearing and support plates proportionally to increasing depth.

The results from Walraven and Lehwalter (1994) were classified as Group 2-1 to Group 2-3 by Chen et al. (2019). Walraven and Lehwalter (1994) had tested 10 deep beams at constant a/d ratio of 0.93. Group 2-1 covered the specimens without vertical reinforcement, Group 2-2 covered specimens with about 0.15% of vertical reinforcement and Group 2-3 covered specimens with about 0.33% of vertical reinforcement. While for the specimen from Zhang and Tan (2007) as presented earlier were classified from Group 2-4 to Group 2-6 by Chen et al. (2019). Group 2-4 covered specimens with vertical reinforcement and increasing width proportional to effective depth, Group 2-5 covered specimens without vertical reinforcement and had constant beam width, and Group 2-6 covered specimens without vertical reinforcement and increasing width proportional to beam depth.

The result of increasing beam depth corresponding to normalised shear strength are shown in Figure 2.7. Chen et al. (2019) had predicted and extrapolated the result in Group 2 up to 4m by using FEM and CSTM. The extrapolated results are as shown in Figure 2.8. It can be observed that the predictions done using FEM and CSTM is well reflecting the decreasing trend of normalised shear strength as the beam height increases. This finding inferred that it is possible to explain the depth size effect of beam by analysing the mechanisms which cause the predicted normalised shear strength by FEM and CSTM to reduce when the beam height increases (Chen, Yi and Ma, 2019).
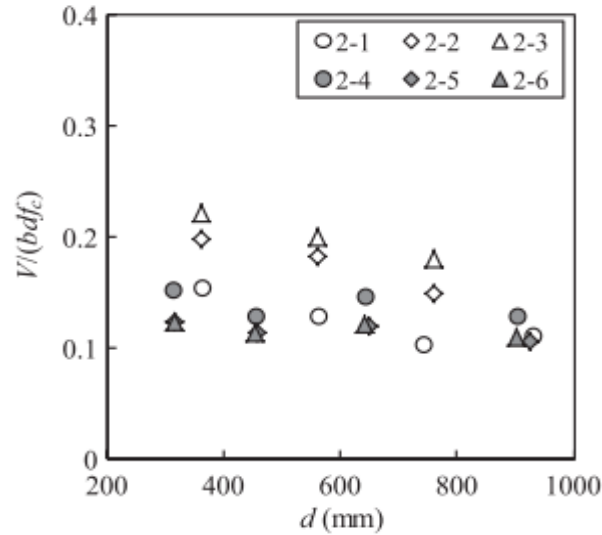
Figure 2.7: Normalised Shear Strength versus Effective Depth Results for
Group 2 (Chen, Yi and Ma, 2019).
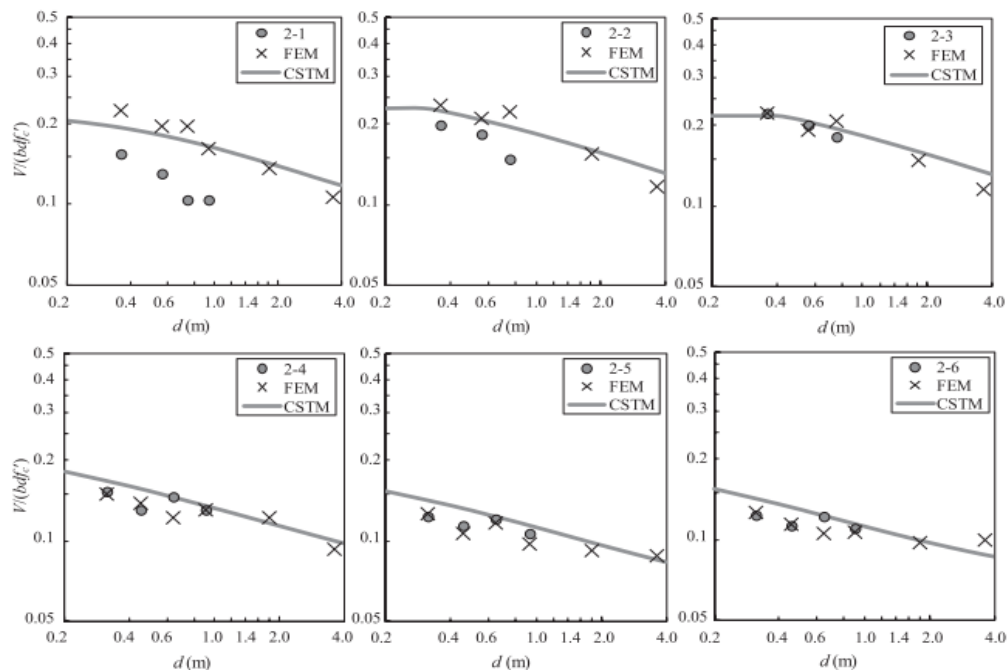
Figure 2.8: Extrapolated Shear Size Effect of Group 2 Specimens (Chen, Yi
and Ma, 2019).

The comprehensive FEM results beams with height of 0.35 m, 1.0 m, and 4.0 m as predicted based on Zhang and Tan (2007) specimens are shown in Figure 2.9. Those specimens are plotted equally in size to ease in direct comparison. As shown in the figure, the relative strut width $\frac{w_s}{d}$ of the models shown a decreasing trend from 0.40 to 0.36 and then 0.32 as the beam height

increases. The 1.0m and 4.0m height beams has smaller relative strut width by 10% and 20% respectively as compared to the 0.35m beam and the normalised shear strength of the 1.0m and 4.0m height beams are lesser than the 0.35m height beam with factor of 0.87 and 0.62 respectively. Therefore, the authors suggest that the decrement of relative strut width is the main factor that contribute to beam depth size effect.
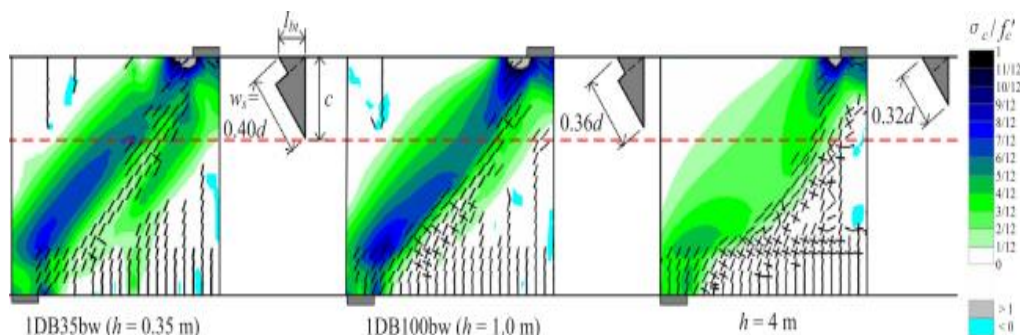
Figure 2.9: Numerical Results by FEM on Beam in Group 2-4 (Chen, Yi and Ma, 2019).

The relatives strut width is affected by the size of bearing plate and the height of compression zone denoted by 'c' as illustrated in Figure 2.9. Since the bearing plate on Group 2-4 specimens are modelled to increase proportionally to beam height, therefore; the relative bearing plate size remains constant for all three specimens. Hence, the decreasing in relative compression zone height c/h is the key factor that causes the reduction of beam's relatives strut width.

Besides that, the author found that the there was considerable portion of principle compressive stress beneath the critical shear crack (CSC) band was transmitted to the support by aggregate interlock through the CSC band. However, the principle compressive stress beneath the CSC band decreased as the beam height increases. This phenomenon is due to when the beam height increases, the CSC width also increases, hence it affect the stiffness and shear transfer strength on the crack face. (Chen, Yi and Ma, 2019). The weaken of shear transfer strength may deteriorate the effective path of principle compressive strength and be the cause of decrement on beam compressive depth. Additionally, Chen, Yi and Ma (2019) also explained the depth size effect by analysing CSTM formula. Based on CSTM, beam shear strength

depends on the strut width and strut efficiency. It is found that the strength carried by the aggregate interlock is the main reason of the depth size effect. Both of the explanations by CSTM and FEM are consistent which is when the cross-sectional depth of beam increases, the width of the diagonal crack will tend to increase which deteriorate aggregate interlock mechanism and finally reduce the shear strength of the beam (Chen, Yi and Ma, 2019).

2.4.3 Explanations on Bearing Plate Size Effect by Numerical and Analytical Model

Bearing plate size effect is different from those beam depth size effect as reviewed on the sections above. The bearing plate size effect is known to be the deterioration on beam shear strength due to the bearing plate sizes. To analyse the bearing plate size effect, the bearing plates on the specimens are no longer varies proportionally to the beam height as done on depth size effect. The bearing plates are often made constant, and the height of the beam is increasing to examine the bearing plate size effect. However, increasing in beam size also induce depth size effect. Therefore, the shear deterioration is often caused by both depth size effect and bearing plate size effect.

Chen et al. (2019) had taken experimental results from other researchers and used those results to serve as reference data and model higher beams size. The authors extrapolated the beam height to 4m using ATENA FEM and CSTM to predict the size effect of deeper beam. The author used results obtained from Tan and Lu (1999) and Birrcher et al. (2014) to assess the effect of deep beams tested by making the bearing plate size and a/d ratio constant while increasing the depth of specimens. The result from Group 1-1 to Group1-3 are contributed by Tan and Lu (1999), while Group 1-4 to Group 1-6 are contributed by Birrcher et al. (2014).

The result of increasing beam depth corresponding to normalised shear strength are shown in Figure 2.10. As could be observed from Figure 2.10, Chen et al. (2019) had predicted and extrapolated the specimens up to 4m by using FEM and CSTM. It can be observed that all the graphs show decreasing trend of normalised shear strength as the beam height increases. However, those graphs from Figure 2.10 show steeper decreasing trend as compared to graphs in Figure 2.8 which are plotted to evaluate for depth size

effect. The steeper line graph implied that larger shear size effect presents in the specimens with constant bearing plate size as compared to proportioned plate size. Therefore, these findings inferred that the bearing plate size on deep beam is more critical than the depth of the beam as the decreasing of normalised shear strength is more dependent on the bearing plate size as compared to the depth of the beam itself. Although the bearing plate size effect is less apparent as compared to the beam depth size effect. However, the beam depth size effect can still result in some degree of deterioration in deep beam shear strength as shown in Figure 2.8. Moreover, the contradicts in findings made by different authors on their experimental depth size effect data as presented in sub-chapter 2.4 further support the needs to reinvestigate the depth size effect in deep beam.
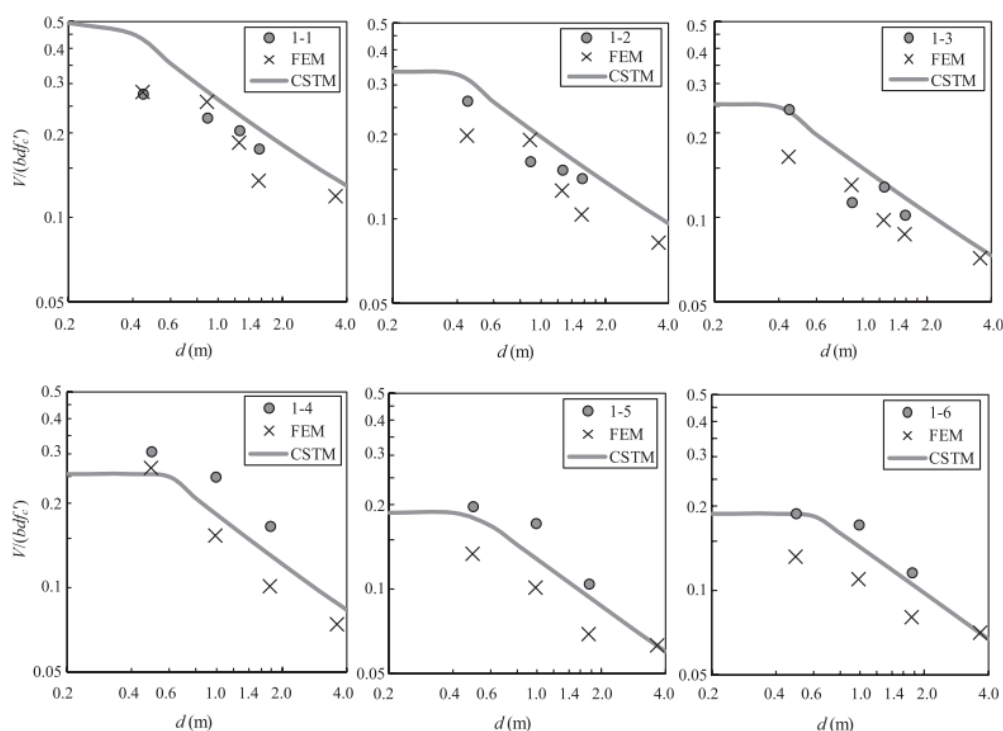
Figure 2.10: Extrapolated shear size effect of Group 2 specimens (Chen, Yi and Ma, 2019).

The bearing plate size effect was study by Tan and Lu (1999) with beam height of 0.5 m, 1.4 m and 4.0 m through FEM approach as shown in Figure 2.11. Those beams are plotted equally in size to ease comparison. As shown in the figure, the relative strut width $\frac{w_s}{d}$ of the models shown a decreasing trend from 0.70 to 0.42 and then 0.32 as the size of the beam

increases. The decreasing width of strut is mainly due to the decrease in relative plate size ℓ_{bt} instead of the relative compression depth c. By comparing among the Figure 2.11 to Figure 2.9, it is noticed that the strut width decrement is larger when size of the bearing plate is made constant as compared to proportioned varied bearing plate size. Zhang and Tan (2007) stated that the depth size effect can be significantly mitigated if the dimension of the bearing and support plates is properly configured. Therefore, Chen et al. (2019) conclude that the bearing size effect is more critical than beam depth size effect.
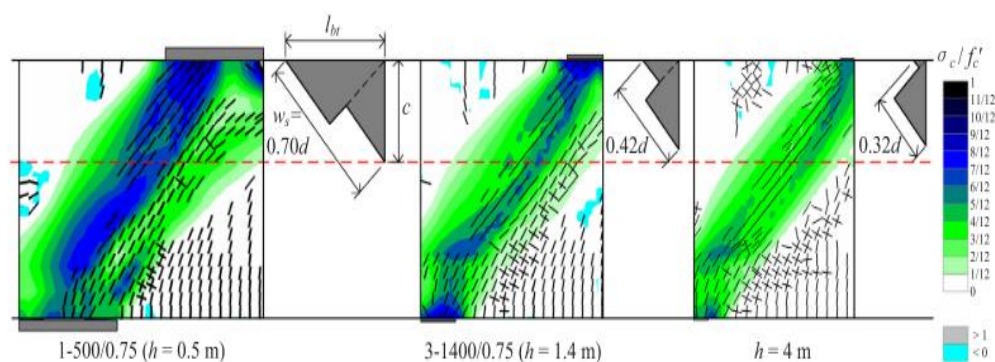
Figure 2.11: Numerical Results by FEM on Beam in Group 1-2 (Chen, Yi and Ma, 2019).

2.5   Summary

In a nutshell, there are several parameters such as the a/d ratio, concrete strength, reinforcement and cross-sectional area that can be controlled to improve the shear capacity of deep beam. However, if the shear capacity is improved by increasing the cross-sectional height of beam; the depth size effect in deep beam can be observed. There are numerous theories proposed by researchers to explain depth size effect. Three of the most popular theories are based upon variation of material strength, interface shear transfer mechanism and the fracture mechanics. However, none of the theories reach consensus agreement among the researchers. STM is introduced to analyse and predict the deep beam depth size effect. However, there are some limitations in the current STM in design codes. Therefore, Chen et al. (2018) proposed a modified STM known as Cracking Strut-and-Tie Model (CSTM) to improve the estimation of shear strength by taking consideration of the diagonal shear crack on the strut efficiency.

Matsuo et al. (2001) and Zhang and Tan (2007) had conducted experiment regarding deep beam depth size effect. The result from Matsuo et al. (2001) shows a relatively huge depth size effect while the result from Zhang and Tan (2007) shows little depth size effect on deep beam. The contradiction of the results might be due to the difference of loading conditions (single point and double point). However, there is limited experimental data available done to study depth size effect and to what extend the depth size effect will deteriorate the deep beam. Besides, Chen et al. (2019) adopts numerical model and experimental model to evaluate size effect in deep beam which had proved that numerical model able to simulate actual beam shear strength accurately. From the findings, the authors conclude that the depth size effect is observed, however it is less critical as compared to bearing size effect. In order to study depth size effect, the steel bearing plates of the specimen in the study should be carefully proportioned to its own overall height to avoid the bearing plate size effect which can affect the contribution of depth size effect. Moreover, to the author knowledge, there is no research paper available to study the motion of stress distribution and crack propagation in various loading stages for different beam heights.

CHAPTER 3

METHODOLOGY AND WORK PLAN

3.1   Introduction

Finite element analysis software ABAQUS was adopted in this project to create the numerical models of deep beam with different cross-sectional height to assess the depth size effect of RC deep beams. This Chapter 3 describes the methodology workflow of the modelling process. The methodology workflow can be divided into three major process which include the numerical modelling, numerical analysis and modelling verification. Before modelling work begins, pre-processing works were carried out to determine the required number of specimens, its geometry and the embedded detailing. The specifications of reference beam were selected based on past experimental work published by researcher. The purpose of modelling a reference beam is to validate the reliability and accuracy of the model.

The first step of the numerically modelling can be further divided into four sub-divisions which includes the modelling of material properties, modelling of interfacial behaviour, boundary condition and loading determination and lastly mesh size definition. After beam modelling is done, numerical analysis was carried out to generate results such as load-deflection curve and concrete tension damage contour. Next, the numerical reference beam results were compared with the experiment result to verify the accuracy and reliability of the modelling technique. Recalibration work was performed when the numerical result and experiment result do not correlate well with each other.

The numerical modelling and numerical analysis were performed again on the proposed control beam and test specimens. Cracking Strut and Tie Model (CSTM) was used to further validate the numerical model. The numerical results such as the load-deflection curve, normalised shear strength versus effective depth, von mises stress contour, tension damage magnitude contour and PEMAG strain distribution were generated from the analysis. The results were discussed in Chapter 4 to assess the depth size effect of RC deep beam. Figure 3.1 presents the summarised version of methodology workflow in a flowchart.
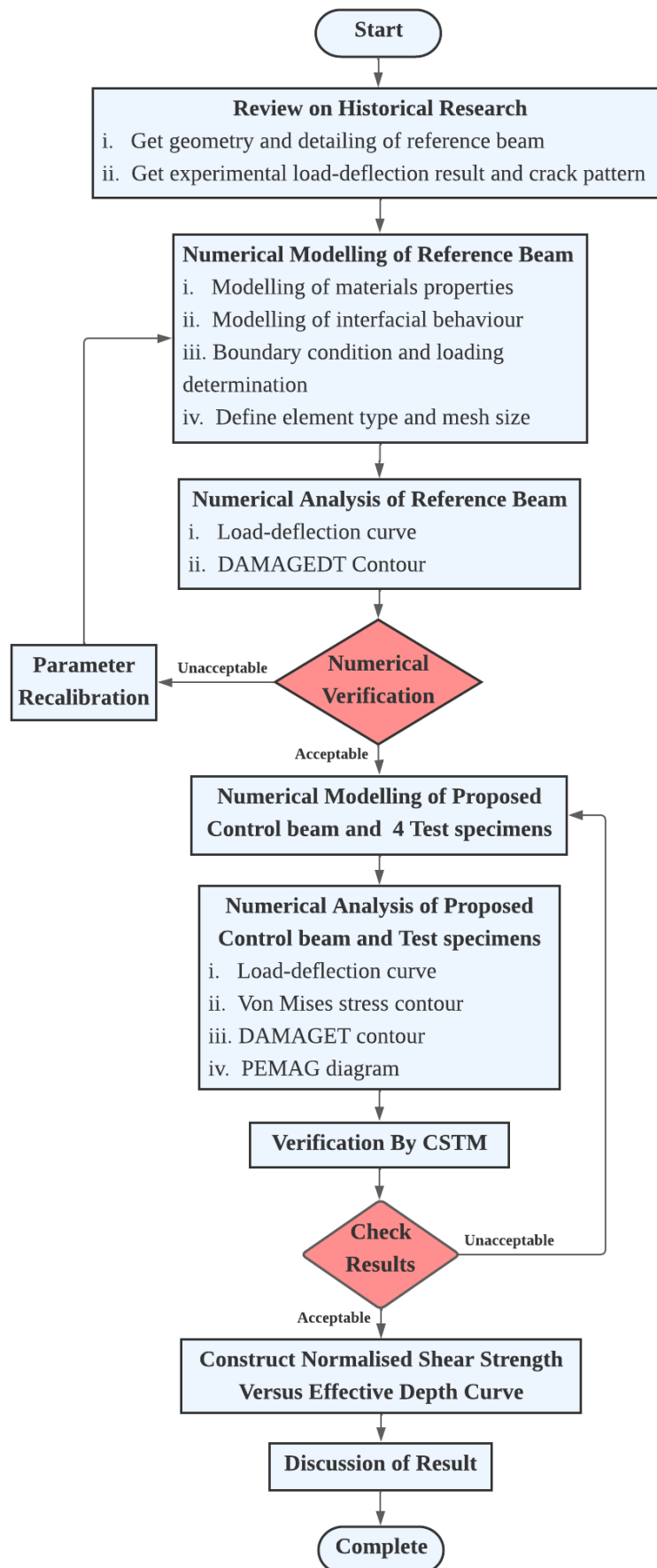
Figure 3.1: Methodology Flowchart.

3.2 Review on Historical Output

The beam specimen and its experimental result conducted by Zhang and Tan (2007) was used in this study to serve as reference for model verification purpose. Numerical analysis was performed by numerically model a reference beam based on the specifications by experimental beam data and the load-deflection curve was constructed from numerical analysis. Comparison between load-deflection curve of beam from experiment done by Zhang and Tan (2007) and load-deflection curve from the numerical model was perform to validate the modelling accuracy and its reliability. When the result showed significant inconsistency, model recalibration on material properties or improvement in technique on modelling were revised to further improve the model reliability and accuracy.

3.3 Specimen Specification

It is necessary to determine the specimen geometry, reinforcement detailing, loading condition and the number of specimens before numerical modelling begins. In this study, a total of 6 specimens were modelled and they consist of 1 reference beam, 1 control beam and 4 test specimens. Modelling was done using ABAQUS finite element software in this study.

3.3.1 Reference Specimen

A reference beam is important in this study where its purpose is to validate the reliability of the numerical analysis approach as well as to define the material properties to be used by the testing specimens. The reference specimen was selected from the experimental study carried out by Zhang and Tan (2007). The dimension of the reference beam selected was 350 mm in height, 80 mm in width and 1330 mm in length, The shear span-to-depth ratio (a/d) is 1.1 for this specimen and it is considered as deep beam as refers on ACI-ASCE Committee 426 where beam which lesser than 2.5 shear span-to-depth ratio can be considered as deep beam. The concrete cylinder compressive strength for the specimen was tested to be 25.9 MPa. Besides that, it is important to note that the experiment was designed using two-point loading. The dimension of the loading and support plates provided were identical which is 52.5 mm in width.

Two R6 of plain round mild bars were provided as top longitudinal reinforcement while four T10 high tensile steel bars are provided as bottom longitudinal reinforcement. Besides that, R6 plain round mild bars with 150 mm spacing were provided as vertical reinforcement. The reference beam's geometry and its material mechanical properties are tabulated in Table 3.1. Figure 3.2 illustrates the detailing of the reference beam.

Table 3.1: Geometry and Material Properties of Reference Beam.

Parameter	Descriptions
Annotation	R01
Dimension	350 mm (height) x 80 mm (width) x 1330 mm (length)
Concrete strength	25.9 MPa
Loading and support plates	52.5 mm width (full length)
Longitudinal reinforcement	2R6 (top), 4T10 (bot)
Vertical reinforcement	4R6@150
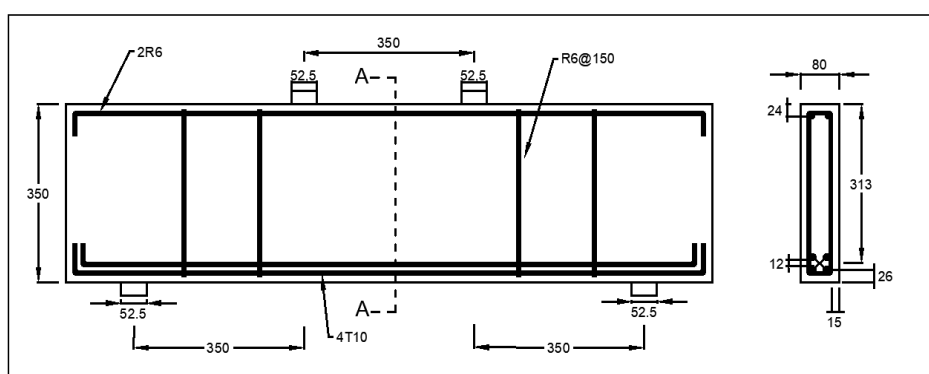
Figure 3.2: Detailing of Reference Beam, R-01 (Zhang and Tan, 2007).

The testing setup by Zhang and Tan (2007) is shown in Figure 3.3. The experimental beam was simply supported by pin and roller support. A swivel head was placed on top of the bearing plate to serve as spreader beam. The loading from the actuator was designed to spread evenly on two bearing plates. The beam was loaded until it fails. The authors had recorded the load-displacement curve as well as the cracking pattern of the reference beam. The load- displacement curve shown in Figure 3.4 was used for model verification

while the cracking pattern showed in Figure 3.5 was used to compared with the numerically predicted crack pattern.

Figure 3.3: Testing Setup (Zhang and Tan, 2007).

Figure 3.4: Load- Deflection Curve of Reference Beam (Zhang and Tan, 2007).

Figure 3.5: Crack Pattern of Reference Beam (Zhang and Tan, 2007).
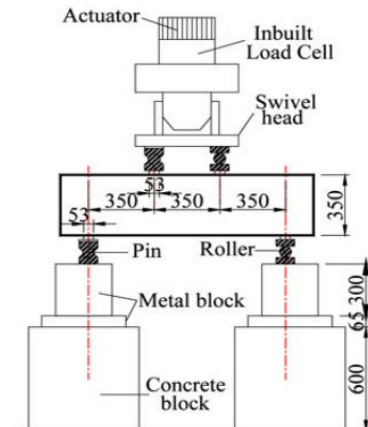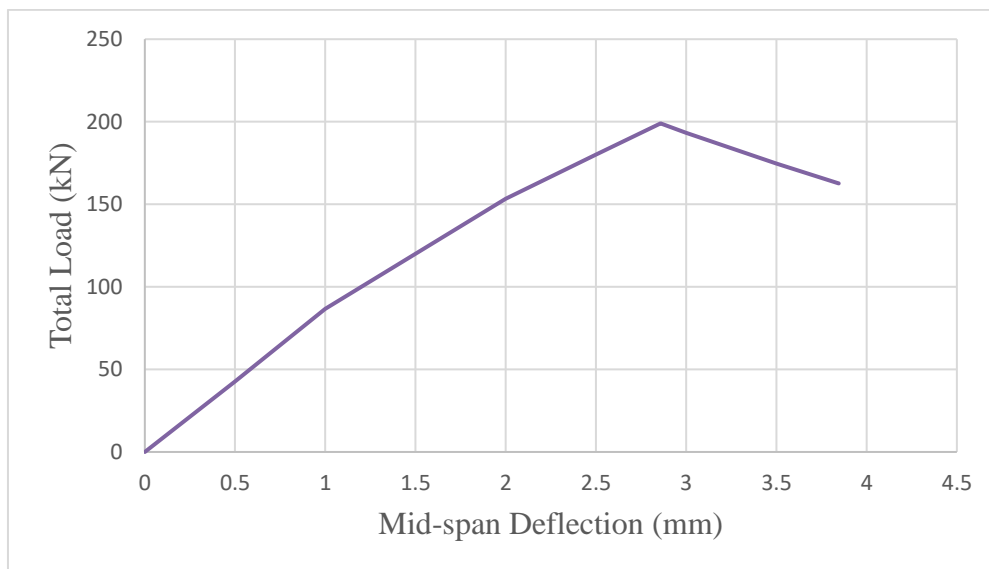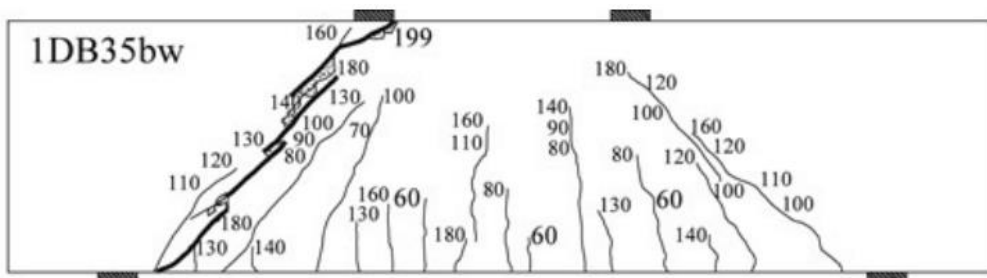
3.3.2 Control Specimen

The numerical control beam is a modelling beam to serve as a reference to compare with other numerical test specimens of different cross-sectional height in order to evaluate the change in percentage of normalised shear strength of deep beam with increasing cross-sectional height of deep beam.

The numerical control beam was designed to be as similar as the numerical reference beam. Since bigger cross-section width was needed for test specimens to allow spaces for its bigger steel reinforcement area, the width of the control beam will be differed with numerical reference beam. To analyse the depth size effect, the numerical control beam width must be the same as the test specimens to exclude the possible influence of width size effect. Besides that, the shear reinforcement area needed to be increase when the beam cross-sectional area increases in order to ensure that the depth size effect is not influence by the lesser percentage of reinforcement provided. Zhang and Tan (2007) suggest that using 1.2% of longitudinal reinforcement and 0.4% of vertical reinforcement to ensure that the specimens will fail by shear compression.

The numerical control beam was designed to have shear span to depth ratio of 1.2. The dimension of the control beam was 300 mm height, 160 mm width and 1140 mm in length. The dimension of the loading and support plates provided were 45 mm in width. Two R8 of steel reinforcement bars were provided as top longitudinal reinforcement while two T10 and two T16 steel reinforcement bars were provided as bottom longitudinal reinforcement. Besides that, R8 steel bars with 150 mm spacing were provided as vertical reinforcement. The concrete compressive strength is designed to be the same as reference beam which was 25.9 MPa. The control beam's geometry and its material properties are tabulated as in Table 3.2. The detailing and geometry of the control beam is illustrated in Figure 3.6.

Table 3.2: Geometry and Material Properties of Control Beam.

Parameter	Descriptions
Annotation	C-01
Dimension	300 mm (height) x 160 mm (width) x 1140 mm (length)
Concrete strength	25.9 MPa
Loading and support plates	45 mm width (full length)
Longitudinal reinforcement	2R8 (top), 2T10 + 2T16 (bot)
Vertical reinforcement	4R8@150
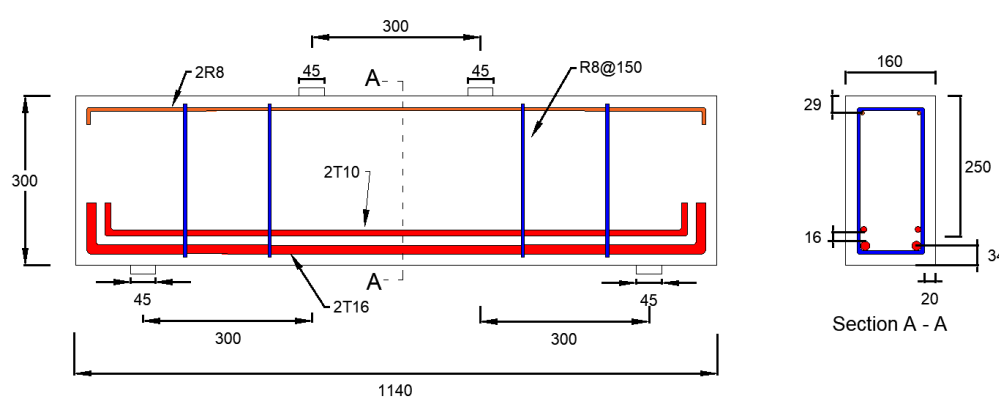
Figure 3.6: Detailing and Geometry of Control Beam, C-01.

3.3.3   Test Specimens

Four numerical test specimens were modelled and compared with control beam. All of the numerical test specimens were designed to have constant shear span to depth ratio of 1.2. The longitudinal reinforcement ratio of 1.20 % and vertical reinforcement ratio of 0.4 % will be provided as recommended by Zhang and Tan (2007). The concrete strength is 25.9 MPa, sectional width of 160 mm, and bearing and support plates proportioned with 0.15 of the overall height were designed consistence with the design of control beam. The only manipulating variable was the cross-sectional height of specimens. The numerical test specimens have different sectional height of 400mm, 500mm, 600mm and 700mm. All the numerical test specimens' geometry and their materials properties are tabulated in Table 3.3, Table 3.4, Table 3.5, and Table 3.6.

Besides, their detailing was illustrated in Figure 3.7, Figure 3.8, Figure 3.9, and Figure 3.10.

Table 3.3: Geometry and Material Properties of 400 mm Height Test Specimen.

| Parameter	Descriptions
Annotation	D-400
Dimension	400 mm (height) x 160 mm (width) x 1560 mm (length)
Concrete strength	25.9 MPa
Loading and support plates	60 mm width (full length)
Longitudinal reinforcement	2R8 (top), 2T10 + 2T20 (bot)
Vertical reinforcement	4R8@150

Figure 3.7: Detailing for Specimen D-400.

Table 3.4: Geometry and Material Properties of 500 mm Height Test Specimen.

Parameter	Descriptions
Annotation	D-500
Dimension	500 mm (height) x 160 mm (width) x 1980 mm (length)
Concrete strength	25.9 MPa
Loading and support plates	75 mm width (full length)
Longitudinal reinforcement	2R8 (top), 2T10 + 2T22 (bot)
Vertical reinforcement	6R8@150

Figure 3.8: Detailing for Specimen D-500.

Table 3.5: Geometry and Material Properties of 600 mm Height Test Specimen.

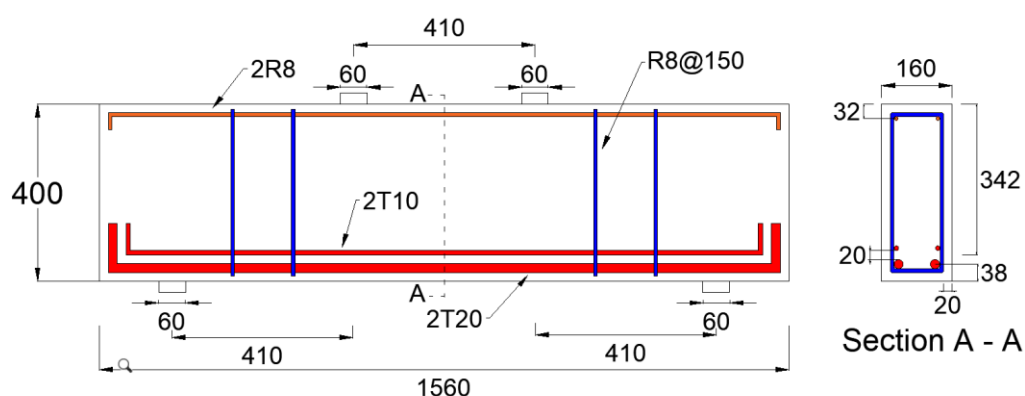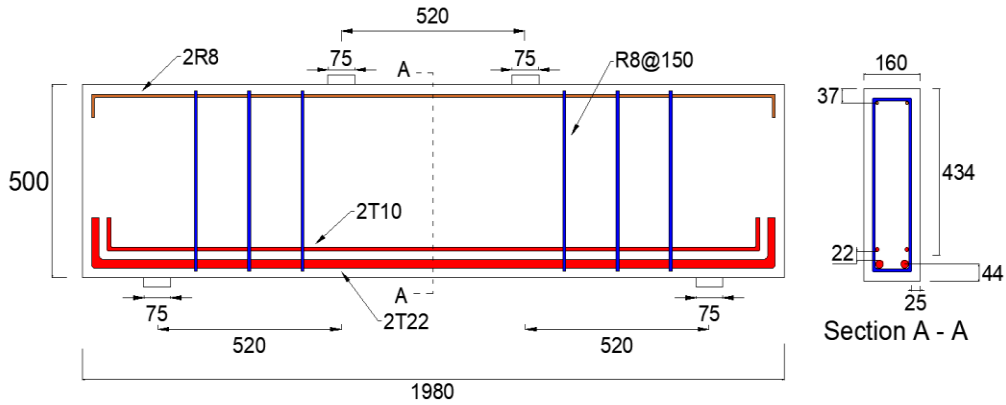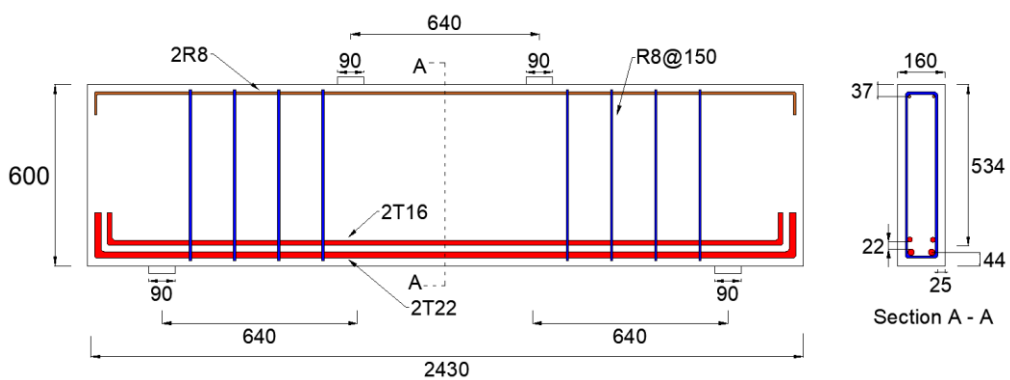| Parameter	Descriptions
Annotation	D-600
Dimension	600 mm (height) x 160 mm (width) x 2430 mm (length)
Concrete strength	25.9 MPa
Loading and support plates	90 mm width (full length)
Longitudinal reinforcement	2R8 (top), 2T16 + 2T22 (bot)
Vertical reinforcement	8R8@150

Figure 3.9: Detailing for Specimen D-600.

Table 3.6: Geometry and Material Properties of 700 mm Height Test Specimen.

Parameter	Descriptions
Annotation	D-700
Dimension	700 mm (height) x 160 mm (width) x 2890 mm (length)
Concrete strength	25.9 MPa
Loading and support plates	105 mm width (full length)
Longitudinal reinforcement	2R8 (top), 2T20 + 2T22 (bot)
Vertical reinforcement	10R8@150
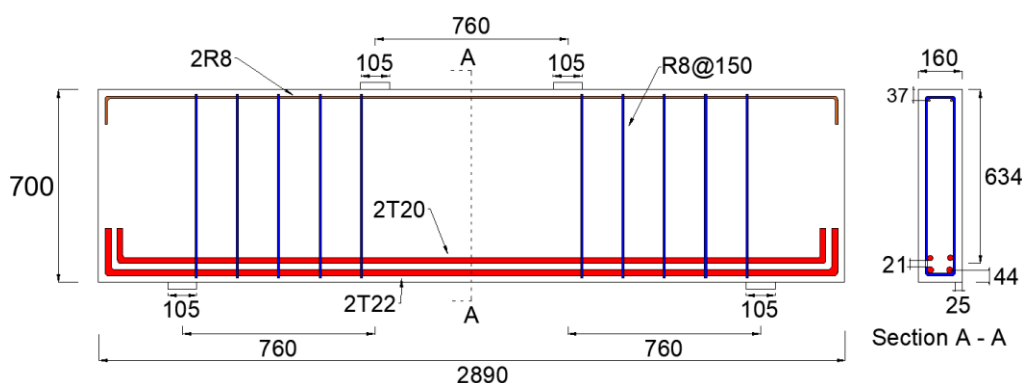
Figure 3.10: Detailing for Specimen D-700.

3.4   Numerical Modelling

In this study, numerically modelling was conducted using finite element analysis software ABAQUS to analyse the behaviour of reinforced concrete deep beam under monotonic loading condition. There are several approaches provided by ABAQUS to represent concrete behaviour which those includes the concrete damaged plasticity model, smeared crack model and discrete crack model. However, out of those available model, Concrete Damaged Plasticity (CDP) model was adopted in this study as it works well to simulate quasi-brittle structure which are ideal for concrete beam. CDP model simulates the inelastic behaviour of concrete by adopting the concepts of isotropic tensile, isotropic damage elasticity, and compressive plasticity.

Numerical modelling can be divided into four stages which started from modelling of material properties, modelling of interfacial behaviour, boundary condition and loading determination and lastly mesh size definition.

Firstly, the properties of concrete as well as the properties of steel reinforcement were defined as the material modelling is important to allow ABACUS to process the linear and non-linear relationship of the materials. Next, interfacial modelling was performed to define the interaction condition between the materials of the model. Those includes the interaction between concrete and steel reinforcements, and interaction between concrete and steel plates. Following, the boundary conditions were defined to specify the support condition such as pin support and roller support by restricting the degree of freedom. The location and type of load were then be defined. Lastly, meshing was created for each component with appropriate seed size.

3.4.1   Properties of Materials

Each type of materials that can be found within the beam model were defined in the first place to allow ABAQUS to process the linear and non-linear relationship of the specimen. The three main types of material which exist in the beam model are the concrete, reinforcing steel and steel plate.

3.4.1.1   Concrete Properties

The CDP model of concrete required the material's compression and tensile constitutive relationship, crushing and cracking damaged parameters, and other parameters such as the characteristic strength of concrete, concrete density, Poisson's ratio, angle of dilation, eccentricity, yield stress ratio, ratio of the second stress invariant on the tensile meridian to compressive meridian for the yield function and viscosity parameter.

In the concrete characteristic cylinder compressive strength selected was 25.9 MPa as defined earlier while the density of the reinforced concrete was taken as 2500kg/m^3 as according to BS EN 1992-1-1:2004 (European Commission, 2004). Besides that, the poisson's ratio for uncrack concrete is taken to be 0.2. By adopting Equation 3.1 suggested by Pauw (1960), with knowing the concrete density and concrete strength, the concrete modulus of elasticity was estimated to be 26409 MPa.

$$E_c = 0.0736 \omega^{1.51} (f_c')^{0.30}$$
(3.1)

where

ω = concrete density, kg/m^3

f_c' = concrete cylindrical compressive strength, MPa

Other required modelling parameters were obtained from Rai (2021). The dilation angle is suggested to be 33° which is within the range of 5° to 42° mentioned by Rewers (2019). The dilation angle influences the amount of plastic volume deformation during modelling where selection of high angle will increase the stiffness of the concrete. For the eccentricity which is to consider the difference between the neutral axis and loading point was taken as 0.1. Next, the yield stress ratio which is the ratio of initial biaxial compressive yield stress to initial uniaxial compressive yield stress was taken as 1.16. The K ratio of the second stress invariant on the tensile meridian to compressive meridian for the yield function was taken as the default value suggested by Abacus user manual which is 0.667. The viscosity parameter was taken as 0.001 which is used to perform viscoplastic regularisation. The parameters of the CDP model are tabulated in Table 3.7.

Table 3.7: CDP parameter for Concrete Material (Rai, 2021).

Parameter	Value
Dilation angle, ψ	33
Eccentricity, ε	0.1
Yield stress ratio, $\dfrac{f_{bo}}{f_{co}}$	1.16
Ratio of the second stress invariant on the tensile meridian to compressive meridian, K_c	0.667
Viscosity, μ	0.001

The concrete stress-strain relationship due to compression and tension were taken into consideration in the simulation. There are numerous stress-strain equations which had derived from various researchers by adopting different school of thought are available to define the concrete compression and tension behaviour. However, out of various types of equations, the stress-strain equations suggested by Carreira and Chu (1985) as shown in Equation 3.2 and

Equation 3.3 were adopted in this study to defined the stress-strain relationship of concrete under compression. The β value from Equation 3.2 was calculated by substituting the defined concrete compressive strength. Then, the β value, compressive strength and the proposed ultimate strain at 0.002 were substituted into Equation 3.3. A concrete stress-strain relationship under compression were then be plotted.

$$\beta = \left[\frac{f_c'}{4.7}\right] + 1.55 \tag{3.2}$$

where

f_c' = concrete ultimate compressive strength, MPa

$$\frac{f_c}{f_c'} = \frac{\beta\,(\varepsilon/\varepsilon')}{\beta - 1 + (\varepsilon / \varepsilon')^{\beta}} \tag{3.3}$$

where

f_c' = concrete ultimate compressive strength, MPa

f_c = concrete compressive strength, MPa

ε = strain, mm/mm

ε' = ultimate strain, mm/mm

For the concrete stress-strain relationship under tension, the modified model suggested by Wahalathantri et al. (2011) was used in this studies. The modified model proposed by Wahalathantri et al. (2011) is designed to eliminate the possible run-time errors during material modelling process. The proposed model created a slanted region between critical tensile strain (ε_{cr}) to 1.25 critical tensile strain (1.25ε_{cr}) as differ from the original model proposed by Nayal and Raheed (2006) which shows sudden drop at critical tensile strain. The modified model is illustrated in Figure 3.11.
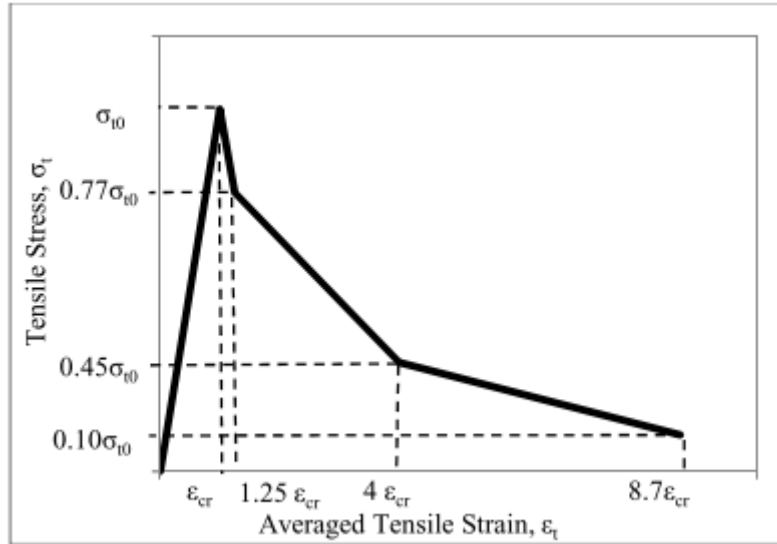
Figure 3.11: Modified Model of Tension Stiffening (Wahalathantri et al., 2011).

For the concrete damage parameter under compression and tension, the formula suggested by Lima et al. (2016) was adopted in this study. The authors assumed that the concrete compression damage and tensile damage will only occur after the concrete reaches its ultimate compressive strength and ultimate tensile strength respectively. Thereafter reaching the peak strength, the damage parameters of concrete will increase monolithically as can be represent by the formula derived by (Lima et al., 2016). Equation 3.4 for the computation of compression damage parameter while Equation 3.5 for the computation of tension damage parameter.

$$d_c = 1 - \frac{f_c}{f_c'} \qquad (3.4)$$

where

f_c = concrete compressive strength on descending limb, MPa

f_c' = concrete ultimate compressive strength, MPa

$$d_t = 1 - \frac{\sigma}{\sigma_{t0}} \qquad (3.5)$$

where

σ = concrete tensile stress on descending limb, MPa

σ_{t0} = concrete peak tensile stress, MPa

The concrete stress-strain curve under compression was plotted as shown in Figure 3.12 by using equations provided by Carreira and Chu (1985) while the concrete stress-strain curve under tension was plotted as shown in Figure 3.13 based on the modified model by Wahalathantri et al. (2011). The concrete compression damage curve and tension damage curve are shown in Figure 3.14 and Figure 3.15 respectively by using equations suggested by Lima et al. (2016).
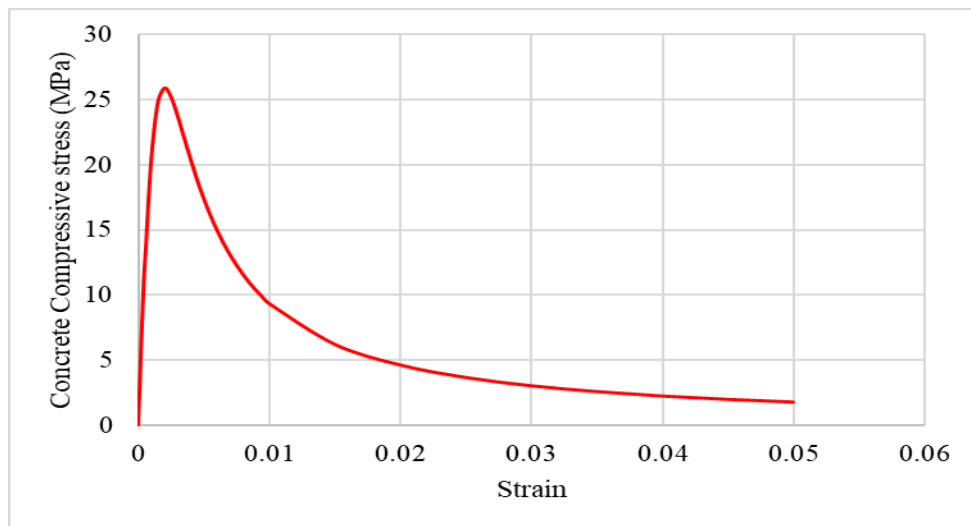

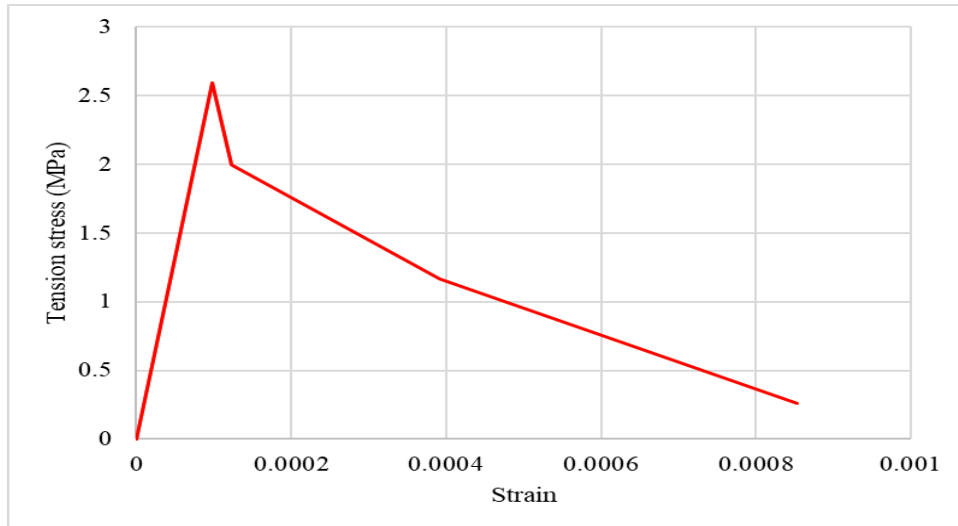Figure 3.12: Concrete Stress-Strain Curve under Compression.

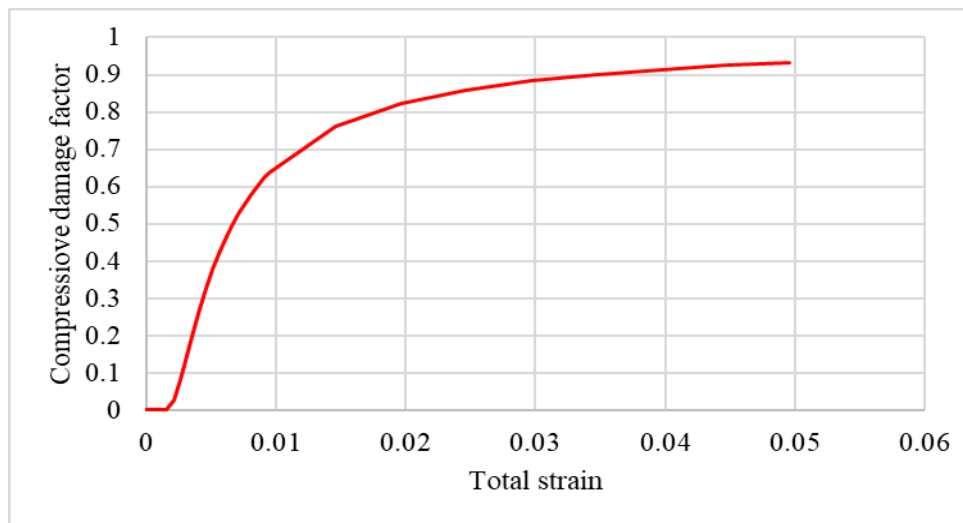Figure 3.13: Concrete Stress-strain Curve under Tension.

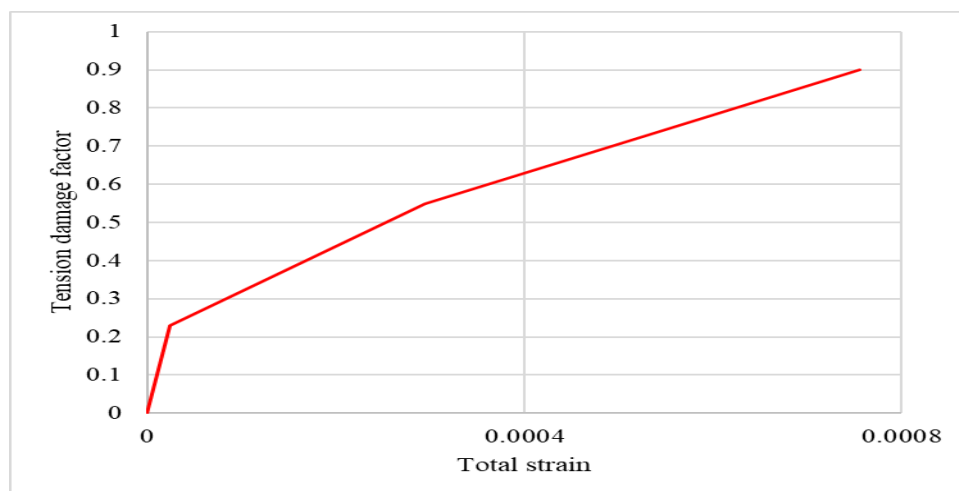Figure 3.14: Concrete Compression Damage Curve.

Figure 3.15: Concrete Tension Damage Curve.

3.4.1.2 Steel Reinforcement Properties

Similar to concrete, steel reinforcement properties are needed to be defined in ABACUS for material modelling. The main steel parameters needed includes the steel density (ρ), Poisson ratio (v), Young's modulus (E) and stress-strain relationship. Some general steel properties will be referring on EN 1993-1-1:2005 (European Commission, 2005). The steel reinforcement density is 7850kg/m^3 and the Poisson ratio was taken as 0.3 in elastic region. The other properties of steel were modelled based on the experiment results by Zhang and Tan (2007). The steel properties were modelled based on bilinear curve of stress-strain relationship. In this case, the ultimate strain of steel was set at 0.2 while other parameters needed for each of the reinforcement sizes are as shown in Table 3.8 provided by Zhang and Tan (2007).

Table 3.8: Properties of Steel Reinforcement (Zhang and Tan, 2007).

Annotation	Young's modulus E, (GPa)	Yield stress f_y, (MPa)	Yield strain ε_y, (mm/mm)	Ultimate Stress f_u, (MPa)
R6	195	426	2.185 x 10^{-3}	488
R8	199	370	1.859 x 10^{-3}	472
T10	198	469	2.369 x 10^{-3}	622
T16	194	499	2.572 x 10^{-3}	648

| T20 | 193 | 522 | 2.705 x 10^{-3} | 592 |
| T22 | 197 | 520 | 2.640 x 10^{-3} | 614 |

3.4.2 Interfacial Behaviour

The interfacial behaviour between each of the materials surfaces are essential to be defined in Abaqus software based on the material actual interfacial contact in real-life. There are two main types of interfacial behaviour needed to be defined in this study which are the interaction between concrete to steel reinforcements and interaction between concrete to steel plates.

For the interfacial behaviour between concrete to steel reinforcement, embedded element technique was adopted to provide perfect bonding. All the steel reinforcements within the concrete were merged to form a steel cage which was then be treated to embed within the concrete. The concrete material was defined as the host element while the steel cage was defined as embedded element. The translational degrees of freedom of the embedded nodes are confined to be the interpolated value of the corresponding degrees of freedom of the host elements (Rai, 2021).

Next, two loading steel plate on top of the concrete beam and two support steel plate under the concrete beam was modelled. The contact between the steel plate and the concrete surface was defined to show no movement during loading analysis. Normal surface contact condition was chosen in the study and the directional behaviours was considered. For the tangential behaviour, friction formulation was selected as rough surface so that no slipping will occur during contact. While for normal behaviour, hard contact was selected for pressure over closure area. The steel plates which have steeper mechanical properties were selected as master surface while the concrete material was selected as slave surface.

3.4.3 Boundary Condition and Loading Determination

The beam specimen was restrained by a pin and roller support at each of the ends. For the pin support, the boundary condition was restricted by translational in all three direction (U1, U2 and U3) and rotational about x and y-axis (UR1 and UR2) has also been restricted as it is unnecessary. Therefore, for pin support,

only rotational about z axis (UR3) was released. Next, the boundary condition for the roller support was restricted by the translational in y and z direction (U2 and U3) and rotational about x and y-axis. Other degrees of freedom were released. Figure 3.17 is provided for reader to ease in the illustration of degrees of freedom.
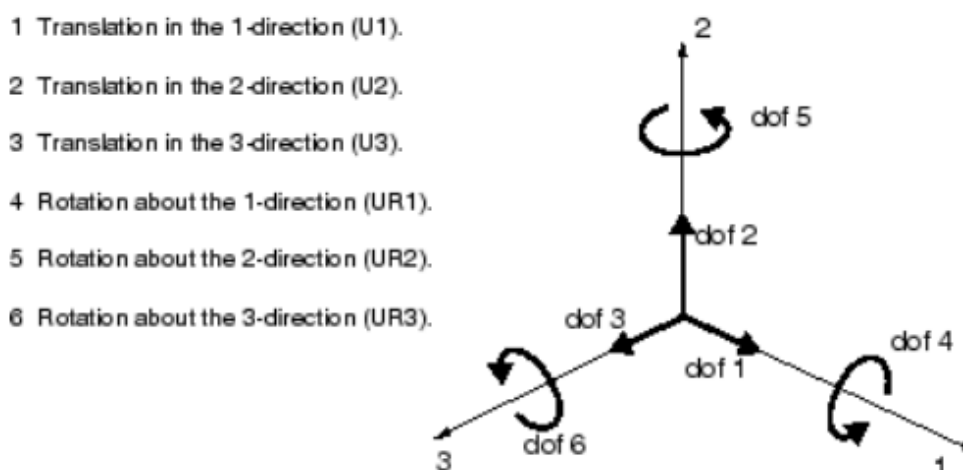

Figure 3.16: Degrees of Freedom in Translation and Rotational.

For loading definitions, two equivalent line load were applied at the centre line of both the bearing plates. Reference point was first created to indicate the loading point acting on the plate. Next, the datum plane was introduced to create partition for bearing plate so that line load can be assigned through the centreline of the bearing plate. Multi-point constraints interaction was adopted for interaction of the bearing plates and loading point. The centreline of the bearing plates was considered as slave node while the reference point act as control point. Furthermore, the load was applied using the static loading step in the direction of negative y-axis (- U2) to indicated loading acting downward.

3.4.4   Element Type and Mesh Size

Concrete was modelled as a three-dimensional solid continuum element consist of 8 nodes linear brick element with 1 integration point (reduced integration) denoted as C3D8R. The model was performed under hourglass control to prevent uncontrolled mesh distortion caused by the reduce integration. This type

of modelling is capable of simulating concrete crushing in compression and cracking in tension. The steel plates which are also a solid continuum element was modelled with similar element type as the concrete which are using the C3D8R. However, steel cage was modelled as a three-dimensional truss element consist of 2 nodes denoted as T3D2. The truss element was chosen as it is suited for modelling of long slender structure such as steel bar. The element only supports axial loading along its centre line where no forces or moment perpendicular to the centreline is supported.

The seed size is required to be determined before meshing process could start. The seed size was based on the coarse aggregate used for the concrete beam casting. The common coarse aggregate used for beam casting are 18mm, 20mm or 25mm. For the initial trial, 25mm of seed size was defined for each part of the model. However, if the result outcomes do not agree well with the experimental data, mesh sensitivity analysis with smaller mesh size will be performed to yield for better result. The smaller mesh size may result in better accuracy. However, it takes longer time to run the analysis as compared to bigger mesh size.

3.4.5   Modelling Verification

The numerical reference beam results were compared with the experimental results done by Zhang and Tan (2007) to justify the accuracy and reliability of the model. The experimental load-deflection curve was compared with the load-deflection curve generated by ABAQUS for verification purpose. Besides that, the numerically generated concrete tension damage contour was compared with the crack pattern observed in experiment done by Zhang and Tan (2007). The purpose of verification is to make sure that the numerically model beam complies well with the actual beam behaviour and if the result shows significant inconsistency, model recalibration is necessary. The model recalibration can be carried out by conducting sensitivity analysis on Concrete Damaged Plasticity model's parameters and mesh sizing.

3.4.6   Analytical Model

After numerical model was verified with the experimental results, the similar simulation technique as well as the material parameters was used for the control specimen and other four test specimens. Load-displacement curves were plotted for each specimen and the ultimate failure load were retrieved. The ultimate failure load of each specimen was compared with the Strut-and-Tie model estimation to further validate the failure load as the failure load is very crucial parameter in determining beam size effect. Cracking Strut-and-Tie Model (CSTM) as has been reviewed in Chapter 2 was used for the computation. A simplified CSTM formulae were adopted in this study. The simplified CSTM had been verified by Chen, Yi and Hwang (2018) with 355 test specimens. The authors had compared the results with other design codes such as ACI 318-14, CSA A23.3-14, and other STMs. And from the findings, the authors concluded that the result predicted by the simplified CSTM showed higher precision as compared to other code. Therefore, simplified CSTM is chosen to be used for the verification purpose.

According to the simplified CSTM formulae, the shear capacity of beam, V_n is calculated by Equation 3.6. The shear capacity is mainly contributed by the resultant force from the uncrack region, F_{si} and cracked region, F_{sc} which can be estimated using Equation 3.7 and Equation 3.8 respectively. Besides that, the coefficient of strut efficiency at uncrack region β_{Si} is taken as 0.85 based on the test results collected by Laughery and Pujol (2015) while for the crack region β_{SC} is calculated based on Equation 3.9. As could be noted, the coefficient of strut efficiency at uncrack region is estimated by taking account on the reinforcement provided as well as the aggregate interlock mechanism. The effective compressive strength contribute by the reinforcements, $\sigma_{cc,s}$ and by aggregate interlock, $\sigma_{cc,ag}$ are calculated based on Equation 3.10 and Equation 3.11 respectively. Moreover, the strut width of both uncracks w_{si} and cracked w_{sc} faces can be calculated by Equation 3.12 and Equation 3.13. The compressive zone depth can be assumed by Equation 3.14. Lastly, the strut angle θ and the critical shear crack angle, α is calculated by Equation 3.15 and Equation 3.16 respectively.

$$V_n = (F_{si} + F_{sc}) \cdot \sin\theta \tag{3.6}$$

where

F_{si} = resultant force from uncrack region, N

F_{sc} = resultant force from cracked region, N

θ = strut angle

$$F_{si} = \left(1 - \frac{f_c'}{250}\right) \beta_{si} f_c' w_{si} b \tag{3.7}$$

where

β_{si} = 0.85

f_c' = cylinder compressive strength of concrete, Mpa

w_{si} = strut width of uncrack face, mm

b = cross-sectional width of specimen, mm

$$F_{sc} = \beta_{sc} f_c' w_{sc} b \tag{3.8}$$

where

β_{sc} = coefficient of strut efficiency at crack region

w_{sc} = strut width of cracked face, mm

$$\beta_{sc} = \frac{\sigma_{cc,ag} + \sigma_{cc,s}}{f_c'} \leq \left(1 - \frac{f_c'}{250}\right) \beta_{si} \tag{3.9}$$

where

$\sigma_{cc,s}$ = effective compressive strength by reinforcement, Mpa

$\sigma_{cc,ag}$ = effective compressive strength by aggregate interlock, Mpa

$$\sigma_{cc,s} = \frac{0.45 f_y \rho_v d \cot^3\alpha}{w_{sc}\sin\theta} \leq \frac{0.9 f_{vy} \rho_v d \cot\alpha}{w_{sc}\sin\theta} \tag{3.10}$$

where

f_y = yield stress of longitudinal bar, Mpa

f_{vy} = yield stress of vertical reinforcement, Mpa

ρ_v = ratio of vertical reinforcement, %

d = effective depth, mm

α = critical shear crack angle

$$\sigma_{cc,ag} = \frac{1.33\sqrt{f_c'}}{0.31 + 0.34a\varepsilon_y/sin\alpha} \tag{3.11}$$

where

ε_y = yield strain of longitudinal reinforcement, mm/mm

$$w_{si} = \left[tan\theta \cdot l_{bt} + \frac{c \cdot (tan\alpha - tan\theta)}{tan\alpha + c/l_{bt}}\right] cos\theta \tag{3.12}$$

$$w_{sc} = \left[c - \frac{c \cdot (tan\alpha - tan\theta)}{tan\alpha + c/l_{bt}}\right] cos\theta \tag{3.13}$$

where

l_{bt} = width of bearing plate, mm

$$c = \left(\sqrt{(np)^2 + 2np} - np\right)d \tag{3.14}$$

where

n = ratio of steel to concrete elastic modular

p = ratio of longitudinal reinforcement

$$\theta = tan^{-1}\left(\frac{d - c/2}{a}\right) \tag{3.15}$$

$$\alpha = 8.53\left(\frac{a}{d} - 2.5\right)^2 + 30.55 \geq tan^{-1}\left(\frac{h}{a + \frac{l_{bt}}{2} - \frac{l_{bs}}{2}}\right) \tag{3.16}$$

where

a = shear span length, mm

l_{bs} = width of support plate, mm

l_{bt} = width of bearing plate, mm

The equations listed above were adopted to compute the ultimate failure load of numerical specimens. The result between CSTM and numerical will be compared to further validate the numerical model.

3.4.7 Normalised Shear versus Effective Depth Curve

In order to evaluate beam depth size effect, ultimate failure load was converted into dimensionless shear strength. The ultimate failure load was normalised by their cross-sectional width, effective depth and characteristic strength of concrete as shown in Equation 3.17. As could be noted from the equation, an additional parameter of f_c' is introduced in the calculation of normalised shear strength as differs from the conventional formula in calculation of ultimate shear strength. The normalised shear strength is widely used by researchers such as Zhang and Tan (2007), Birrcher et al. (2014), and Chen, Yi and Ma (2019) in their researches related to beam depth size effect. Normalised shear strength versus effective depth curve was plotted. If the curve obtained is in flat trend, then depth size effect is said to have not taken place. While if a curve of decreasing trend is observed, it means that the depth size effect is present in the specimens.

$$\text{Normalised Shear Strength} = \frac{V}{f_c' b d} \qquad (3.17)$$

where;

V = ultimate failure load, kN

f_c' = concrete compressive cylinder strength, kPa

b = specimen width, mm

d = specimen effective depth, mm

3.4.8 Summary

In this study, the reference beam which serve for verification purpose was adopted from the experimental work done by Zhang and Tan (2007). All the numerical beam specimens were modelled using Abaqus software. The methodology workflow can be divided into three major process which include the numerical modelling, numerical analysis and modelling verification. Numerical modelling described the specimens with input such as the material and mechanical properties. Following, numerical analysis was carried out to generate results such as load-deflection curve and concrete tension damage contour. Next, the numerical reference beam results were compared with the

experiment result to verify the accuracy and reliability of the model. Recalibration work by conducting sensitivity analysis on Concrete Damaged Plasticity model's parameter was conducted when the result shows significant inconsistency, thus achieving the first study objective. Then, the numerical modelling and numerical analysis was performed on one control beam and four test specimens with different cross-sectional height to study the depth size effect of deep beams. Manual calculation by Cracking Strut-and-Tie method was used to further validate the numerical result. Lastly, ultimate failure load was converted into normalised shear strength to evaluate the depth size effect of the specimens.

CHAPTER 4

RESULTS AND DISCUSSIONS

4.1 Introduction

This chapter mainly discussed the depth size effect of deep beam from the designed numerical specimens which had 100mm of cross-sectional height increment each as being tabulated in Table 4.1. The discussion started with validation of the stimulation technique and material properties by numerically simulate a reference beam R-01 and compared it to the experimental result by Zhang and Tan (2007). Then by adopting the validated modelling technique, a control beam and four numerical test specimens namely as D-400, D-500, D-600, and D-700 were generated. The numerical results have then been analysed in term of the load-displacement curve, normalised shear strength, von Mises stress contour, plastic strain magnitude (PEMAG), and concrete tension damage to study the depth size effect in deep beam.

Table 4.1: Specification of Numerical Model.

Specimen	Dimension		
	Height (mm)	Width (mm)	Length (mm)
C-01	300	160	1140
D-400	400	160	1560
D-500	500	160	1980
D-600	600	160	2430
D-700	700	160	2890
All beams are proportioned with: 1) Shear to span depth ratio a/d = 1.2 2) Longitudinal reinforcement ratio = 1.2% 3) Vertical reinforcement ratio = 0.4% 4) Plate width to height ratio = 0.15			

4.2   Model Verification between Numerical Modelled Reference Beam and Experimental Beam

The analysis of this study begins with model verification by utilised the load-displacement curve result retrieved from the numerically generated reference beam and compared it to the experimental beam's result. As mentioned from the previous chapter, the key purpose of comparing experimental beam's result and the numerical model result is to verify the accuracy of the ABAQUS software on stimulating the actual behaviour of beam in real-life as well as to provide the best set of Concrete Damaged Plasticity (CDP) parameters to be used for the following test specimens. The main CDP parameters to be validate are the viscosity and the dilation angle of the concrete, which were later selected as 0.03 and $30°$ respectively. The numerical reference beam R-01 was modelled in accordance with the experimental beam by Zhang and Tan (2007) where the dimension and the detailing of the beam was mentioned in Chapter 3, which can be referred on Table 3.1 and Figure 3.2 respectively. The load-displacement curve of numerical reference beam R-01 and experimental beam are presented in Figure 4.1, and the important data from the findings are tabulated in Table 4.2.
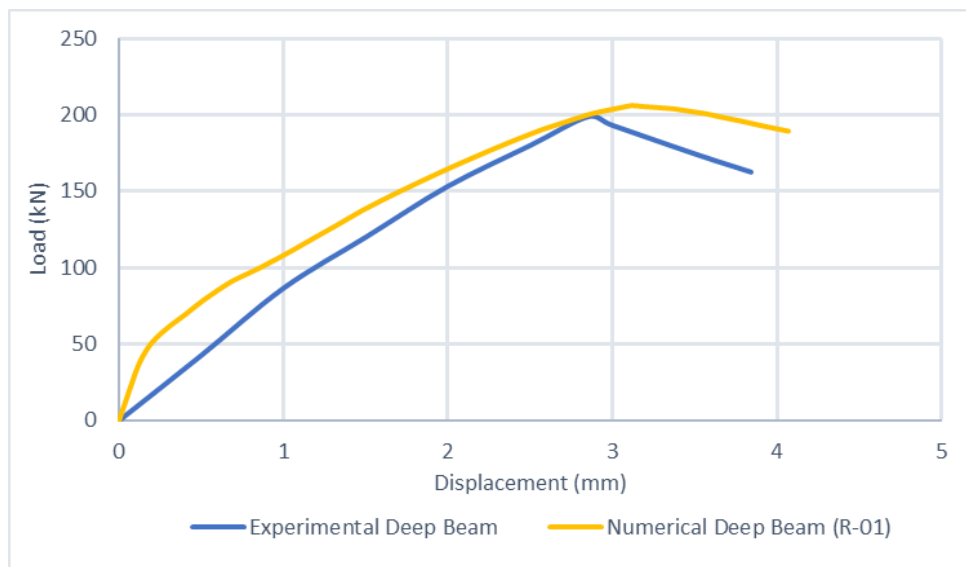
Figure 4.1: Load-Displacement Curve of Numerical Deep Beam (R-01) and Experimental Deep Beam from Zhang and Tan (2007).

Table 4.2: Important Data from Load-Displacement Curves.

Deep Beam Specimen	Ultimate Fail Load (kN)	Percentage Difference (%)	Deflection at Ultimate Fail Load (kN)	Percentage Difference (%)
Experimental Beam	199	3.52	2.86	8.74
R-01	206		3.11	

Based on the visualised load-displacement curves in Figure 4.1, the numerical specimen R-01 curve is generally steeper as compared to the experimental beam. This outcome is common as there are many researchers who have done similar study using numerical results generated by Abaqus software to compare with experimental specimens have obtained same trend of result. Those researchers were including Rai (2021) who modelled RC deep beam, Mohamed, Shoukry and Saeed (2014) who modelled beam with web opening, and Shahnewaz (2013) who modelled deep beam under monotonic load. They have all obtained numerical curve steeper than their experimental curve. Therefore, the analysis was continued even though the numerical curve obtained is steeper than experimental curve.

As can be observed in Figure 4.1, during the initial loading stage which happened before concrete started to crack, the R-01 is noticed to have a steeper curve compared to the experimental beam. There are several factors that may cause higher stiffness of numerical beam which include ABAQUS software unable to simulate microcracks behaviour during loading condition where microcracks is likely to develop in the experimental beam due to concrete drying shrinkage (Ibrahim and Mohmood, 2009). Besides that, the bonding condition between concrete and reinforcement is assumed to be perfect by ABAQUS software. However, in actual condition, the bonding between them may slip which resulted in the loss of composite action in experimental beam (Jasim, Tahnat and Halahla, 2020). Therefore, the stiffness of the numerical beam is found to be higher than the experimental beam.

However, when the R-01 specimen started to crack after the applied load reached 56kN at 0.25mm deflection, the R-01 started to show milder curve

all the way toward experimental beam until the ultimate failure load had occurred. The reduction in stiffness of R-01 at higher loading stage was due to the magnitude of the principal strains increases which causes the concrete material to undergo compression crushing and diagonal tensile failure as illustrate by the stress-strain curve in Figure 3.12 and Figure 3.13. When the value of maximum principal tensile strain goes beyond the strain value corresponding to the concrete tensile strength, and the minimum principal compressive strain goes beyond the strain value corresponding to the concrete compressive strength, the beam stiffness will then start to reduce (Rai, 2021). This explained the reason of reduction in stiffness. After ultimate fail load occur, both R-01 and experimental beam shown abrupt decline which indicates the beam failure taking place.

The ultimate failure load of R-01 fall at 206kN with deflection of 3.11mm while the ultimate failure load of the experiment beam occurred at 199kN with 2.86mm deflection. Therefore, the ultimate failure load analysed by numerical model was 3.52% higher, and the corresponding deflection was 8.74% greater than the experiment data. The percentage difference of ultimate load and deflection length between R-01 and experimental beam were quite small which shows good evident that the Concrete damage plasticity model is useful in reflecting the load-displacement behaviour of actual specimen.

Besides on comparing the specimen strength, the numerical tension damage contour was compared with the experimental crack patterns of the beam. Figure 4.2 presents the experimental cracking pattern of the reference beam while Figure 4.3 shows the numerical tension damage contour of R-01 extracted from ABAQUS software which predicted R-01 cracks pattern numerically. Both figures shows that the critical crack occurs at the compressive strut location which originate from the support plate and propagate diagonally towards loading point. Besides that, some vertical flexural cracks are developed at the midspan of the tension region. Although there are horizontal cracks showed at both edges of the R-01 specimen which is non noticed on the experiment beam but still the overall cracking pattern of R-01 appear to match well with the experimental cracking pattern. Therefore, ability of the CDP Model in simulating the crack patterns is verified.
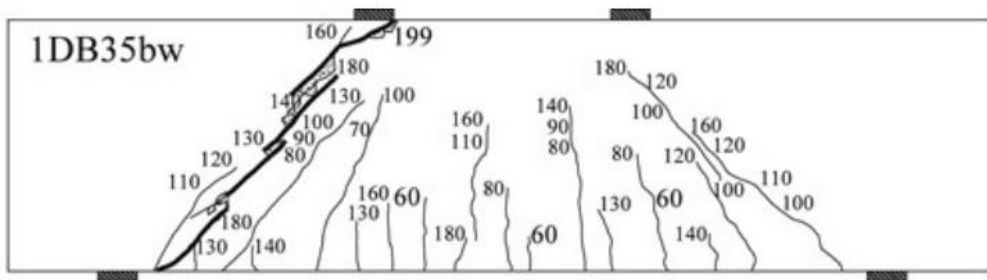
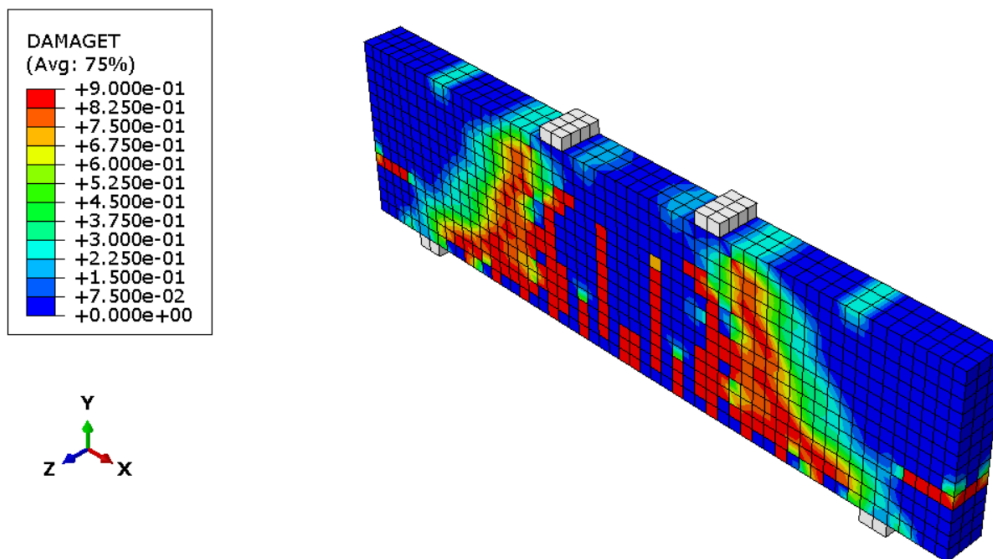Figure 4.2: Experimental Cracking Pattern (Zhang and Tan, 2007).

Figure 4.3: Tension Damage Contour of R-01.

In short, the numerical specimen R-01 is way stiffer than the experimental beam before the cracking occurs. But after cracking occurred, stiffness of R-01 decrease gradually all the way ultimate failure load and closing the gap between experimental beam and R-01. A well matching load-displacement curve was observed where difference of the ultimate failure load was only 3.52 % and the difference in the corresponding deflection was 8.74 %. Moreover, the numerical cracking pattern of R-01 is in good agreement with the experimental observation. Therefore, the modelling technique and material properties applied in this study are proven accurate. Hence, the same modelling technique and material properties are reliable to be used for the following test specimens for evaluating the depth size effect of deep beam.

4.3   Control Beam and Numerical Test Specimens with Increasing Cross-Sectional height

A control beam and 4 numerical test specimens were all designed to have constant shear span to effective depth ratio a/d of 1.2, longitudinal reinforcement ratio of 1.2% and vertical reinforcement ratio of 0.4%. Besides that, loading and support plates were proportioned with 0.15 of the overall specimen height to exclude the bearing plate size effect on the result outcomes. Therefore, the only variable among the control beam and all four numerical test specimens were the cross-sectional height. The height of the control beam C-01 is 300 mm while the height of the following 4 specimens which denoted as D-400, D-500, D-600, D-700 was designed with height of 400 mm, 500 mm, 600 mm, and 700 mm respectively in order to determine the shear strength behaviour of deep beam under increment of cross-sectional height. Those specimens' dimension and geometry can be referred on sub-chapter 3.3. All the specimens were modelled using ABAQUS software by adopting the proven accurate modelling technique and Concrete Damaged Parameters as been done on reference beam R-01.

4.3.1   Load-Displacement Curve of Numerical Models

The modelling and analyses of a control beam C-01 and 4 numerical test specimens D-400, D-500, D-600 and D-700 was performed. The load-displacement curve of each of the numerical beams was plotted separately and are presented in Appendix B while Figure 4.4 combined all the load-displacement in a single graph for better visualisation on its failure point. Table 4.3 tabulates the numerical specimens' ultimate fail load and displacement at failure as well as their respective percentage difference to the control beam.
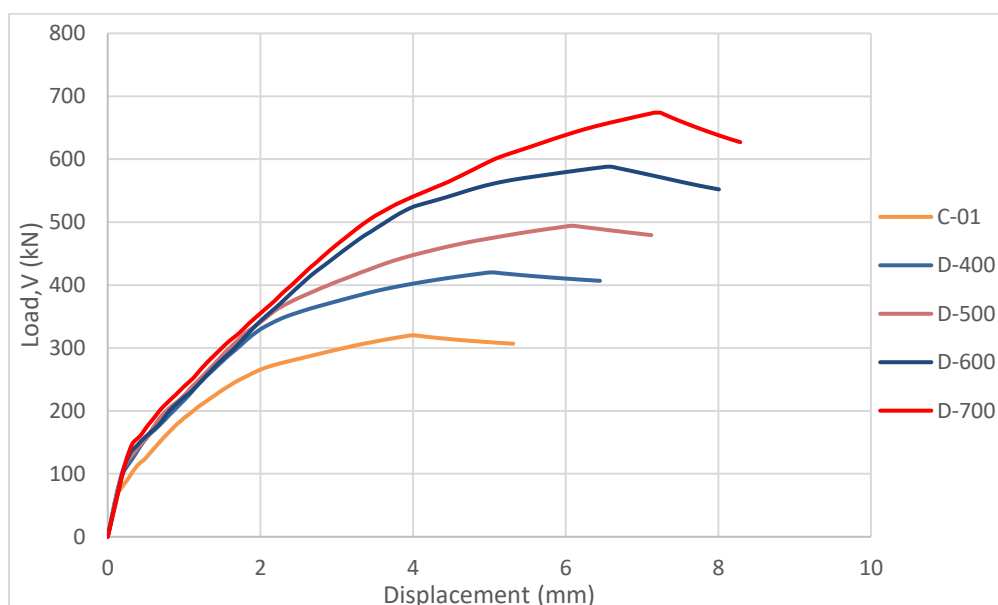
Figure 4.4: Load-Displacement of Numerical Beam with Different Height.

Table 4.3: Numerical Specimens Data from Load-Displacement Curve.

Specimen	Ultimate Fail Load, V (kN)	Percentage Increment based on C01 (%)	Deflection at Failure (mm)	Percentage Difference Based on C-01 (%)
C-01	320	-	3.97	-
D-400	415	29.7	4.68	17.8
D-500	494	54.4	6.06	52.5
D-600	588	83.8	6.53	64.5
D-700	674	110.6	7.17	80.4

As can be observed from Figure 4.3, all five numerical specimens' load-displacement curves show similar trend where all the curves showed constant steep gradient in the initial stage until when the applied load is enough to induce cracking, then the curves became milder. Those curves continue its path up until a sharp dropping of applied load happened which the load at the point is defined as ultimate failure load. As can be seen from Figure 4.3, the ultimate failure load of the specimen increases when the sectional height of

beam increases. Along with the increment of fail load, the deflection at failure load also increases respectively. The cumulative percentage of ultimate failure load of beam increases for every additional of 100 mm beam height incremental measured based on C-01. On the first 100 mm beam height increment, the ultimate failure load increased by 29.7 % and for the following 100 mm beam height incremental, the cumulative ultimate failure load increment are found to be 54.4 %, 83.8 % and 110.6% respectively.

The increment of failure load at larger cross-sectional height is theoretically correct for either slender beam or deep beam. As the cross-sectional height increases, the cross-sectional area susceptible to load transfer will also increase. Therefore, the load carrying capacity increases. However, the load transfer mechanism of deep beams is governed by arch-action. Hence, the load carrying capacity increment in deep beam was due to the depth increment which led to the increment of the back face of CCT and CCC nodes. The increment of the nodes directly contributes to the increase in size of node-strut interface (Birrcher et al., 2009). Subsequently, it contributes to higher load carrying capacity.

Cracking Strut-and-Tie Model (CSTM) which had been mentioned in the Literature chapter as a reliable model was used in this section to serve as a reference on how well the analytical model can predicts the failure load of numerically generated beam. The analytical model calculated failure loads were tabulated as shown in Table 4.4 and a set of sample calculation is attached in Appendix A. As can be seen from the Table 4.4, the simplified CSTM formulae estimated fail load slightly lower compared to the numerical result. The percentage difference between the numerical result and the analytical model ranged from 5.13% to 7.24%. The results show that the simplified CSTM formulae are slightly more conservative in predicting the failure load of numerical deep beam. This reason is due to the simplified CSTM formulas are formulated based on actual deep beam behaviour and the coefficients are regressed from historical experimental results (Chen, Yi and Hwang, 2018). Therefore, the calculated value from CSTM can better resembled the actual beam's load capacity and causes it to have lower value than numerical result. The results show consistency as in Section 4.2 the ultimate failure load of the

experimental beam was also found to be lower than numerical reference beam R-01. Thus, this implies that the simplified CSTM formula can well predicts the failure load of deep beam and since the percentage difference between fail load calculated by CSTM and numerical results are not excessively high. Therefore, numerical results are said to be reliable.

Table 4.4: Ultimate Fail Load by Finite Element Analysis and CSTM.

Specimen	Numerical Ultimate Fail Load, V (kN)	CSTM Ultimate Fail Load, V_{cstm} (kN)	Percentage Difference (%)
C-01	320.0	303.6	5.13
D-400	415.0	390.4	6.83
D-500	494.0	458.5	7.19
D-600	588.0	548.0	6.80
D-700	674.0	625.2	7.24

In short, when the deep beam height increases, the ultimate failure load increases due to arch action. The failure load is very crucial in examining the depth size effect. Therefore, CSTM model was used to further validate the numerical results. The failure load calculated manually based on simplified CSTM are lower than the numerical results. However, the percentage difference between the numerical analysed failure load and the manual calculated failure load are low. Therefore, the numerical result was proven to be reliable.

4.3.2   Analyses on Depth Size Effect by Normalised Shear Strength versus Effective Depth Curve

As referring back to the study aim which is to study the depth size effect. With the ultimate failure load alone can't be enough to perform the analysis on the depth size effect. Therefore, to evaluate on how the depth of deep beam actually affect its shear strength, dimensionless normalised shear strength (V/bdf'_c) versus specimen's effective depth curve must be plotted to aid in analysis of depth size effect as mentioned in Chapter 3. The calculated normalised shear

strength at failure of all the numerical specimens and their respective depth were tabulated as shown in Table 4.5, while Figure 4.5 shows the normalised shear strength versus effective depth curve.

Table 4.5: Beam Normalised Shear Strength and its respective Effective Depth.

Specimen	Height (mm)	Effective Depth, d (mm)	Normalised Shear Strength at failure (V/bdf_c')	Difference of Normalised strength based on C-01 (%)
C-01	300	250	0.309	-
D-400	400	342	0.293	-4.29
D-500	500	434	0.275	-11.07
D-600	600	534	0.266	-13.97
D-700	700	634	0.257	-16.95
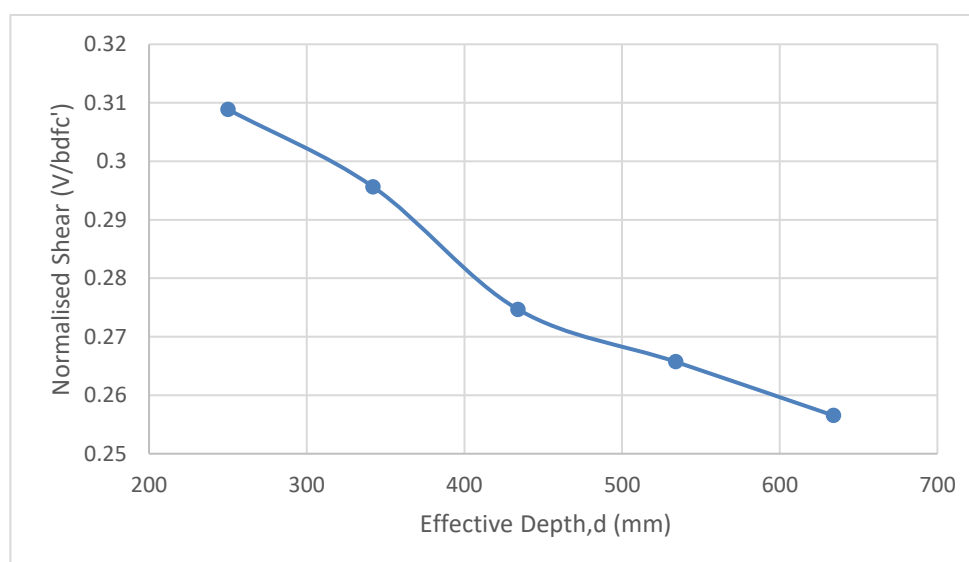
Figure 4.5: Normalised Shear Strength versus Effective Depth.

As could be observed from Table 4.5 and Figure 4.5, it could be noted that when the beam effective depth increases, the normalised shear strength decreases. The decrement of normalised shear strength started from C-01 all the way toward the highest beam D-700. The decreasing in normalised shear strength inferred that the load carrying capacity of the deep beam did not increase proportionally to the increment of depth. Therefore, the depth size

effect was proven exist in this study. The cumulative percentage of decrement in normalised shear strength increases for every additional 100 mm height incremental measured based on C-01 as shown in Table 4.5. On the first 100 mm beam height incremental, the cumulative normalised shear strength decreased by 4.29 % and then to 11.07 %, 13.97 % and 16.95 % for the following 100 mm beam height incremental respectively. It could be noticed from Figure 4.5 that the gradient between D-400 to D-500 is steeper as compared to other parts of the curve. The steeper trend is due to the normalised shear strength of C-01 and D-400 are comparatively higher as compared to normalised shear stress at D-500, D-600 and D-700. This may be due to the capacity of the vertical reinforcement provided to the specimens did not been fully utilised. As the arrangement of vertical reinforcements provided for C-01 and D-400 are located relatively away from the bearing and support plates. Therefore, due to deep beam's arch mechanism, the vertical reinforcement can be utilised fully. However, for specimens D-500, D-600 and D-700, due to the beam cross-sectional area increases, a greater number of vertical reinforcements were provided. Due to this reason, some vertical reinforcements are located nearer to the face of the bearing and support plate. Therefore, when the strut and tie action developed, the vertical reinforcements were not fully utilised. Hence, D-500, D-600, D-700 resulted in comparatively lower normalised strength as compared to C-01 and D-400. However, the depth size effect of all the specimens is still very obvious.

The existence of the depth size effect in this study agreed with the finding by Matsuo et al. (2001) as by reviewing back to the Literature chapter, it has been mentioned that the depth size effect on the experiment tested by Matsuo et al. (2001) did show size effect but contradictorily to the finding by Zhang and Tan (2007) which the specimens tested by the authors did not show obvious size effect. Zhang and Tan (2007) mentioned that the size effect was greatly mitigated as the authors proportioned the size of the bearing and support plates to the specimen height. However, the result in Figure 4.5 does show obvious depth size effect even though the bearing and support plates of each numerical specimen was designed proportioned to the height of beam. Same goes to the specimens tested by Matsuo et al. (2001) who also proportioned their

specimens in the same way yet the size effect still obvious. Therefore, this comparison inferred than the size effect does exist even though the bearing and support is proportioned to the beam height. Besides that, it is previously mentioned that the contradictorily in findings between Matsuo et al. (2001) and Zhang and Tan (2007) may be due to the loading condition on the specimen where Matsuo et al. (2001) used single point loading while Zhang and Tan (2007) used two-point loading. However, two-point loading was performed in this study, yet the size effect could still obviously be detected. Therefore, the load condition may not be the cause of size effect mitigation in the finding by Zhang and Tan (2007). Hence, further research may be done in the future to study the reason behind the cause of size effect mitigation by the finding by Zhang and Tan (2007).

The depth size effect of deep beam can be explained by using Strut-and-Tie Model (STM). As have been mentioned in the Literature Review chapter, the strength of deep beam is mainly governed by its struts width where the struts width is directly influence by the width of bearing-support plates and the depth of compression zone. The depth of compression zone is predicted by double of the distance between the bottom face of the beam to the centre of the longitudinal tie. To assess the shear capacity of the deep beam, the relative struts size was measured. As can be seen from Table 4.6, the struts width did increase along with the increment of specimens' height. However, the relative struts width decreases as the depth of the beam increases. Since the bearing-support plates of the beams were designed to increased proportionally to the beam height. Therefore, bearing-support plates did not affect the relative struts size. Hence, the decrement on relative depth of compression zone (c/h) is the main factor that caused the decrement of relative strut width (w_s/h). As tabulated in Table 4.6, the compression depth for specimens D-500, D-600 and D-700 are about the same. This is due to the compression depth was calculated based on the concrete cover and longitudinal bar size, since the specimen D-500, D-600 and D-700 were having almost similar concrete cover and bar sizes. Therefore, their compression depth was computed to be about the same value. However, when all the specimens' compression depth are divided by their respective beam height, the relative compression depth is under a decrement trend. The

decrement of the relative compressive depth resulted in the decrement of relative struts width which then directly resulted in the decrement of normalised shear strength. The decrement of normalised strength implies that the load carrying capacity of beam did not increased proportionally with its depth therefore explained the depth size effect in deep beam. To make it short, the depth size effect of deep beam is cause by the decrement of relative strut width which is due to its decrement in relative depth of compressive zone. Figure 4.6 presented the relative strut size of specimen C-01, D500 and D-700 where the specimens was plotted as equally large to ease in visualisation of the decrement of relative strut width.

Table 4.6: Data for Struts Size Estimation.

Specimen	Compression Depth c, (mm)	Struts Width w_s,(mm)	Relative Compression depth, c/h	Relative Plate Width, ℓ/h	Relative Struts Width, w_s/h
C-01	100	107.0	0.33	0.15	0.36
D-400	116	128.8	0.29	0.15	0.32
D-500	132	150.6	0.26	0.15	0.30
D-600	132	159.6	0.22	0.15	0.27
D-700	131	167.8	0.19	0.15	0.24
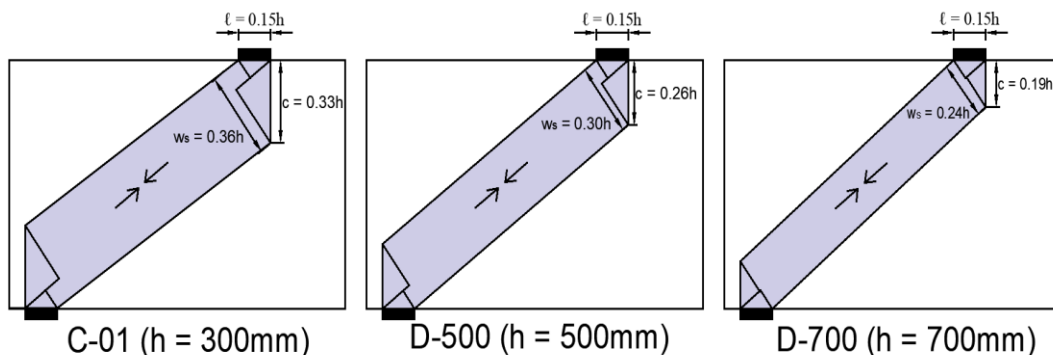
Figure 4.6: Normalised strut size for specimen C-01, D-500 and D-700.

In short, depth size effect does exist in deep beam when the cross-sectional height of the beam increases. The cumulative decrement of beam shear

strength increases for every additional of 100 mm incremental measured started from C-01. On the first 100 mm beam height increment, the normalised shear strength decreases by 4.29% and then to 11.07 %, 13.97 %, and 16.95 % for the following 100 mm beam height incremental respectively. Besides that, the location of vertical reinforcement is suggested to have influence on the beam strength. Moreover, the depth size effect was compared to the finding by Matsuo et al. (2001) and Zhang and Tan (2007). The findings conclude that size effect does exist even though the bearing and support plates are proportioned to the beam height. Furthermore, the reason of depth size effect was explained by STM model where the depth size effect of deep beam happened was caused by the decrement of relative strut width which was mainly due to the decrement in relative depth of compressive zone when beam height increases.

4.4 Graphical Contour generated by Finite Element Analysis

The discussion continues with the comparison of graphical contour among beam specimens. The numerical graphical contour such as von Mises stress contour, concrete tension damage contour and plastic strain magnitude contour were generated by ABAQUS software for every specimen. The main reason of this section is to study the behaviour of deep beam at different cross-sectional height in term of the stress distribution and direction of crack propagation.

4.4.1 Von Mises Stress Contour

The von Mises stress contour is a 3-dimensional graphical diagram that generated numerically by ABAQUS software through the finite element analysis. It is useful for visualising the stress-distribution within the specimen beam on different level of applied loading. While two types of von Mises stress contour could be generated for RC deep beam which are the concrete von Mises stress contour and the von Mises stress contour of reinforcement cage. Both types of the contours were captured and was discussed under the following sub-section.

4.4.1.1   Concrete von Mises Stress Contour

The von Mises stress contour is able to describe the distribution of stress within the beam specimens. The concrete von Mises stress contour at different loading level was generated for all specimens. The contour for control beam, C-01 at different loading stages are presented as shown in Figure 4.7, Figure 4.8 and Figure 4.9 while for other specimens were attached in Appendix C. As been compared, the stress distribution pattern at each loading level were similar for all the numerical specimens.

The stress contour started to form initially when the load applied on the bearing plates, where the stress was then been distributed evenly on top of the beam and eventually the stress propagates downward to the support plates diagonally. Besides that, it could be noticed that the compression region and the tension region within the diagonal struts were taking considerable amount of stress at the initial stress as being presented in Figure 4.7. However, when the load applied went larger than the diagonal cracking load, where the specimens was likely to start cracking diagonally, the stress started to concentrate at the diagonal struts and the stress at the tension region began to reduce. Where this support the findings by Tan and Lu (1999) which stated that the load transfer mechanism of deep beam started to shift into arch action after diagonal crack formation. Therefore, the compressive stress will be taken by compressive strut while the tension will be taken by longitudinal reinforcement. The stress distribution right after diagonal crack is presented in Figure 4.8. After diagonal crack, the stress started to be more concentrated on the compressive strut until failure occurred. As can be seen from Figure 4.9 where the failure load was applied, a more obvious bottle-shaped struts were observed forming diagonally connecting bearing and support plates. While a minimal amount of flexural stress was observed at the tension region. Therefore, from the concrete von Mises stress contour, it inferred that all the deep beam specimens were undergone the same set of stresses distribution even though they have different cross-sectional height.
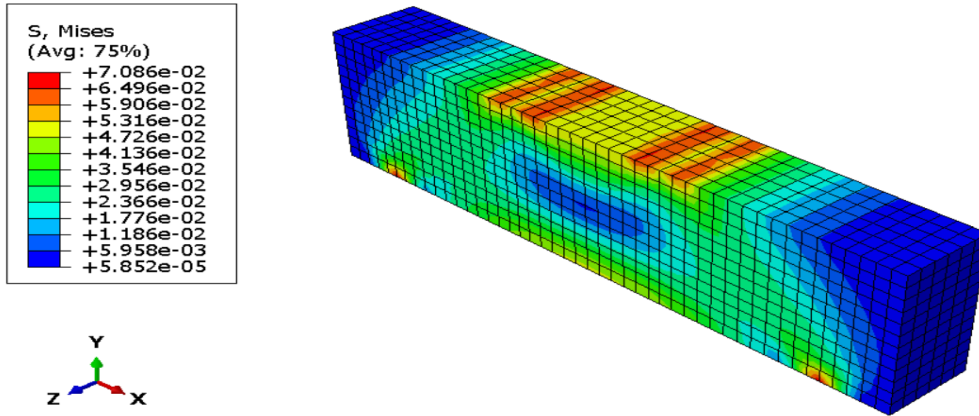
Figure 4.7: Concrete von Mises Stress Contour of C-01 at Initial Loading
Stage.
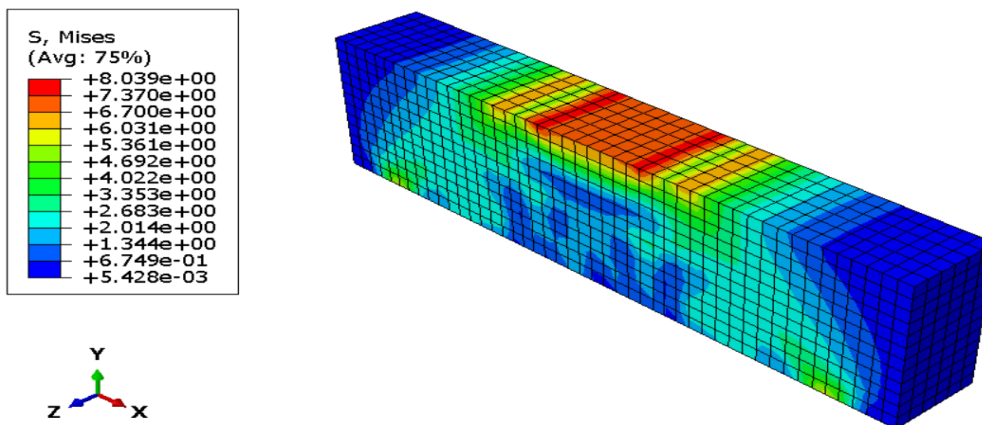
Figure 4.8: Concrete von Mises Stress Contour of C-01 at Diagonal Cracking
Stage.
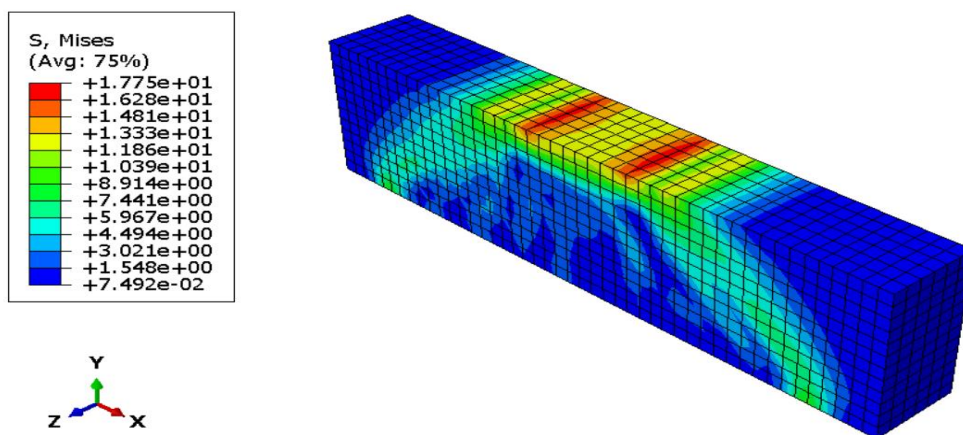
Figure 4.9: Concrete von Mises Stress Contour of C-01 at Final Loading
Stage.

4.4.1.2 Reinforcement Cage von Mises Stress Contour

Von Mises stress contour of reinforcement cage which composing of longitudinal reinforcements as well as vertical reinforcements were generated to visualise the stress distribution of those reinforcements throughout the loading process. When the load was applied initially, the stress contour concentrated at the bottom longitudinal reinforcements. As this could be explained based on the Strut-and-Tie Model (STM) where the reinforcement was designed as tension tie component which is to resist tensile force. When the concrete started to show significant flexural cracks, most of the tensile force in the beam will be resisted by the bottom longitudinal reinforcement. While, when the applied load continues to increase, formation of stress could be noticed at the vertical reinforcement. The formation of stress is due to the bursting tensile force within the concrete strut caused the widening of strut, which led to further cracking. Therefore, the vertical reinforcement was responsible to counteract the tensile force within the concrete strut for preventing further cracking. Therefore, this explained the present of stress in a diagonal pattern among the vertical reinforcement. The von Mises stress contour at failure load was generated for all specimens. The contour for numerical control beam, C-01 and numerical specimens D-700 were presented in Figure 4.10 and 4.11 respectively while stress contour for other specimens were attached in Appendix C. As been observed, the stress distribution pattern of reinforcement cage at failure load were almost similar for all specimens. Therefore, it is concluded that the stress distribution of reinforcement cage is not affected by the height of the deep beam specimens.
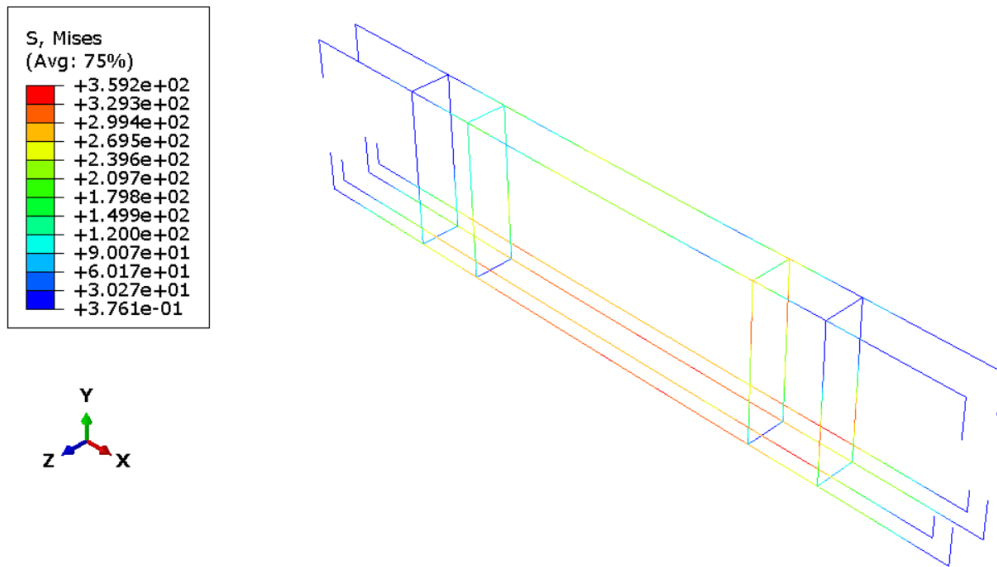
Figure 4.10: Reinforcement von Mises Stress Contour for C-01 at Failure Load.
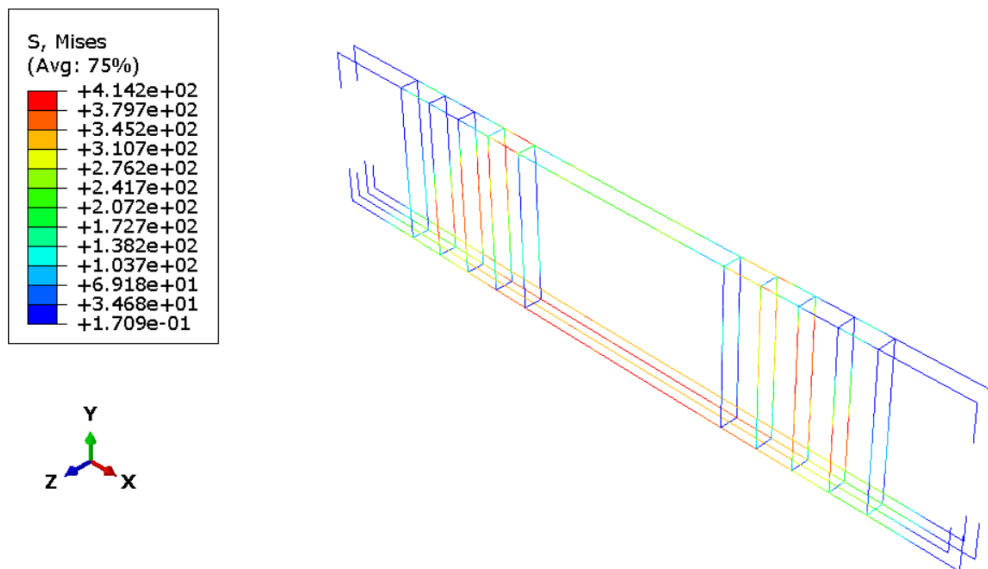
Figure 4.11: Reinforcement von Mises Stress Contour for Specimen D-700 at Failure Load.

4.4.2   Concrete Tension Damage Contour

Concrete Tension Damage Contour is able to describe the development of cracking path motion in the concrete beam. The concrete tension damage contour at different loading level was generated for all specimens. The cracking development of concrete specimen at each loading stages were observed to be similar for each specimen. Therefore, we can conclude in this section that the height of specimen does not affect the cracking path on each loading stages. The contour for control beam, C-01 at different loading stages are presented as shown in Figure 4.12, Figure 4.13 and Figure 4.14 while for other specimens were attached in Appendix C.

At the beginning of the loading stage, vertical crack started to form at the bottom midspan of the specimen. As loading increased, the vertical crack started to propagate upward and at the same time more vertical cracks were formed as shown in Figure 4.12. The vertical cracks are defined as flexural crack, and it is caused by the tensile stress formation at the bottom block of the beam. As the load started to increase further, diagonal crack will start to develop from the support plate and propagate diagonally toward the loading plate as shown in Figure 4.13. The diagonal cracks formation further proven the arch transfer mechanism in deep beam where the diagonal cracks is due to the bursting tensile force within the concrete struts. When the loading was further applied as shown in Figure 4.14, the diagonal cracks formation started to widen which indicating that more bursting tensile force happened at the concrete struts. Besides that, it could also be noticed that there are horizontal cracks and vertical cracks started to propagate from the edge and top face of the beam respectively. However, no obvious upward extension of vertical crack could be noticed for further applied loading. This is due to most of the tensile stress at the bottom part of the beam was resisted by the bottom longitudinal reinforcement. Therefore, no obvious flexural crack extension could be noticed.

In short, all beam specimens with different cross-sectional height shows similar cracking development where the specimens started with flexural cracks and then diagonal cracks. The diagonal cracks then widen and at the same time horizontal and vertical cracks develop at the edge and top of the specimen

respectively. Finally, the diagonal cracks further extend which lead to failure of specimens.
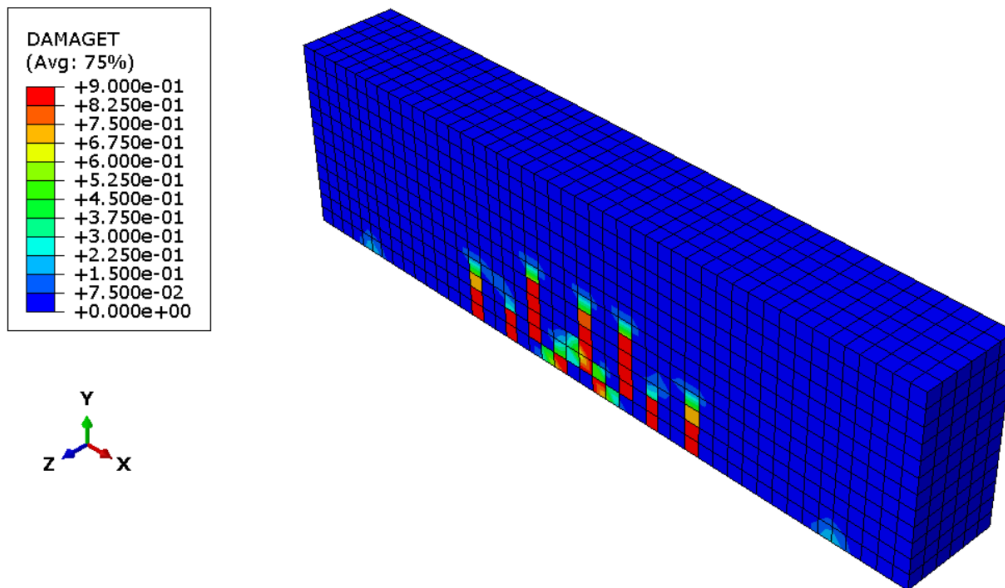
Figure 4.12: Concrete Tension Damage for C-01 at Initial Loading Stage.
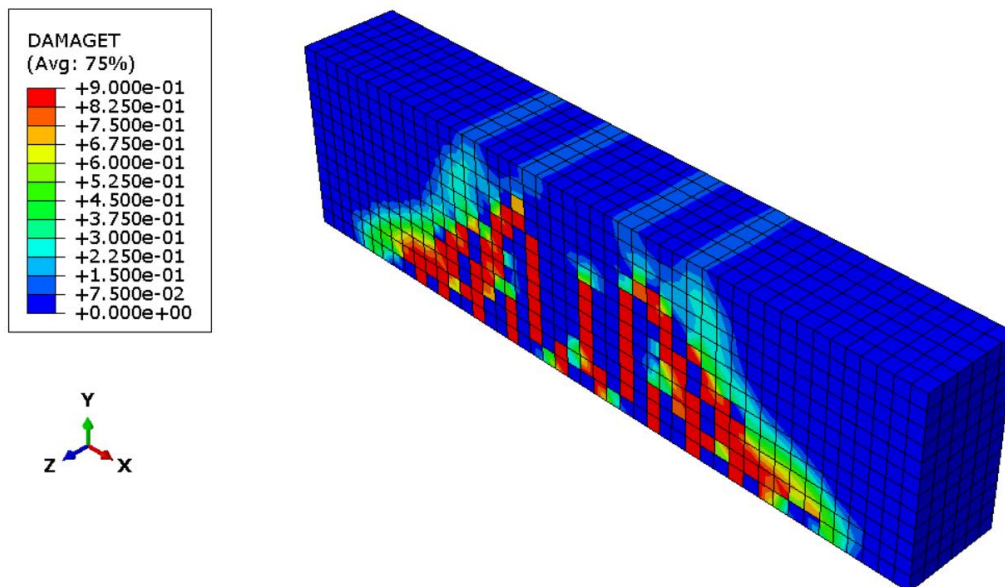
Figure 4.13: Concrete Tension Damage for C-01 at Diagonal Cracking Stage.
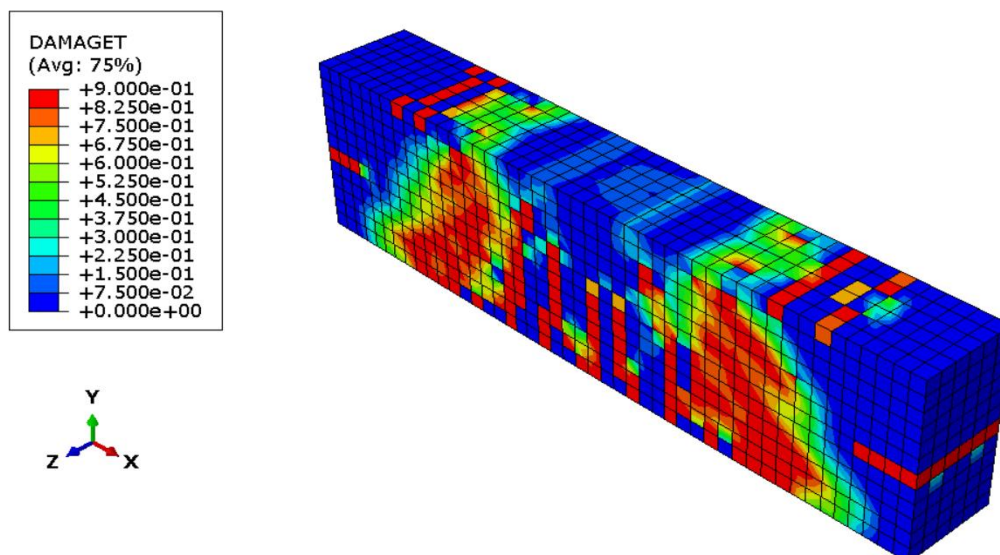
Figure 4.14: Concrete Tension Damage for C-01 at Final Loading Stage.

4.4.3   Plastic Strain Magnitude (PEMAG) Diagram

The plastic strain magnitude (PEMAG) diagram provides illustration of crack distribution of concrete in term of the plastic strain of concrete. When the load was applied initially, the concrete plastic strain could be noticed to form vertically at the bottom mid-span of the beam. As the load applied increased, the PEMAG diagram showed similar trend which has been noticed in Concrete Tension Damage Contour discussed earlier where the plastic strain elongated upwards and later diagonal plastic strains started to take place until failure occurred. The PEMAG diagram at failure load was generated for all specimens. The diagram for control beam, C-01 and specimens D-700 were presented in Figure 4.15 and 4.16 respectively while plastic strain diagram for other specimens were attached in Appendix C. All the specimen's PEMAG diagrams at failure load are rather similar. As could be seen from Figure 4.15 and 4.16, where both specimens have great amount of plastic strain at diagonal sections as well as horizontal strain at the side of the beam. Besides that, there were also flexural strain, however the strain values are smaller than the dominant diagonal strain. Therefore, the flexural strains were less visible in the diagrams.
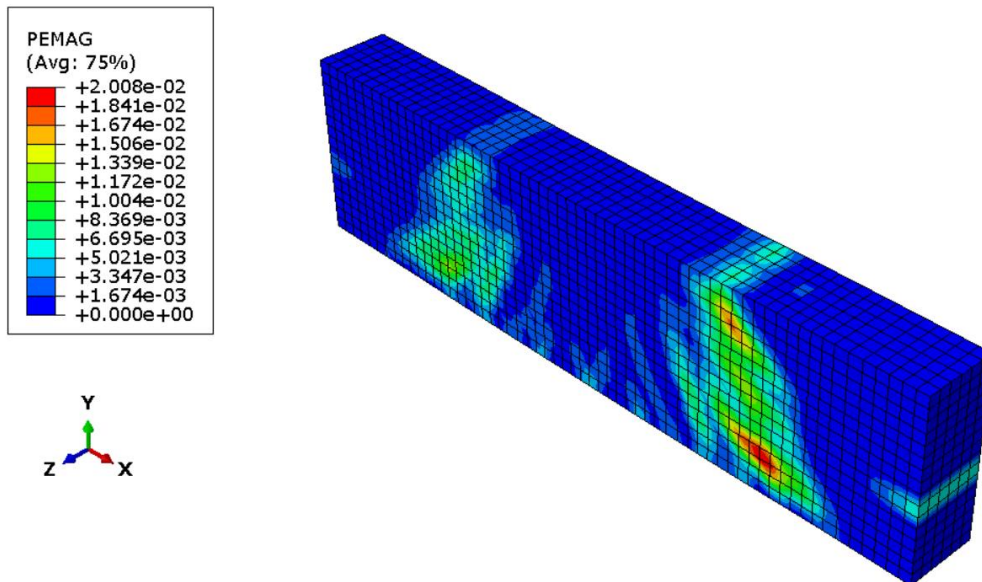
Figure 4.15: Plastic Strain Magnitude (PEMAG) Diagram for C-01at Failure
Load.
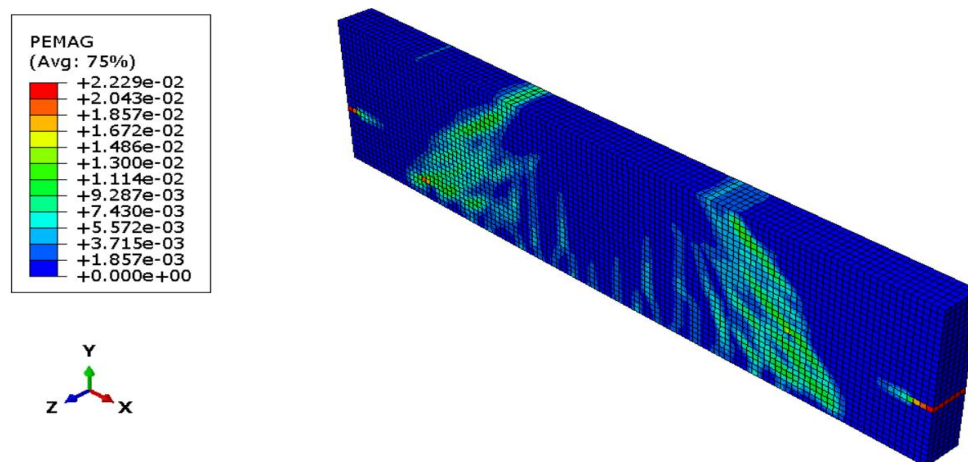
Figure 4.16: Plastic Strain Magnitude (PEMAG) Diagram for D-700 at Failure
Load.

4.5   Summary

All in all, a numerically modelled reference beam results generated using
ABAQUS software is resemble well with the experimental data by Zhang and
Ta (2007). Therefore, the modelling technique and material properties applied
in this study are proven accurate. A numerical control beam and 4 numerical
test specimens with different cross-section height were modelled and simulated
using ABAQUS software. A single combined load-displacement graph was

plotted and the ultimate failure load for each specimen were retrieved. It has been noticed that the ultimate failure of specimen increased as the cross-sectional height of beam increased. On the first 100 mm cross-sectional height increment, the ultimate failure load increased by 29.7 % and for the following 100 mm height incremental, the cumulative increments are computed as 54.4 %, 83.8 % and 110.6 % respectively. However, the normalised shear strength is detected to decreased which means that the increment of specimen's ultimate load is not proportional to the incremental of depth of the specimen. On the first 100 mm cross-sectional height increment, the normalized shear strength decreased by 4.29 % and for the following 100 mm height incremental, the cumulative decrements are found to be 11.07 %, 13.97 % and 16.95 % respectively. Therefore, the depth size effect is said to be taking place when the height of beam increases. Besides that, since the ultimate failure load is crucial in examining the depth size effect. CSTM calculation had been done to further validate the numerical results where the analyses showed low percentage of difference which ranged between 5.13% to 7.24 %. Besides that, the numerical graphical contours such as von Mises stress contour, concrete tension damage contour and plastic strain magnitude contour and were compared between specimens and it is concluded that the general behaviour of deep beam at each loading phases are about similar even though the cross-sectional height beams is increased.

CHAPTER 5

CONCLUSION AND RECOMMENDATIONS

5.1　Conclusion

In conclusion, deep beam finite element analysis was completed using ABAQUS software with the aim to study the depth size effect in simply supported reinforced concrete deep beams. Six numerical deep beam specimens were created which including one reference beam, R-01, one control beam, C-01, and 4 numerical test specimens with different cross-sectional height of 400 mm, 500 mm, 600 mm, and 700 mm which are denoted as D-400, D-500, D-600 and D-700 respectively. All the objectives of study were accomplished throughout the numerical analysis process.

The first objective of this study is to create a numerical reference beam using ABAQUS software and verify the numerical reference beam results with the experimental beam results. A numerical reference beam was modelled according to the modelling methodology as presented in Chapter 3 which covered the material properties modelling, interfacial properties modelling, boundary conditions, loading definition and assignment of mesh sizing. The numerical reference beam results generated were compared with the experimental results obtained by Zhang and Tan (2007) after fine-tuning process was done by conducting sensitivity analysis on the parameters of Concrete Damaged Plasticity model. A well matching load-displacement curve was observed where difference of the ultimate failure load was only 3.52 % and the difference in the corresponding mid span deflection was just 8.74 %. Moreover, the numerical cracking pattern generated by the concrete tension damage contour is in good agreement compared to the experiment observed pattern. Therefore, the numerical beam was verified to be reliable in simulating the actual behaviour of beam in real-life. Hence, the same modelling technique and material properties are reliable to be used to construct numerical control beam and numerical test specimens for the study of depth size effect.

The second objective is to evaluate the change in percentage of normalised shear strength of deep beam corresponding to the increment of

beam's cross-sectional height. Based on the result, the depth size effect was observed where the normalised shear strength versus effective depth curve shows a decreasing trend. The normalised shear strength decreased by 4.29 % for the first 100 mm beam height incremental and for the following additional of 100 mm beam height incremental, the normalised shear strength decreased by 11.07 %, 13.97 % and 16.95 % respectively. The decrement in relative depth of compressive zone which causes lower relative compressive struts strength is the contributing factor that causes the size effect.

The third objective is to study the stress behaviour and cracking pattern of deep beam when the cross-sectional height of the beam increases. From the graphical contours obtained, all the numerical deep beam specimens show similar traits of stress behaviour and cracking propagation. The stress distribution within the numerical specimen was observed by von Mises stress contour while the motion of crack propagation was observed through concrete tension damage contour. The stress distribution and cracking propagation at different loading level were similar between all different height of numerical specimens which inferred that the stress distribution and cracking path of deep beam does not greatly influence by beam height. All the numerical specimens were seen to be exhibiting characteristic of arch mechanism where the specimen stress level and tension cracking damage becomes critical at the location of diagonal struts when loading is applied to certain level.

5.2   Recommendations

The research on depth size effect in reinforced concrete deep beam are relatively scarce at this moment. Hence, there is room for improvement and modification could be done to meet various goals and objectives. The following recommendations could be considered to further study on this subject topic.

The first recommendation is to conduct laboratory test for numerical model verification purposes. As the current difficulties on carrying out physical experiment in the laboratory due to Covid-19 pandemic, the experimental test results were obtained from Zhang and Tan (2007). The experimental data provided by the authors is insufficient especially on the crack propagation data. Therefore, laboratory testing should be performed to generate experimental data

and validate it to numerical results in order to deliver a more persuasive conclusion.

Secondly, the depth size effect of reinforced concrete deep beam in other type of support condition such as partially fixed or fully fixed end could be studied. The deep beam with partially fixed or fully fixed end are more likely to be used in practical structures rather than simply supported conditions. However, the related study on such support condition available is extremely scarce as to the author knowledge, there is none being published. Therefore, it could be very helpful to carry out such research study.

Lastly, depth size effect of deep beam with larger cross-sectional height could be studied. As found from the literature, the study on experimental deep beam with height larger than 2 m is relatively scare and the numerical deep beam specimen found from other researchers was only up to 4 m height which is by Chen, Yi and Ma (2019). However, the height of deep beam could goes up to 6 m in practical (Yu et al., 2016). Therefore, the research study in the future could consider on selecting deep beam with larger cross-sectional height.

REFERENCES

American Concrete Institution, 2014. ACI 318R-14 Commentary on building code requirements for structural concrete. [online] Available at: <http://aghababaie.us c. ac.ir/files/150650520336 5.pdf> [Accessed 12 Jun 2021].

Bazant, Z. P., and Xiang, Y., 1997. *Size effect in compression fracture: Splitting crack band propagation*. [online] Journal of Engineering Mechanics. Available at:<https://eds-a-ebscohost com.libezp2.utar.edu.my/eds/pdfviewer/pdfviewer? vid=1&sid=f25b347a-4800-445e-8da0-d81a50e75dc9%40sessionmgr4007> [Accessed 9 Aug. 2021].

Beres, A.B. and Rabbatm B.G., 2007. Strut-and-Tie Model for Structural Concrete Design. [e-book] Portland Cement Association. Available at: Structure Point website <https://structurepoint.org/publication/pdf/pdh-Strut-And-Tie-Design-Method.pdf> [Accessed 20 July 2021].

Birrcher, D., Tuchscherer, R., Huizinga, M., Bayrak, O., Wood, S. and Jirsa, J., 2009. Strength and Serviceability Design of Reinforced Concrete Deep Beams. FHWA/TX-09, p.400.

Birrcher, D.B., Tuchscherer, R.G., Huizinga, M. and Bayrak, O., 2014. Depth effect in deep beams. *ACI Structural Journal*, 111(4), pp.731–740.

British Standard. 2004. Eurocode 2: Design of concrete structures – Part 1-1: General rules and rules for buildings. [online] Available at: <https://people.utm.my/noornabilah/files/2012/09/BSOL_DOWNLOADS_20 13-09-30-02-39-29.pdf> [Accessed 12 Jun 2021].

Carreira and Chu, 1985. Stress-Strain Relatonship for Reinforced Concrete in Compression. *ACI Structural Journal*, (November-December), pp.797–804.

Chen, H., Yi, W.J. and Hwang, H.J., 2018. Cracking strut-and-tie model for shear strength evaluation of reinforced concrete deep beams. *Engineering Structures*, [online] 163(November 2017), pp.396–408. Available at: <https://doi.org/10.1016/j.engstruct.2018.02.077>.

Chen, H., Yi, W.J. and Ma, Z.J., 2019. Shear size effect in simply supported RC deep beams. *Engineering Structures*, [online] 182(August 2018), pp.268–278. Available at: <https://doi.org/10.1016/j.engstruct.2018.12.062>.

Dassault Systèmes Simulia Corp., 2017. *Applying Boundary Conditions to the Frame*. [online] Available at: <https://abaqus-docs.mit.edu/2017/ English/SIM ACAEGSARefMap/simagsa-t-applyingboundaryconditionstotheframe.htm> [Accessed 10 August 2021].

Dassault Systèmes Simulia Corp., 2017. *Embedded Elements*. [online] Available at: <https://abaqus-docs.mit.edu/2017/English/SIMACAECSTRefMap/simacst-c-embeddedelement.htm> [Accessed 10 August 2021].

European Commision, 2004. BS EN 1992-1-1:2004 Eurocode 2: Design of concrete structures – Part 1-1: General rules and rules for buildings.

Ghugal, Y.M. and Dahake, A.G., 2012. Flexural analysis of deep beam subjected to parabolic load using refined shear deformation theory. *Applied and Computational Mechanics*, 6, pp.163–172.

Hussein, G., Sayed, S.H., Nasr, N.E. and Mostafa, A.M., 2018. Effect of loading and supporting area on shear strength and size effect of concrete deep beams. *Ain Shams Engineering Journal*, 9(4), pp.2823–2831.

Ibrahim, A.M. and Mohmood, M., 2009. *Finite Element Modeling of Reinforced Concrete Beams Strengthened with FRP Laminates*. [online] European Journal of Scientific Reseach. Available at: <https://www.researchgate.net/publication/242163873_Finite_Element_Modeling_of_Reinforced_Concrete_Beams_Strengthened_with_FRP_Laminates> [Accessed 21 Mar. 2022].

Ismail, K.S., Guadagnini, M. and Pilakoutas, K., 2017. Shear behavior of reinforced concrete deep beams. *ACI Structural Journal*, 114(1), pp.87–99.

Jasim, W.A., Tahnat, Y.B.A. and Halahla, A.M., 2020. Behavior of reinforced concrete deep beam with web openings strengthened with (CFRP) sheet. [online] Available at: <https://doi.org/10.1016/j.istruc.2020.05.003> [Accessed 24 Jun. 2021].

Lertsrisakulrat, T., Yanagawa, A., Matsuo, M., and Niwa, J., 2001. Shear Behaviour of RC Deep Beam with Stirrups, *Transaction of the Japan Institute*, Vol. 23, pp. 385-390.

Lafta, Y.J. and Ye, K., 2016. Specification of deep beams affect the shear strength capacity. *Civil and Environmental Research*, 8(2), pp.56–68.

Laughery, L. and Pujol, S., 2015. Compressive strength of unreinforced struts. *ACI Structural Journal*, 112(5), pp.617–623.

Lima, M.M., Doh, J.H., Hadi, M.N.S. and Miller, D., 2016. The effects of CFRP orientation on the strengthening of reinforced concrete structures. *Structural Design of Tall and Special Buildings*, 25(15), pp.759–784.

Matsuo, M. Lertsrisakulrat, T., Yanagawa, and Niwa, J., 2001. Shear Tests of Reinforced Concrete Deep Beams. *JCI committee report on test method for fracture property of concrete*.

Matsuo, M., Lertsrisakulrat, T., Yanagawa, A. and Niwa, J. (2002). Shear Behavior of RC Deep Beams with Stirrups, Transaction of the Japan Concrete Institute, Vol. 23, pp. 385- 390.

Mohamed, A.R., Shoukry, M.S. and Saeed, J.M., 2014. Prediction of the behavior of reinforced concrete deep beams with web openings using the finite element method. *Alexandria Engineering Journal*, 53(2), pp.329–339.

Mphonde, A. G. and Frantz G.C., 1984. Shear tests of high-and low-strength concrete beams without stirrups. ACI Journal Proceedings, ACI.

Niranjan, B.R. and Patil, S.S., 2012. Analysis of R.C Deep Beam by Finite Element Method. *International Journal of Modern Engineering Research*, 2(6), pp.4664–4667.

Pauw, A., 1960. Static modulus of elasticity of concrete as affected by density. ACI Jorunal, Proceedings,[e-journal] 57(12), pp.679-687.https:// doi.org/10.14 359/8040.

Rai, P., 2021. Non-Linear Finite Element Analysis of RC Deep Beam Using CDP Model. *Advances in Technology Innovation*, 6(1), pp.01–10.

Reinhardt, H. W., 1981. Similitude of brittle fracture of structural concrete. Proc. Advanced Mechanics of Reinforced Concrete, IABSE Colloquium, Delft, The Netherlands, 175–184.

Rewers, I., 2019. Numerical Analysis of RC beam with High Strength Steel Reinforcement using CDP model. *IOP Conference Series: Materials Science and Engineering*, 471(2).

Said, M., Adam, M.A., Arafa, A.E. and Moatasem, A., 2020. Improvement of punching shear strength of reinforced lightweight concrete flat slab using different strengthening techniques. Journal of Building Engineering, [online] 32(August), p.101749. Available at: <https://doi.org/10.1016/j.jobe.2020.1017 49> [Accessed 24 Jun 2021].

Saurabh and Yadav, Y., 2016. Literature review on finite element method. International Journal of Enhanced Research in Science, Technology & Engineering, 5(3).
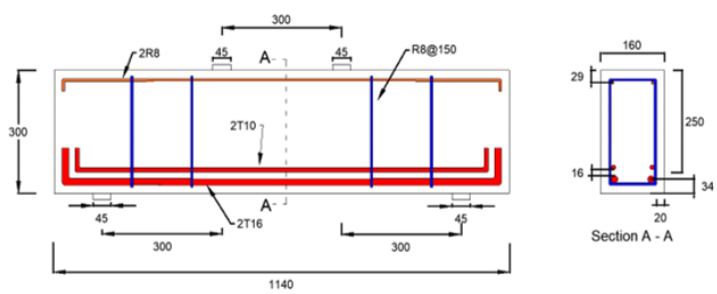
Shah, A., Haq, E. and Khan, S., 2011. Analysis and design of disturbed regions in concrete structures. *Procedia Engineering*, [online] 14, pp.3317–3324. Available at: <http://dx.doi.org/10.1016/j.proeng.2011.07.419>.

Shahnewaz, M., 2013. Shear behavior of reinforced concrete deep beams under static and dynamic loads. Master. University of British Columbia. Available at: <https://www.researchgate.net/publication/343083828_SHEAR_BEHAVIOR _OF_REINFORCED_CONCRETE_DEEP_BEAMS_UNDER_STATIC_AN D_DYNAMIC_LOADS> [Accessed 26 Jun 2021].

Tan, K.H. and Cheng, G.H., 2006. Size Effect on Shear Strength of Deep Beams: Investigating with Strut-and-Tie Model. *Journal of Structural Engineering*, 132(5), pp.673–685.

Tan, K.H., Kong, F.K., Teng, S. and Guan, L., 1995. High-strength concrete deep beams with effective span and shear span variations. ACI Structural Journal 92(4).

Tan, K. H., and Lu, H. Y. (1999). Shear behaviour of large reinforced concrete deep beams and code comparisons. *ACI Struct. J.,* 96(5), 836 - 845.

Taylor, H. P. J., 1972. Shear strength of large beams. J. Struct. Div. ASCE, 98(11), 2473–2490.

Wahalathantri, B.L., Thambiratnam, D.P., Chan, T.H.T. and Fawzia, S., 2011. A material model for flexural crack simulation in reinforced concrete elements using ABAQUS. *First International Conference on Engineering, Design and Developing the Built ENvironment for Sustainable Wellbeing*, (April), pp.260–264.

Weibull, W., 1939. Phenomenon of rupture in solids. Ingen.-skapsakad. Handl., 153, 1–55.

Yu, Q., Le, J.L., Hubler, M.H., Wendner, R., Cusatis, G. and Bažant, Z.P., 2016. Comparison of main models for size effect on shear strength of reinforced and prestressed concrete beams. *Structural Concrete*, 17(5), pp.778–789.

Zhang, N. and Tan, K.H., 2007. Size effect in RC deep beams: Experimental investigation and STM verification. *Engineering Structures*, 29(12), pp.3241–3254.

APPENDICES

Appendix A: CSTM Sample Calculation

Reference	Calculation	Output
	Specification of Control Beam Cylinder compressive strength, $f_c' = 25.9$ Mpa Modulus elasticity of concrete $E_c = 26409$ Mpa Modular elasticity of steel $E_s = 200$ Gpa Yield stress of longitudinal reinforcement, $f_y = 499$Mpa Yield stress of vertical reinforcement, $f_{vy} = 370$Mpa Ratio of vertical reinforcement, $\rho_v = 0.4$ % Ratio of longitudinal reinforcement, $p = 1.2\%$ Yield strain of longitudinal reinforcement, $\varepsilon_y = 0.00264$ 	
Chen, Yi and Hwang (2018)	Ratio of Elastic Modular, $n = \dfrac{E_S}{E_C}$ $$= \frac{200,000\text{Mpa}}{26409 \text{ Mpa}} = 7.57$$ Compressive zone depth, $\text{c} = \left(\sqrt{(np)^2 + 2np} - np\right)d$ $$= \left(\sqrt{(7.57\text{x}0.012)^2 + 2\text{x}7.57\text{x}0.012}\right.$$ $$\left. - 7.57\text{x}0.012\right)250$$ $$= 86.3\text{mm}$$ Strut angle, $\theta = tan^{-1}\left(\dfrac{d-\frac{c}{2}}{a}\right)$ $$= tan^{-1}\left(\frac{250-\frac{86.3}{2}}{300}\right)$$ $$= 34.6°$$	

Reference	Calculation	Output
	Critical shear crack angle, α $$\alpha = 8.53 \left(\frac{a}{d} - 2.5\right)^2 + 30.55 \geq tan^{-1}\left(\frac{h}{a + \frac{l_{bt}}{2} - \frac{l_{bs}}{2}}\right)$$ $$= 8.53 \left(\frac{300}{250} - 2.5\right)^2 + 30.55 \geq tan^{-1}\left(\frac{300}{300 + \frac{45}{2} - \frac{45}{2}}\right)$$ $$= 45.0° \geq 45.0°$$	Ok
	Width of strut at uncrack face, w_{si} $$w_{si} = \left[tan\theta \cdot l_{bt} + \frac{c \cdot (tan\alpha - tan\theta)}{tan\alpha + c/l_{bt}}\right] cos\theta$$ $$w_{si} = \left[tan(34.6) \cdot 45 + \frac{86.3 \cdot (tan45 - tan34.6)}{tan45 + 86.3/45}\right] cos34.6$$ $$w_{si} = 33.1 \text{ mm}$$	
	Width of strut at cracked face, w_{sc} $$w_{sc} = \left[c - \frac{c \cdot (tan\alpha - tan\theta)}{tan\alpha + c/l_{bt}}\right] cos\theta$$ $$w_{sc} = \left[86.3 - \frac{86.3 \cdot (tan45 - tan34.6)}{tan45 + 86.3/45}\right] cos34.6$$ $$w_{sc} = 63.5 \text{ } mm$$	
	Effective compressive strength by reinforcement, $\sigma_{cc,s}$ $$\sigma_{cc,s} = \frac{0.45\rho_v d cot^3 \alpha}{w_s sin\theta} \leq \frac{0.9f_{vy}\rho_v d cot\alpha}{w_{sc} sin\theta}$$ $$\sigma_{cc,s} = \frac{0.45 \text{x} 499 \text{x} 250 \text{x} cot^3 45}{63.5 sin\theta} \leq \frac{0.9 \text{x} 370 \text{x} 0.004 \text{x} 250 cot45}{63.5 sin34.6}$$ $$\sigma_{cc,s} = 6.25 \text{ Mpa} \leq 9.25 \text{ Mpa}$$	Ok

Reference	Calculation	Output
Laughery and Pujol (2015)	Effective compressive strength by aggregate interlock, $$\sigma_{cc,ag} = \frac{1.33\sqrt{f_c'}}{0.31 + 0.34\alpha\varepsilon_y/sin\alpha}$$ $$\sigma_{cc,ag} = \frac{1.33\sqrt{25.9}}{0.31 + 0.34 \text{x} 250 \text{x} 0.00264/sin45}$$ $$\sigma_{cc,ag} = 9.80 \text{ Mpa}$$ Coefficient of strut efficiency at crack region, β_{sc} $$\beta_{sc} = \frac{\sigma_{cc,ag} + \sigma_{cc,s}}{f_c'} \leq \left(1 - \frac{f_c'}{250}\right)\beta_{si}$$ $$\beta_{sc} = \frac{9.80 + 6.25}{25.9} \leq \left(1 - \frac{25.9}{250}\right)0.85$$ $$\beta_{sc} = 0.62 \leq 0.76$$ Resultant force from uncrack region, F_{si} $$F_{si} = \left(1 - \frac{f_c'}{250}\right)\beta_{si}f_c'w_{si}b$$ $$F_{si} = \left(1 - \frac{25.9}{250}\right)0.85 \text{x} 25.9 \text{x} 33.1 \text{x} 160$$ $$F_{si} = 104.4 \text{ kN}$$ Resultant force from cracked region, F_{sc} $$F_{sc} = \beta_{sc}f_c'w_{sc}b$$ $$F_{sc} = 0.62 \text{x} 25.9 \text{x} 63.5 \text{x} 160$$ $$F_{sc} = 163.0 \text{kN}$$ Shear capacity, V_n $$V_n = (F_{si} + F_{sc}) \cdot sin\theta$$ $$V_n = (104.4 + 163.0) \cdot sin34.6$$ $$V_n = 151.8 \text{ kN}$$ For two-point loading, Total shear strength, $2V_n = 303.6 \text{ kN}$	Ok

Appendix B: Load Displacement Curves
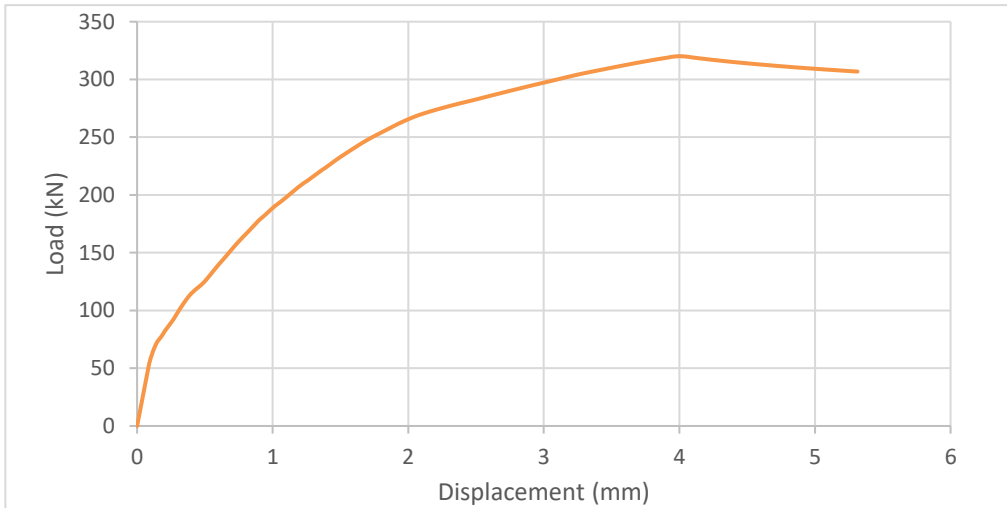
Figure B-1: Load-Displacement Curve of Numerical Control Beam, C01.
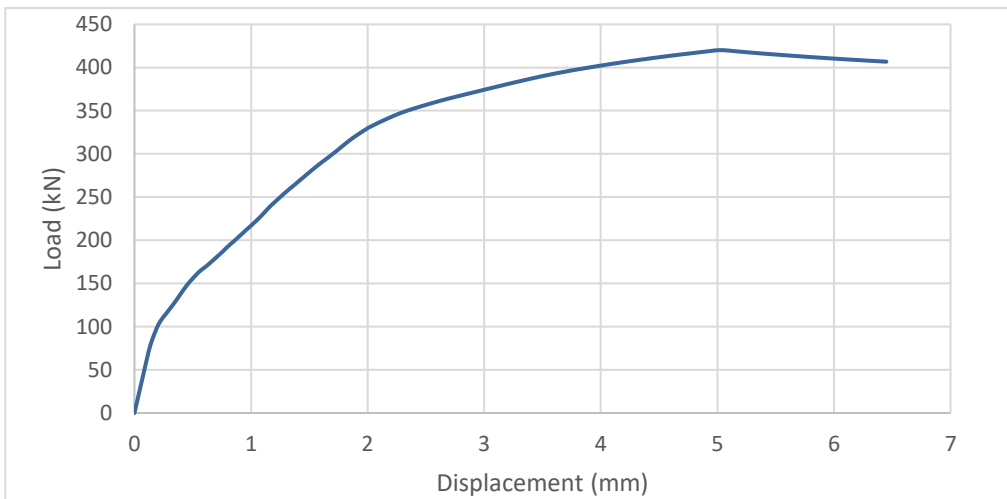
Figure B-2: Load-Displacement Curve of Numerical Test Specimen, D-400.
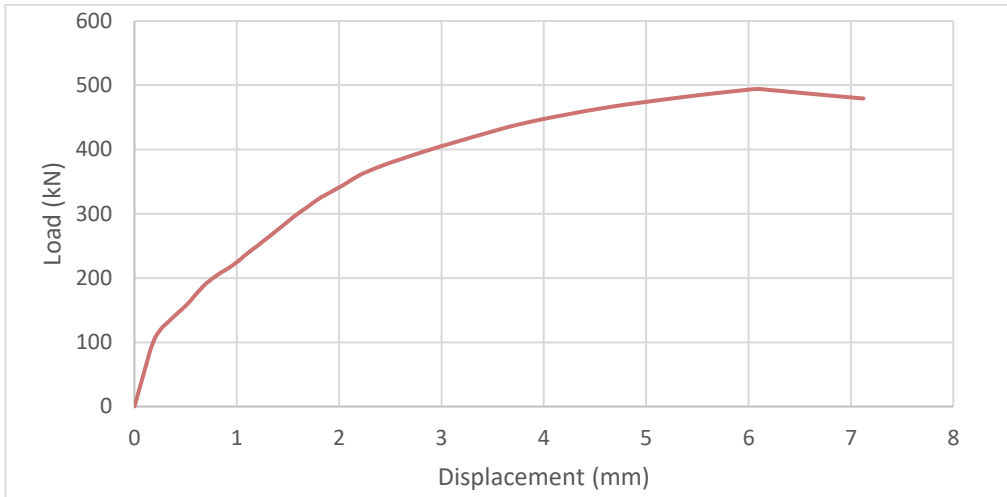
Figure B-3: Load-Displacement Curve of Numerical Test Specimen, D-500.
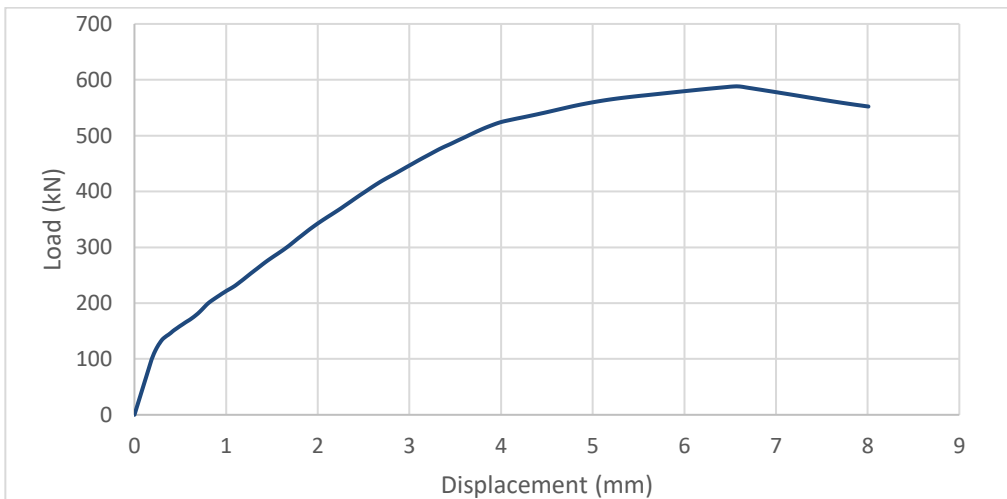
Figure B-4: Load-Displacement Curve of Numerical Test Specimen, D-600.
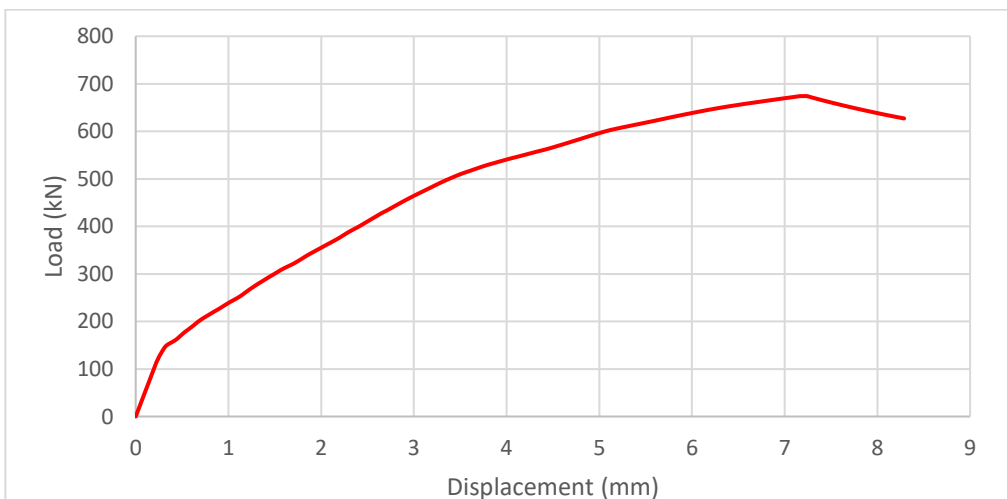
Figure B-5: Load-Displacement Curve of Numerical Test Specimen, D-700.

Appendix C: Graphical Contours
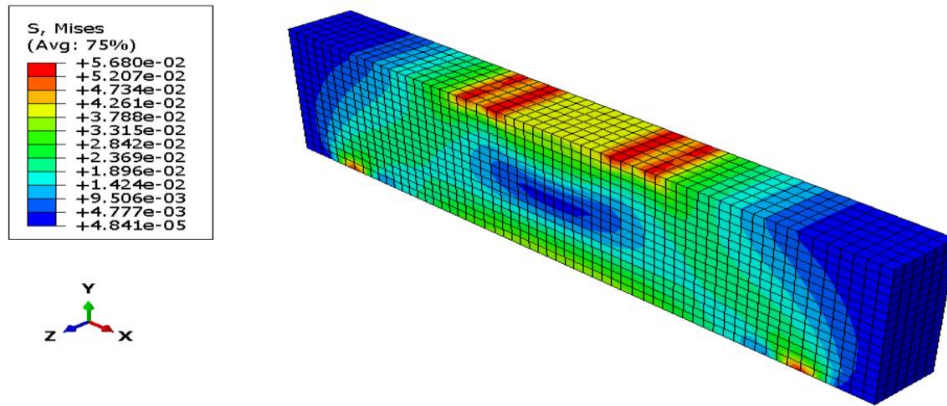
Figure C-1: Concrete von Mises Stress Contour of D-400 at Initial Loading
Stage.
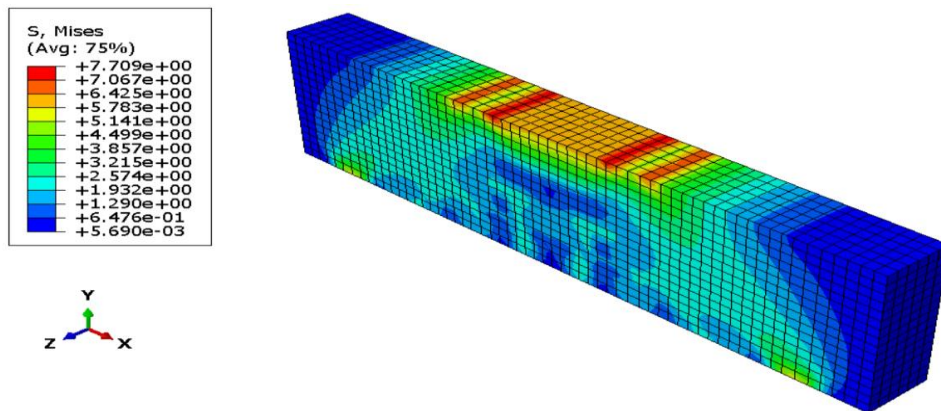
Figure C-2: Concrete von Mises Stress Contour of D-400 at Diagonal
Cracking Stage.
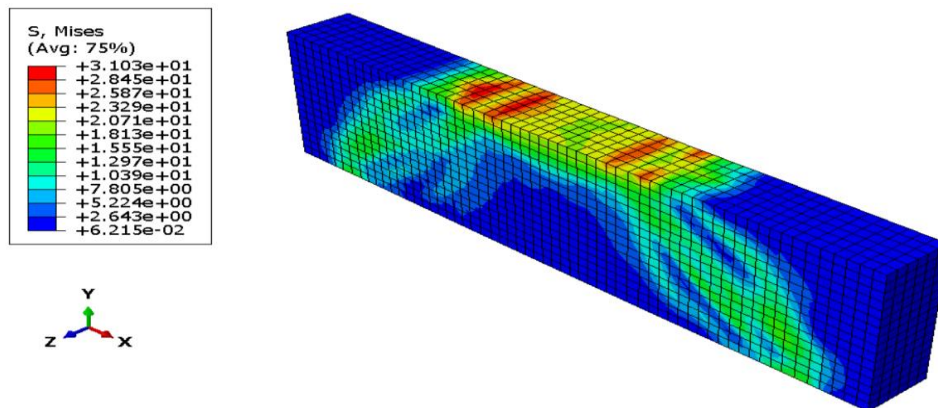
Figure C-3: Concrete von Mises Stress Contour of D-400 at Final Loading
Stage.
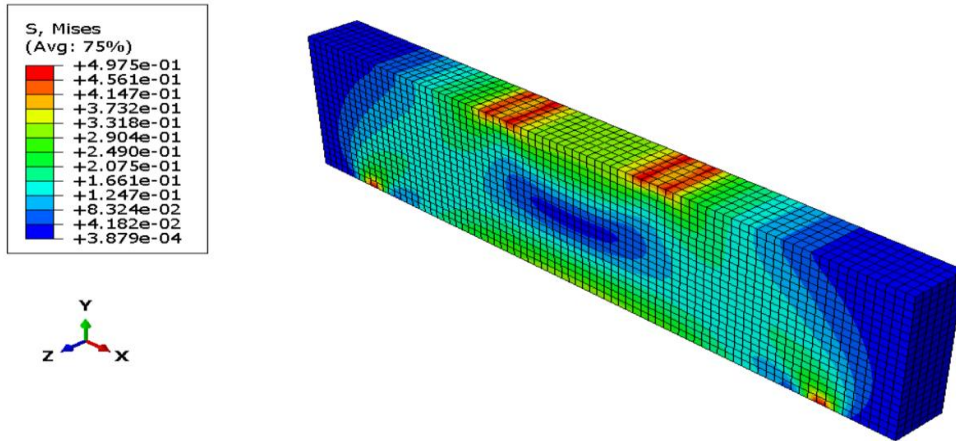
Figure C-4: Concrete von Mises Stress Contour of D-500 at Initial Loading
Stage.
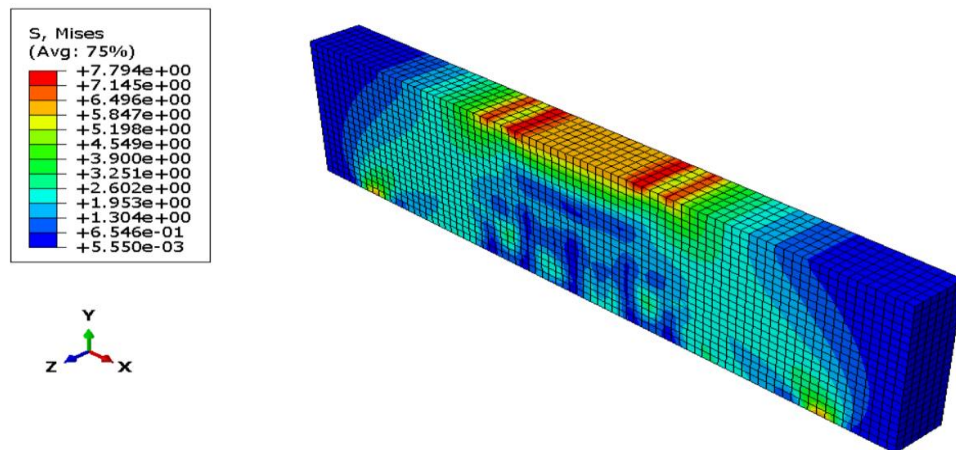
Figure C-5: Concrete von Mises Stress Contour of D-500 at Diagonal
Cracking Stage.
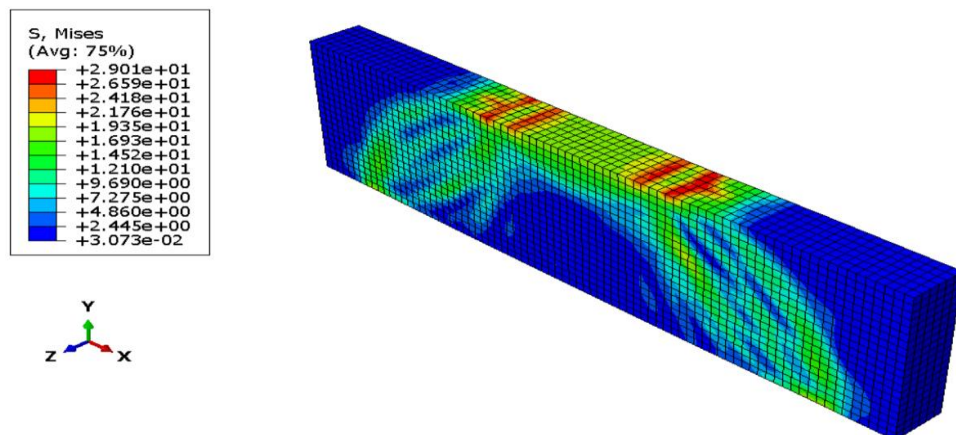
Figure C-6: Concrete von Mises Stress Contour of D-500 at Final Loading
Stage.
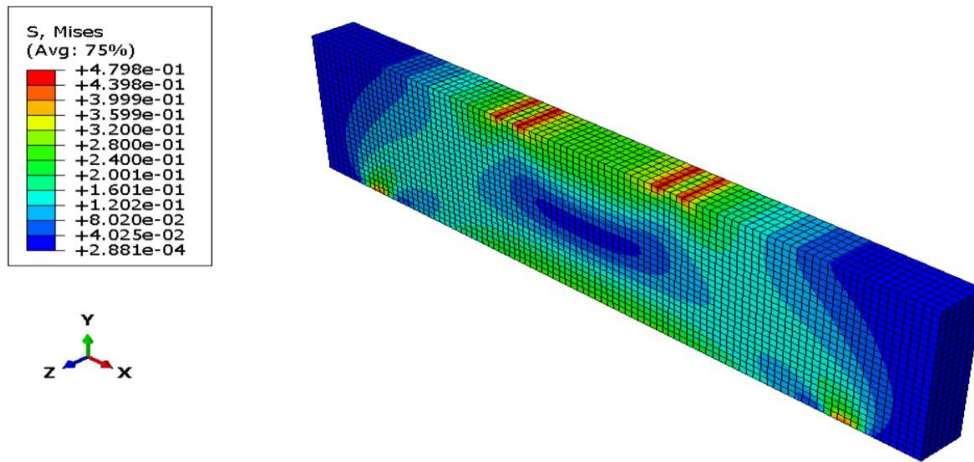
Figure C-7: Concrete von Mises Stress Contour of D-600 at Initial Loading
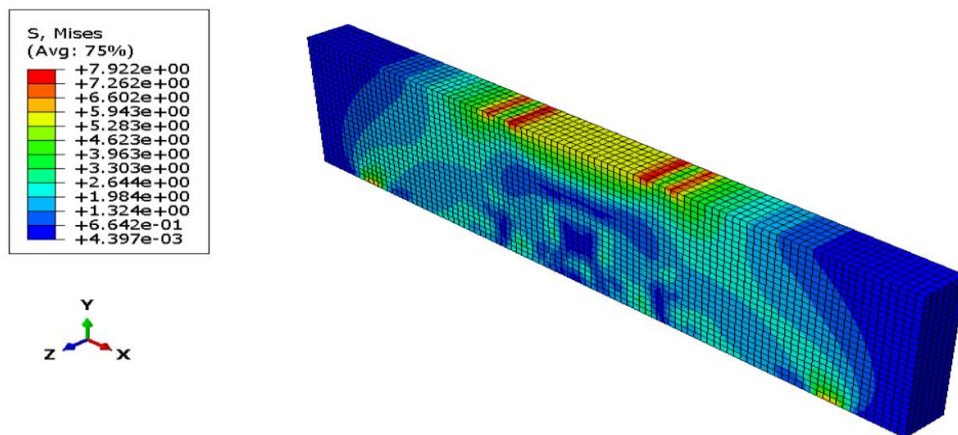
Stage.

Figure C-8: Concrete von Mises Stress Contour of D-600 at Diagonal

Cracking Stage.
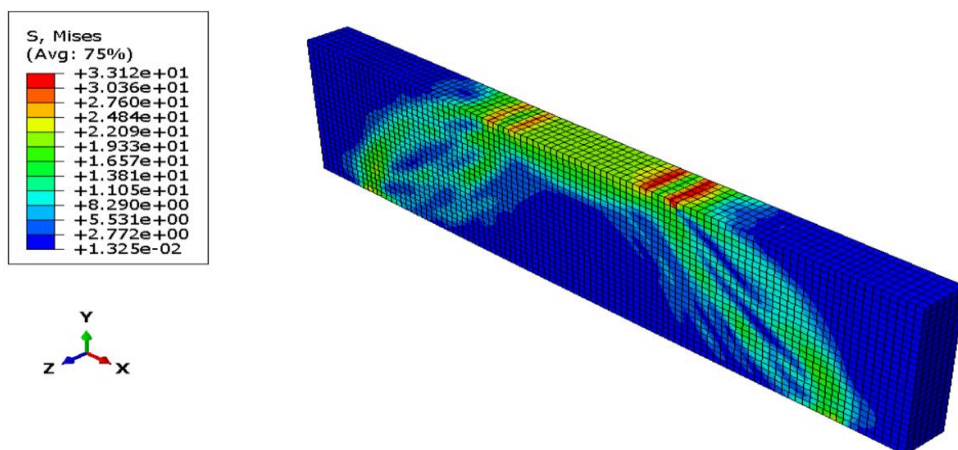
Figure C-9: Concrete von Mises Stress Contour of D-600 at Final Loading
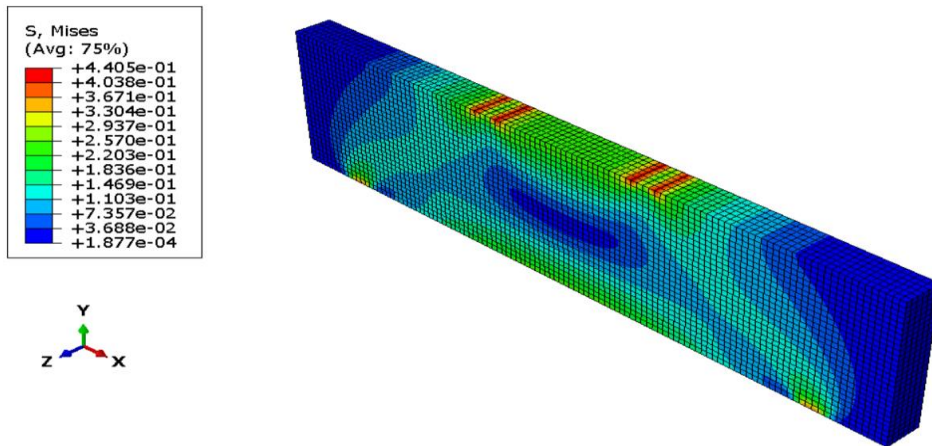
Stage.

Figure C-10: Concrete von Mises Stress Contour of D-700 at Initial Loading
Stage.
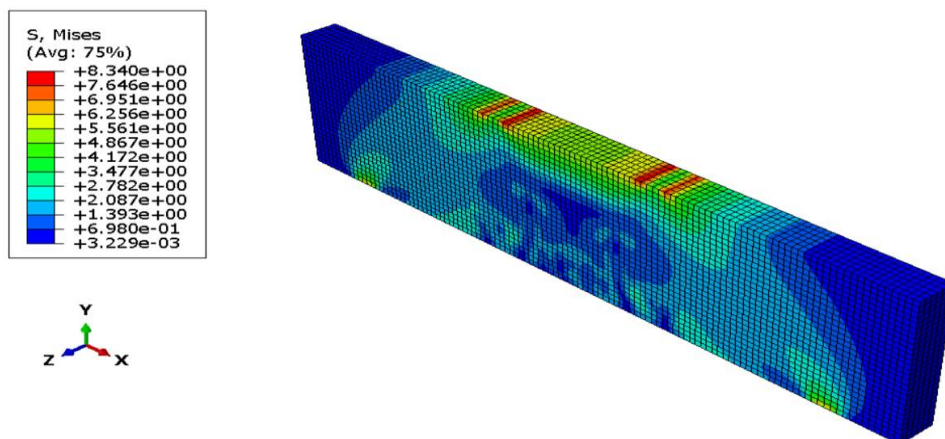
Figure C-11: Concrete von Mises Stress Contour of D-700 at Diagonal
Cracking Stage.
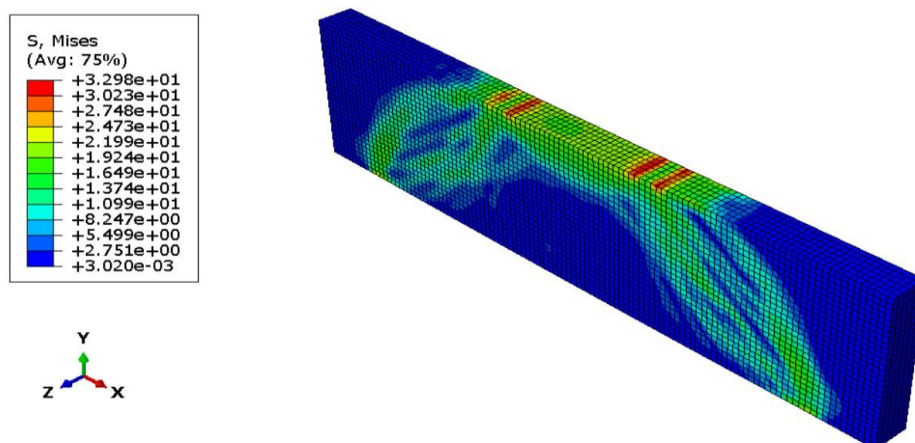
Figure C-12: Concrete von Mises Stress Contour of D-700 at Final Loading
Stage.
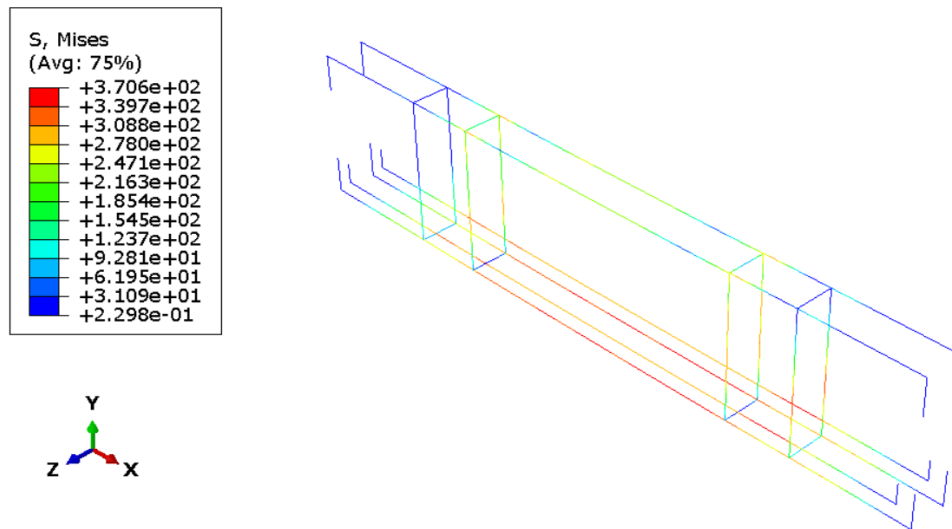
Figure C-13: Reinforcement von Mises Stress Contour for Specimen D-400 at Failure Load.
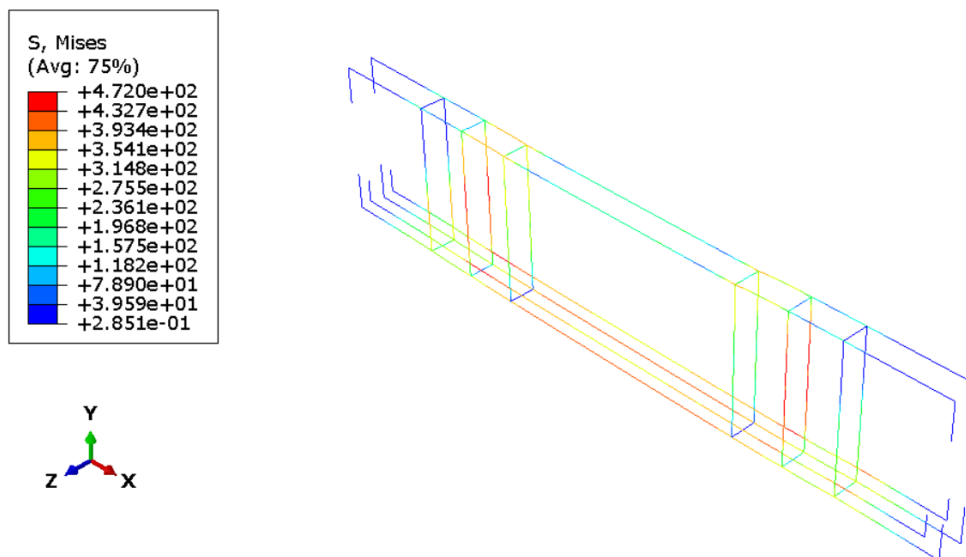
Figure C-14: Reinforcement von Mises Stress Contour for Specimen D-500 at Failure Load.
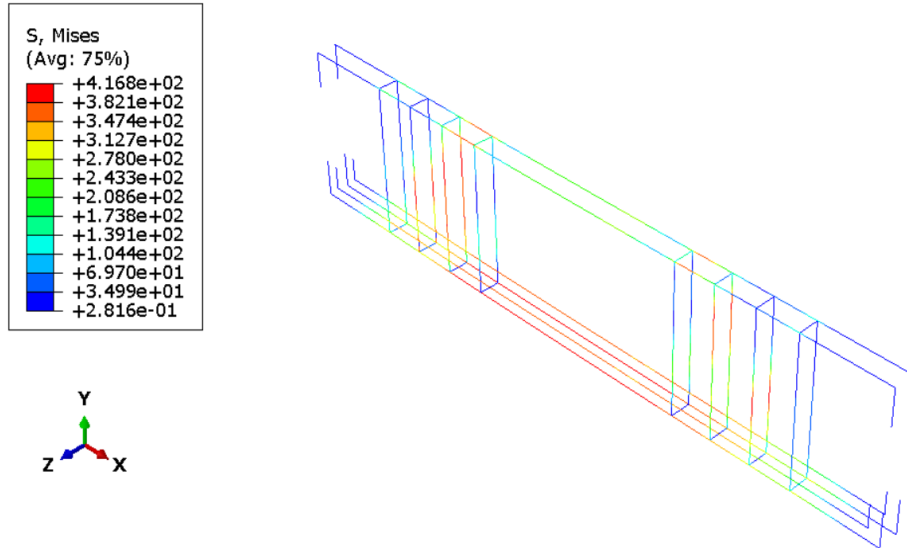
Figure C-15: Reinforcement von Mises Stress Contour for Specimen D-600 at Failure Load.
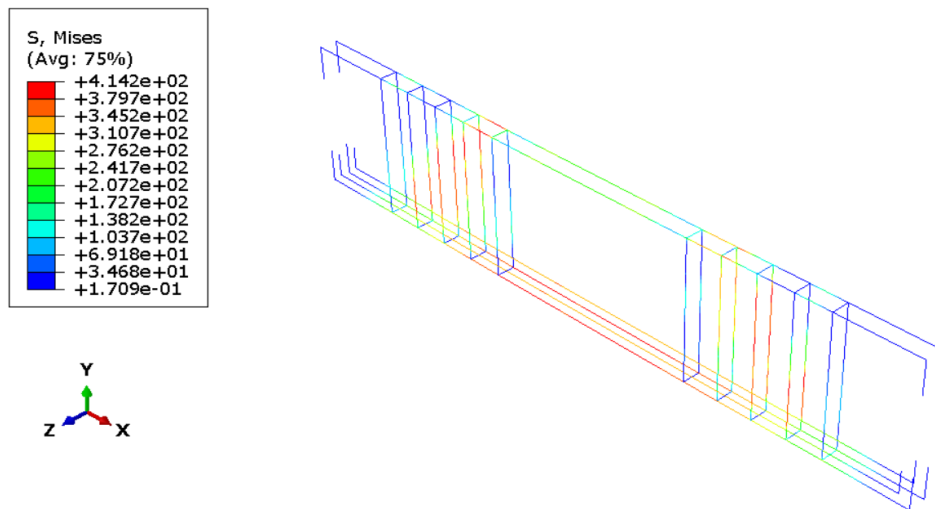
Figure C-16: Reinforcement von Mises Stress Contour for Specimen D-700 at Failure Load.
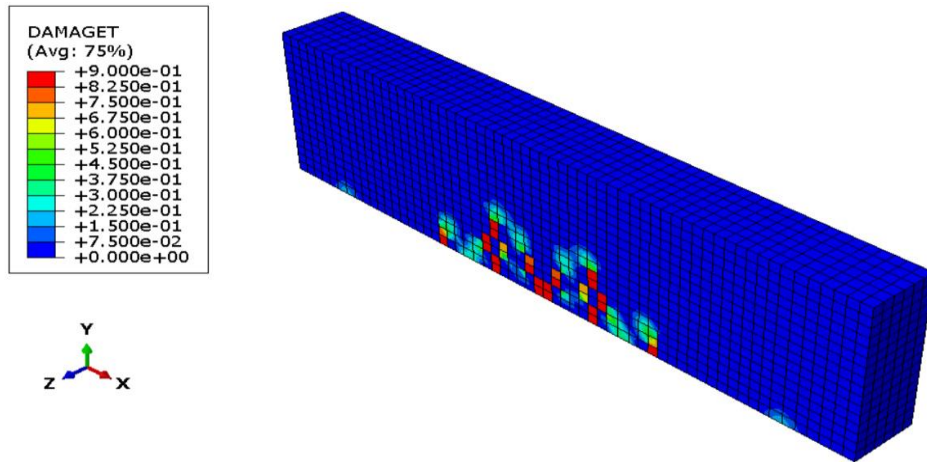
Figure C-17: Concrete Tension Damage for Specimen D-400 at Initial Loading
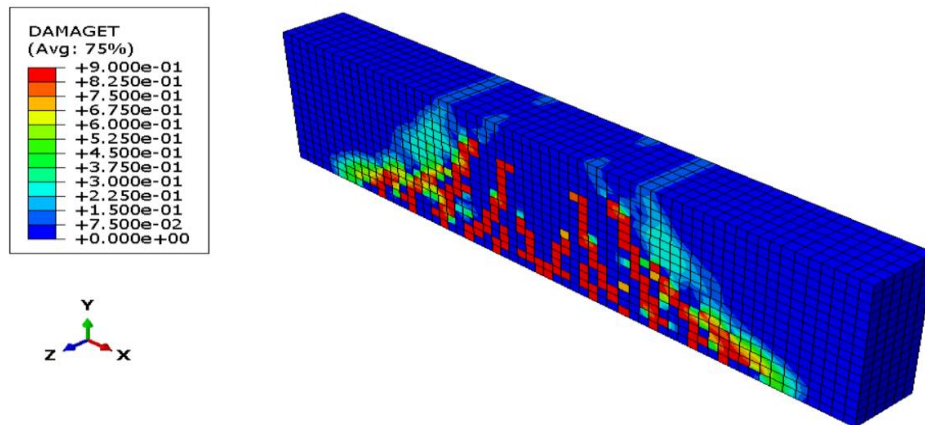
Stage.

Figure C-18: Concrete Tension Damage for Specimen D-400 at Diagonal

Cracking Stage.
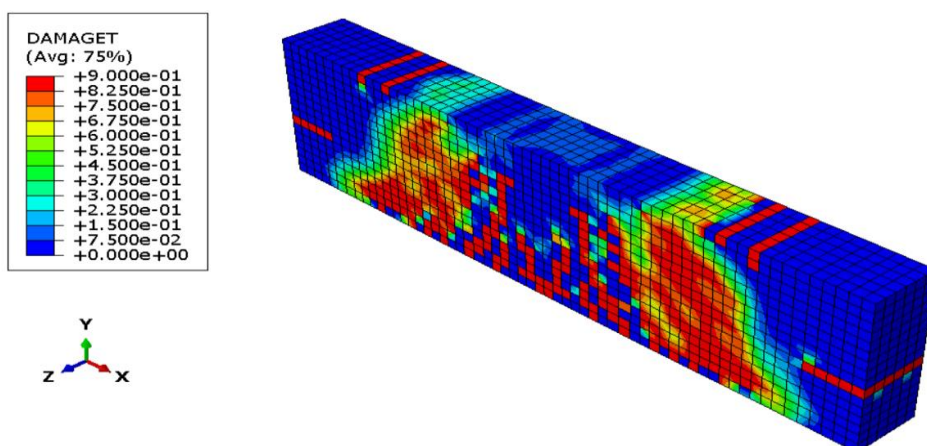
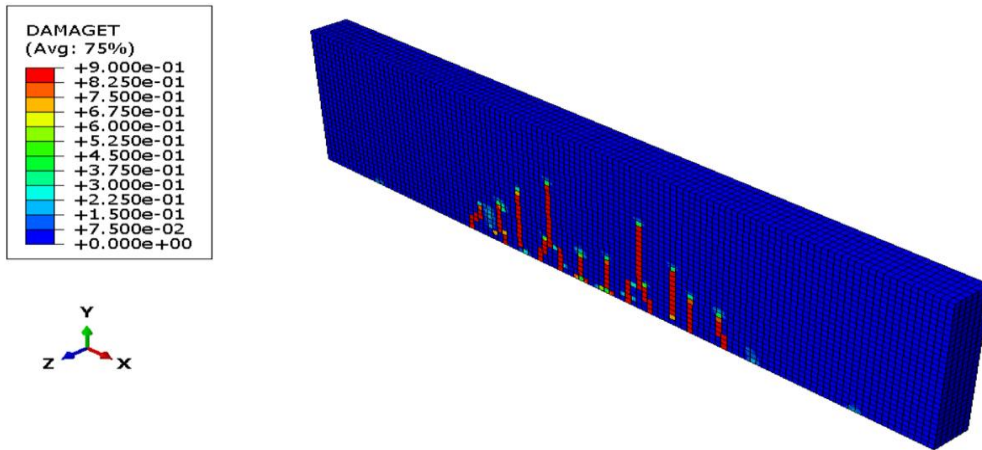Figure C-19: Concrete Tension Damage for Specimen D-400 at Final Loading
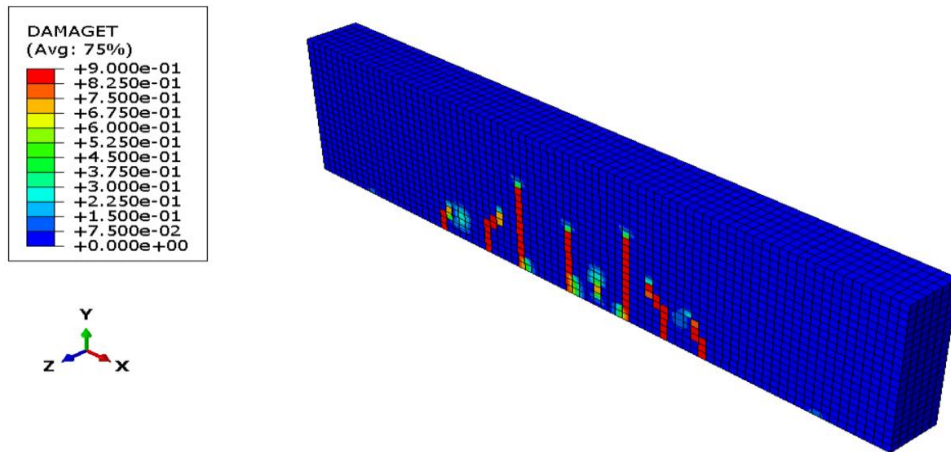
Stage.

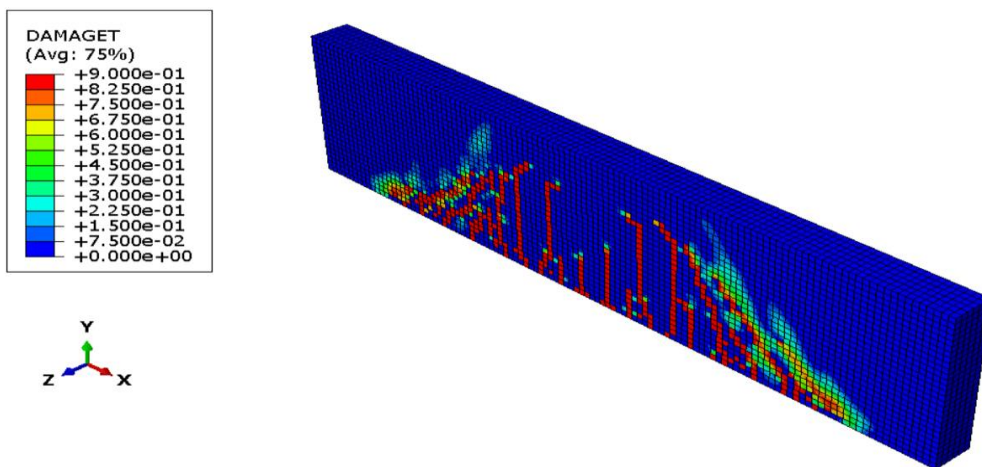Figure C-20: Concrete Tension Damage for Specimen D-500 at Initial Loading
Stage.
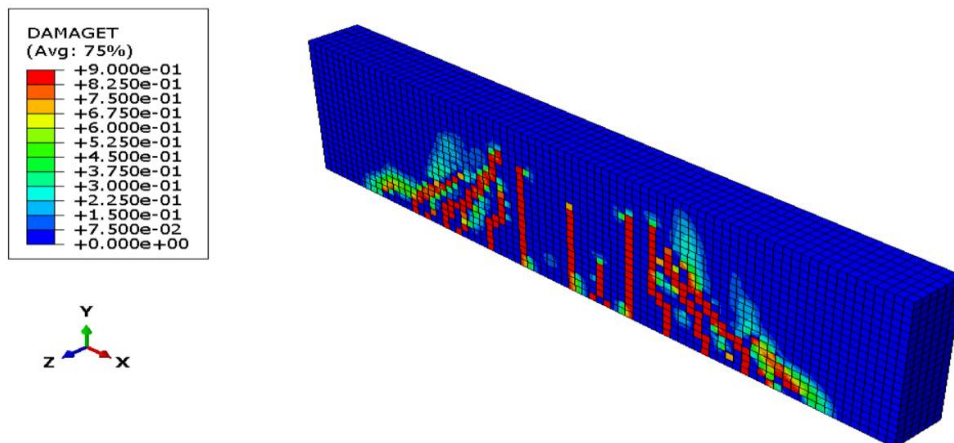
Figure C-21: Concrete Tension Damage for Specimen D-500 at Diagonal
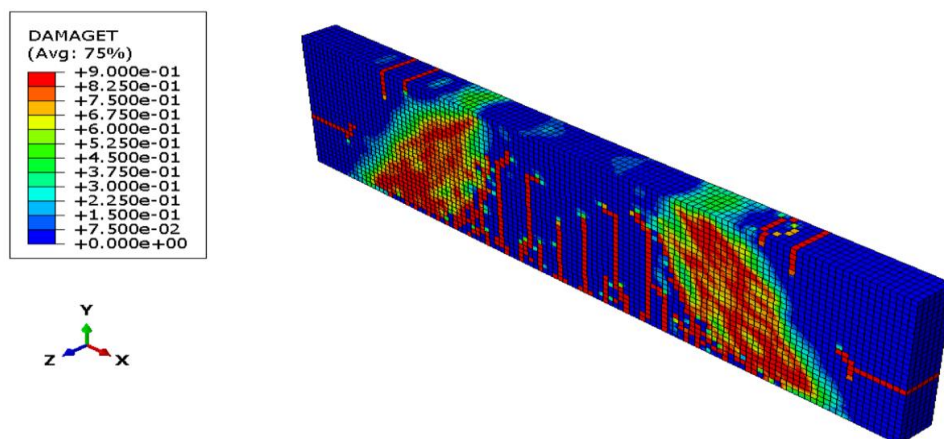Cracking Stage.
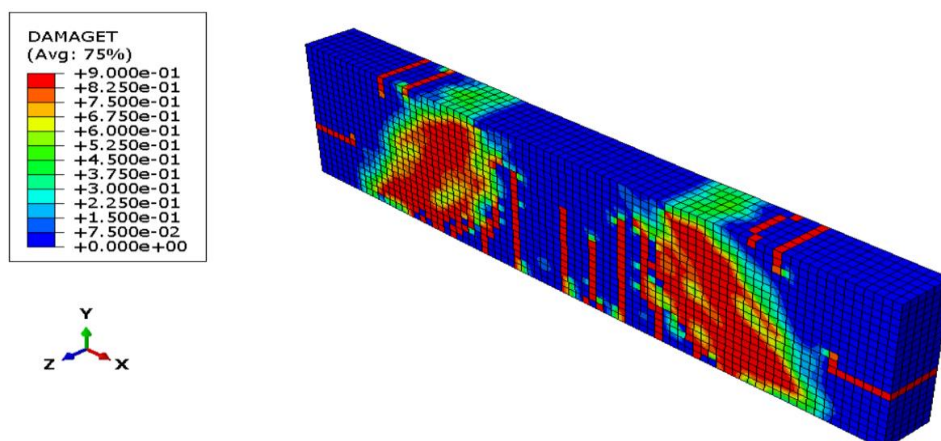
Figure C-22: Concrete Tension Damage for Specimen D-500 at Final Loading
Stage.
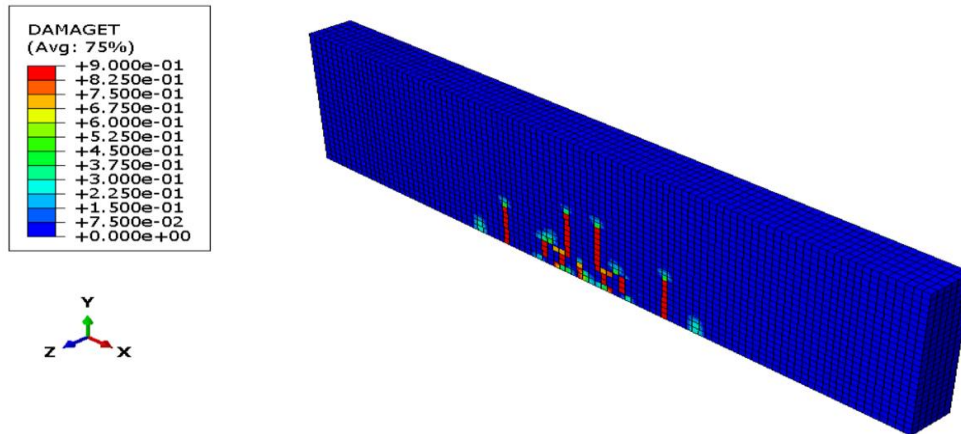
Figure C-23: Concrete Tension Damage for Specimen D-600 at Initial Loading
Stage.
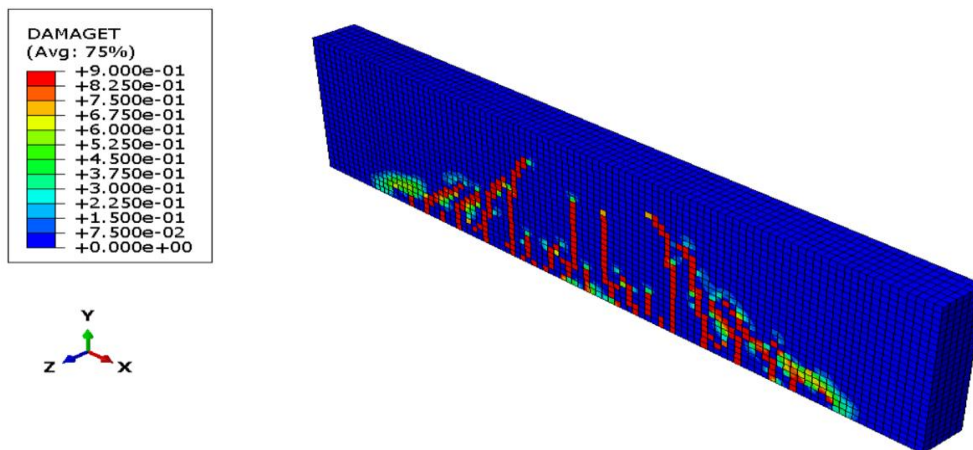
Figure C-24: Concrete Tension Damage for Specimen D-600 at Diagonal
Cracking Stage.
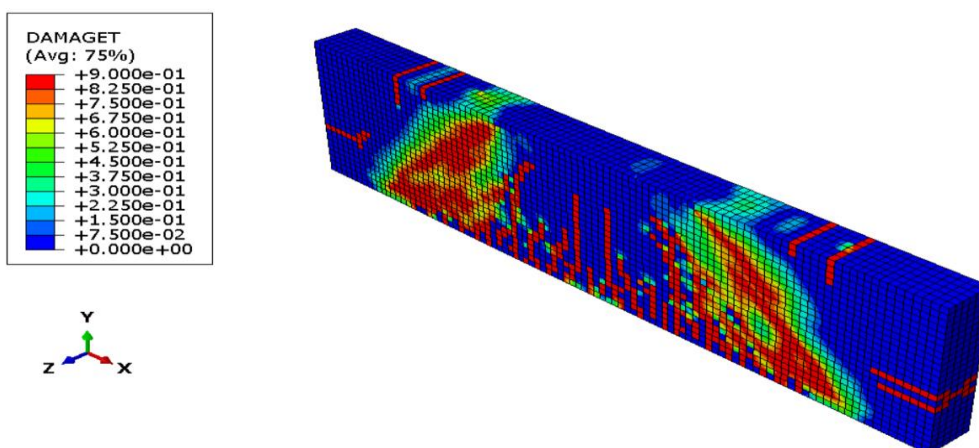
Figure C-25: Concrete Tension Damage for Specimen D-600 at Final Loading
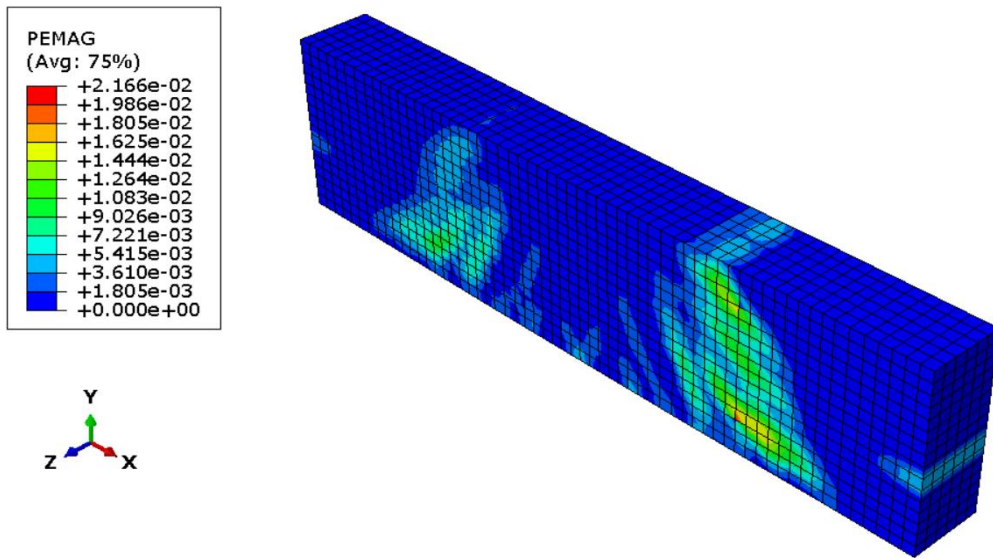Stage.

Figure C-26: Concrete Tension Damage for Specimen D-700 at Initial Loading
Stage.

Figure C-27: Concrete Tension Damage for Specimen D-700 at Diagonal
Cracking Stage.

Figure C-28: Concrete Tension Damage for Specimen D-700 at Final Loading
Stage.

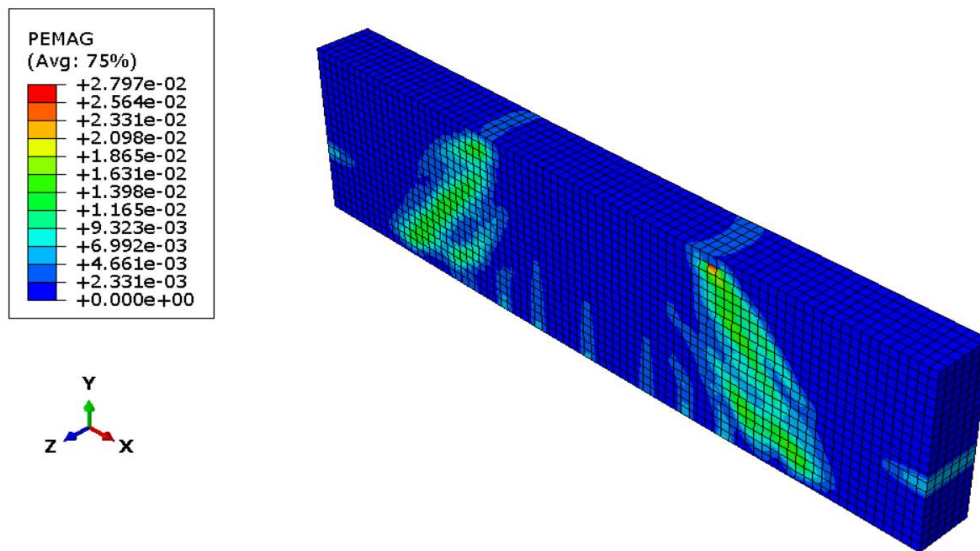Figure C-29: Plastic Strain Magnitude (PEMAG) Diagram for D-400 at
Failure Load.

Figure C-30: Plastic Strain Magnitude (PEMAG) Diagram for D-500 at
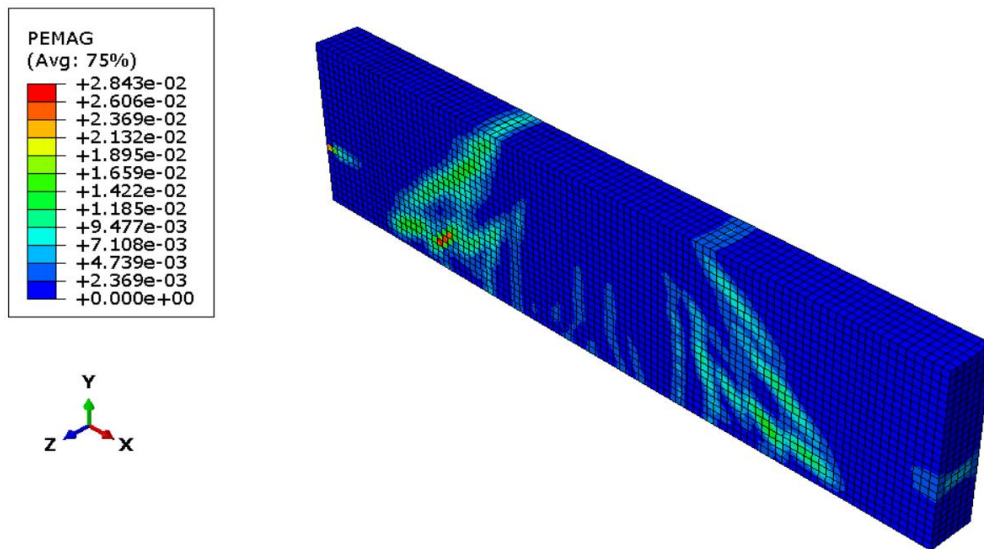Failure Load.

Figure C-31: Plastic Strain Magnitude (PEMAG) Diagram for D-600 at
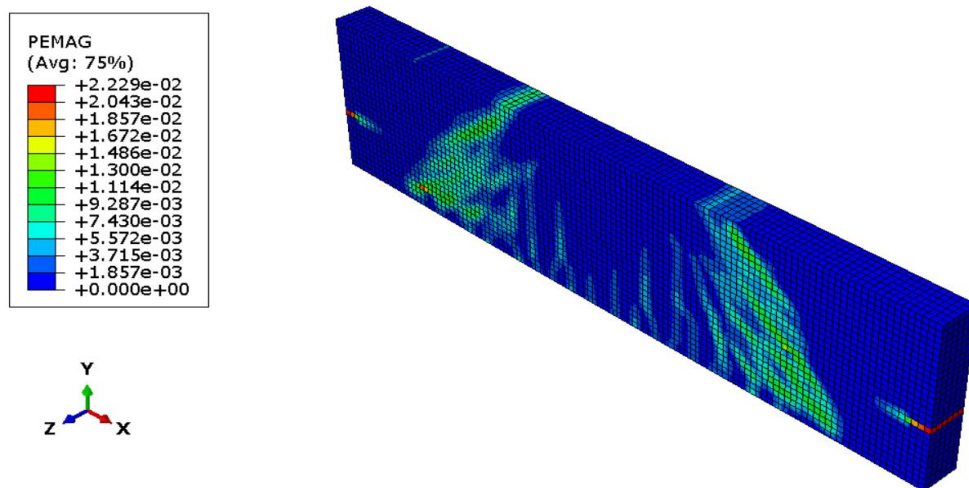Failure Load.

Figure C-32: Plastic Strain Magnitude (PEMAG) Diagram for D-700 at
Failure Load.